

CARBONATION CONVERSION OF  $\text{Na}_2\text{S}$  TO  $\text{H}_2\text{S}$

Dedicated to my sister,  
for her encouragement and support.

KINETICS AND MECHANISMS OF CARBONATION  
CONVERSION OF AQUEOUS  
SODIUM SULFIDE TO HYDROGEN SULFIDE

By

STEVEN HOI-CHIU NG, B.Sc.(Hons.)

A Thesis

Submitted to the School of Graduate Studies  
in Partial Fulfilment of the Requirements  
for the Degree  
Master of Science

McMaster University,

September 1990

MASTER OF SCIENCE (1990)  
(Chemical Metallurgy)

McMASTER UNIVERSITY  
Hamilton, Ontario

TITLE: Kinetics and Mechanisms of Carbonation Conversion  
of Aqueous Sodium Sulfide to Hydrogen Sulfide

AUTHOR: Steven Hoi-chiu Ng, B.Sc. (Dalhousie University)

SUPERVISOR: Dr. W-K Lu

NUMBER OF PAGES: xii, 144

## ABSTRACT

The objectives of the present study were to investigate the reaction mechanisms and the effects of certain physical variables on the overall reaction rate of the conversion of aqueous  $\text{Na}_2\text{S}$  to gaseous  $\text{H}_2\text{S}$  by bubbling with  $\text{CO}_2$  gas, which is a simultaneous absorption-desorption reaction.

The dependence of reaction rate on the physical variables investigated were the volumetric flow rate and the  $\text{CO}_2$  partial pressure of inlet gas and reaction temperature. Potential advantages of a pressurized reaction system were also studied. It was found that the effect of reaction temperature on the overall reaction rate was relatively small as compared to that of inlet gas flow rate and  $\text{CO}_2$  partial pressure.

Gas-liquid interfacial area was estimated and the overall reaction rate constant determined. It was found that the carbonation conversion of  $\text{Na}_2\text{S}$  is first order with respect to both the  $\text{HS}^-$  ion concentration of the liquid phase and the  $\text{CO}_2$  partial pressure of the inlet gas.

The rate limiting step of the overall conversion reaction, under the present laboratory conditions, appeared to be the desorption of hydrogen sulfide.

## ACKNOWLEDGEMENTS

The author wishes to express his gratitude to his supervisor, Dr. W-K Lu, for his inspiring guidance and highly motivating encouragement throughout the course of this work.

Grateful acknowledgements are due to the Natural Science and Engineering Research Council of Canada for the financial support in the form of a graduate scholarship, and an operating grant to his supervisor.

Special thanks are also due to those who in various ways have contributed to the work embodied in this thesis. The author is particularly indebted to:

Dr. P. Hegde for his valuable advise and discussions.

Dr. J.S. Chang and Dr. R.L. Judd for their high speed movie camera and movie projector.

V. Kupec, T. Bryner and M.V. Oosten for their valuable assistance in experimental and photographic work.

His fellow graduate students for many helpful discussions.

All Faculty members of the Department of Materials Science and Engineering for their thoughtful support.

## TABLE OF CONTENTS

	<u>Page</u>
Chapter 1 - Introduction	1
Chapter 2 - Literature Review	3
2.1 Summary.	3
2.2 The development of LB furnace at McMaster University.	4
2.3 Direct reduction and smelting of sulfide concentrates in LB furnace.	7
2.3.1 Lime enhanced reduction.	8
2.3.2 Separation of CaS from reduced metals and generation of H <sub>2</sub> S.	9
2.3.2.1 Through pyrometallurgical process.	10
2.3.2.2 Through hydrometallurgical process.	11
2.3.3 Soda enhanced reduction.	12
2.4 Generation of H <sub>2</sub> S from aqueous Na <sub>2</sub> S solution.	13
2.5 Measurement of the extent of Na <sub>2</sub> S conversion to H <sub>2</sub> S.	16
2.6 Chemical kinetics and reaction mechanisms.	19
2.7 Gas-liquid reaction.	21
2.7.1 Physical absorption.	23
2.7.2 The film model.	23
2.7.3 Absorption accompanied by chemical reaction.	25
2.7.4 Gas desorption.	27
2.8 Absorption of carbon dioxide in carbonate-bicarbonate buffer solutions.	29
2.8.1 Reaction between carbon dioxide and water.	30
2.8.2 Reaction between carbon dioxide and hydroxyl ion.	32
2.8.3 Overall absorption rate of carbon dioxide in carbonate-bicarbonate buffer solution.	33
2.9 Solubility of gas in aqueous solution.	36
2.10 Generation of elemental sulfur from hydrogen sulfide.	39
2.10.1 Clause process.	39
2.10.2 Bioreactor-based H <sub>2</sub> S treatment system.	

Chapter 3 - Experimental work	47
3.1 Introduction.	47
3.2 Experimental design.	47
3.2.1 Na <sub>2</sub> S stock solution.	47
3.2.2 Physical variables.	48
3.3 Experimental technique.	51
3.3.1 Description of experimental set up and equipment.	51
3.3.2 Calibration of mass flow meter.	52
3.3.3 Experimental procedures.	53
3.3.3.1 Preparation of solutions.	53
3.3.3.2 Determination of the concentrations of master and standard solutions.	55
3.3.3.3 Conversion of Na <sub>2</sub> S to H <sub>2</sub> S.	57
3.3.3.4 Estimation of interfacial area	60
Chapter 4 - Results	66
4.1 Summary.	66
4.2 Calibration of mass flow meter.	66
4.3 Temperature dependence of Na <sub>2</sub> S conversion rate.	69
4.4 The dependence of Na <sub>2</sub> S conversion on CO <sub>2</sub> flow rate.	71
4.5 The dependence of Na <sub>2</sub> S conversion on partial pressure of CO <sub>2</sub> .	73
4.6 Pressurized experiments.	75
4.7 Evaluation of interfacial area.	77
4.7.1 Gas hold-up volume.	77
4.7.2 Bubble size distribution and interfacial area.	79
Chapter 5 - Calculations and discussion.	94
5.1 Ionic composition of NaHCO <sub>3</sub> -Na <sub>2</sub> S solution.	94
5.1.1 At reaction time t = 0	94
5.1.2 During the course of reaction.	98
5.2 Exit gas composition.	104
5.2.1 H <sub>2</sub> S desorbed.	105
5.2.2 CO <sub>2</sub> absorbed.	105
5.2.3 Outgoing gas P <sub>H<sub>2</sub>S</sub> to P <sub>CO<sub>2</sub></sub> ratio.	108
5.3 Reaction kinetics of carbonation	

	conversion of aqueous sodium sulfide to hydrogen sulfide.	114
5.4	Reaction mechanisms and rate determining step of the carbonation conversion of aqueous sodium sulfide to hydrogen sulfide.	121
	5.4.1 Reaction mechanisms.	121
	5.4.2 Rate determining step.	125
5.5	Pressurized reaction system.	129
Chapter 6 - Conclusions		138
References		140

## LIST OF FIGURES

<u>Chapter 2</u>		<u>Page</u>
2.1	Cross section of bench-scale LB Furnace	43
2.2	Equilibrium constant as a function of temperature, for lime or soda enhanced carbothermic reduction of chalcopyrite.	44
2.3	Dependence of $K'_{2-18}$ on total sodium ion concentration.	45
2.4	Partial pressure ratio of hydrogen sulfide and carbon dioxide over sodium bisulfide-bicarbonate solutions.	45
2.5	Film model of gas-liquid reaction.	46
 <u>Chapter 3</u>		
3.1	Experimental set-up for H <sub>2</sub> S generation.	63
3.2	(a) Titration burette, with inner \$24 joint at the tip. (b) Titration flask, with matching joint and gas bag on side arm.	64
3.3	Experimental set-up for pressurized H <sub>2</sub> S generation.	65
 <u>Chapter 4</u>		
4.1	Calibration curve of CO <sub>2</sub> and N <sub>2</sub> transducer of Matheson mass flow controller.	89
4.2	Percent conversion of Na <sub>2</sub> S to H <sub>2</sub> S vs. reaction time at different temperatures.	90
4.3	Percent conversion of Na <sub>2</sub> S to H <sub>2</sub> S vs. reaction time with different CO <sub>2</sub> flow rates.	91
4.4	Percent conversion of Na <sub>2</sub> S to H <sub>2</sub> S vs. reaction time at different CO <sub>2</sub> partial pressures.	92
4.5	Percent conversion of Na <sub>2</sub> S to H <sub>2</sub> S vs.	

	reaction time of pressurized systems.	93
4.6	CO <sub>2</sub> bubbling at 1 min. reaction time.	80-2
4.7	CO <sub>2</sub> bubbling, at a flow rate of 155 ml/min, at the second reaction period.	83
4.8	CO <sub>2</sub> bubbling in distilled water, at a flow rate of 265 ml/min.	83
4.9	CO <sub>2</sub> bubbling at a rate of 397 ml/min at one minute reaction time.	87
 <u>Chapter 5</u>		
5.1	Ln(C/[Na <sub>2</sub> S] <sub>o</sub> ) verses reaction time at different temperatures.	131
5.2	Ln(C/[Na <sub>2</sub> S] <sub>o</sub> ) verses reaction time with different CO <sub>2</sub> flow rates.	132
5.3	Ln(C/[Na <sub>2</sub> S] <sub>o</sub> ) verses reaction time at different CO <sub>2</sub> partial pressures.	133
5.4	Ln(C/[Na <sub>2</sub> S] <sub>o</sub> ) verses reaction time of pressurized systems.	134
5.5	[Ln(C/[Na <sub>2</sub> S] <sub>o</sub> )]/P <sub>CO<sub>2</sub></sub> verses reaction time at different CO <sub>2</sub> partial pressures.	135
5.6	[Ln(C/[Na <sub>2</sub> S] <sub>o</sub> )]/(P <sub>CO<sub>2</sub></sub> ) <sup>2</sup> verses reaction time at different CO <sub>2</sub> partial pressures.	136
5.7	Gas-liquid interfacial area verses gas flow rate.	137

## LIST OF TABLES

<u>Chapter 2</u>		<u>Page</u>
2.1	Henry's law constant of CO <sub>2</sub> and H <sub>2</sub> S in pure water at various temperatures.	38
 <u>Chapter 4</u>		
4.1	Actual flow rate of mass flow controller, at room temperature and atmospheric pressure.	67
4.2	Volume and composition of gas flows of the N <sub>2</sub> -CO <sub>2</sub> mixtures.	68
4.3	Residual sulfide concentration (M), as functions of temperature and reaction time.	69
4.4	Percent conversion of Na <sub>2</sub> S to H <sub>2</sub> S as functions of temperature and reaction time.	70
4.5	Residual sulfide concentration (M), after pre-determined reaction time, with various CO <sub>2</sub> flow rates.	71
4.6	Percent conversion of Na <sub>2</sub> S, in experiments with various flow rates.	72
4.7	Residual sulfide concentration (M), and pH value of solution, as functions of inlet gas CO <sub>2</sub> partial pressure and reaction time.	73
4.8	Percent conversion of Na <sub>2</sub> S to H <sub>2</sub> S after various reaction time, as functions of inlet gas CO <sub>2</sub> partial pressure.	74
4.9	Residual sulfide concentration (M), and pH value of solution, as functions of gaseous pressure and reaction time.	75
4.10	Percent conversion of Na <sub>2</sub> S to H <sub>2</sub> S, as functions of gaseous pressure and reaction time.	76
4.11	Gas hold-up volume (ml), as functions of CO <sub>2</sub> flow rate and reaction time.	78
4.12	Ratio of gas hold-up volume to total	

	volume, as functions of CO <sub>2</sub> flow rate and reaction time.	78
4.13	Summary of bubble size distributions and interfacial areas in the system with various CO <sub>2</sub> flow rates.	85
4.14	Variation in bubble size distribution and interfacial area of figure 4.9.	88
 <u>Chapter 5</u>		
5.1	Composition of solution, with 0.716 atm partial pressure of CO <sub>2</sub> in the inlet gas.	101
5.2	Composition of solution, with 0.417 atm partial pressure of CO <sub>2</sub> in the inlet gas.	102
5.3	Composition of solution, with 0.121 atm partial pressure of CO <sub>2</sub> in the inlet gas.	103
5.4	Average P <sub>H<sub>2</sub>S</sub> to P <sub>CO<sub>2</sub></sub> ratio of outgoing gas, of the 0.716 atm CO <sub>2</sub> partial pressure experiments.	109
5.5	Average P <sub>H<sub>2</sub>S</sub> to P <sub>CO<sub>2</sub></sub> ratio of outgoing gas, of the 0.417 atm CO <sub>2</sub> partial pressure experiments.	110
5.6	Average P <sub>H<sub>2</sub>S</sub> to P <sub>CO<sub>2</sub></sub> ratio of outgoing gas, of the 0.121 atm CO <sub>2</sub> partial pressure experiments.	110
5.7	Slopes of the linear regions of the plots of figure 5.1, together with the calculated rate constants.	119
5.8	Slopes of the linear regions of the plots of figure 5.2, together with the calculated rate constants.	119
5.9	Slopes of the linear regions of the plots of figure 5.3, together with the calculated rate constants.	120
5.10	Slopes of the linear regions of the plots of figure 5.4, together with the calculated rate constants.	120

5.11	Slopes of the linear regions of the plots of figure 5.5, together with the calculated rate constants.	120
5.12	Solubility of CO <sub>2</sub> in reaction solution at various reaction time of the 0.716 atm CO <sub>2</sub> partial pressure experiments.	128

## CHAPTER 1

### Introduction

Conventional processes for the winning of metals from sulfide concentrates generally involve roasting and converting<sup>(1,2)</sup>, i.e. the oxidation of metal sulfides by air or oxygen. In these processes, essentially all sulfur from concentrates is oxidized to sulfur dioxide. At the present time, in order to reduce its emission to the atmosphere, sulfur dioxide is converted to sulfuric acid as much as the market could take. In Canada, however, many smelters are located in remote area. The requirement of long distance transportation of sulfuric acid or the establishment of an operation to convert it to a chemically stable compound posts immense problems.

As an alternative the novel LB Furnace technology which is being developed at McMaster University may be used<sup>(3)</sup>. It involves carbothermic reduction, rather than oxidation, in the presence of basic oxides, of sulfide concentrates to produce metal and sulfide slag. Hydrogen sulfide may be generated from the sulfur-containing slag after being separated from the other reduced metallic products. The gaseous hydrogen sulfide can then be converted to elemental sulfur for storage or shipping to far away markets. The main potential advantage of this new reduction process of sulfide concentrates is the

elimination of sulfur dioxide formation, hence emission to the atmosphere.

The generation of hydrogen sulfide from sodium sulfide, which would be the major component in the sulfur-containing slag if soda is used as flux in the direct reduction of sulfide concentrates, can be accomplished by the addition of an acid. Carbonation conversion of aqueous sodium sulfide, i.e. bubbling with  $\text{CO}_2$  gas, is particularly favourable since  $\text{CO}_2$  is readily available in the furnace flue gas. The thermodynamics of this process has been described in the literature but there is a lack of kinetic data which are needed for practical applications. The objectives of this project are to study the kinetics and mechanisms, which are crucial information for industrial reactor design, of the carbonation conversion of aqueous sodium sulfide to gaseous hydrogen sulfide.

This research program are mainly concerned with the dependence of sodium sulfide conversion rate on various physical variables. Four variables are considered important, namely reaction temperature,  $\text{CO}_2$  flow rate, inlet gas  $\text{CO}_2$  partial pressure, and the potential advantages of a pressurized system. Gas-liquid interfacial area at various gas flow rates will be estimated in order to evaluate the overall reaction rate constants.

## CHAPTER 2

### Literature review

#### 2.1 Summary

This chapter introduces the development of the novel ironmaking technology, the LB Furnace, and its potential application to the smelting reduction of sulfide concentrates. The selection of flux, with considerations concerning downstream separation of reduction products and subsequent conversion, is discussed.

The carbonation conversion of sodium sulfide (from slag) to hydrogen sulfide is studied. It also describes the common volumetric method used in the measurement of aqueous sulfide content.

One section of this chapter is dedicated to the definition of chemical kinetics, reaction mechanism and the concept of a rate controlling step in a sequence of elementary reactions.

The phenomena of gas-liquid reactions including physical gas absorption, gas absorption facilitated by chemical reaction and gas desorption are reviewed. The solubility of gas in liquid, and that of carbon dioxide in carbonate-bicarbonate buffer solutions in particular, is also covered.

The last part of this chapter describes some of the processes which generate elemental sulfur from hydrogen

sulfide.

## 2.2 The development of LB Furnace at McMaster University

The Blast Furnace, which has been recognized as a mature process, is the most productive and energy efficient ironmaking smelting reduction reactor with about 85% pre-reduction of iron ore before melting occurs when it is operated under optimum conditions. This most efficient operation, however, requires the preparation of raw materials (coke and fluxed agglomerates of iron ore) of specific physical and chemical properties. The growing overwhelming concern over the problems associated with coke plants, and the strong desire for the elimination of the step of agglomeration of iron ore and carbonization of coal appears to have come to the point that it is too costly to take the advantage of the technical superiority of the Blast Furnace. It has also become increasingly clear that the most efficient operating conditions for the Blast Furnace, coke oven and sinter plant are usually technically incompatible with flexible operation in terms of the properties of raw materials and productivity.

The potential of a new ironmaking technology, namely the LB Furnace<sup>(3,4)</sup>, has been substantiated in a bench scale unit at McMaster University. One of the basic principles of the LB Furnace is to utilize coal (a source of both energy and reducing agent) as efficiently as possible by first carrying out direct reduction (which

requires heat at moderately high temperature) and indirect reduction, and finally burning all of the remaining carbon monoxide and hydrogen by oxygen in air to release all the chemical energy within the reactor to provide the heat required for the process.

For the reduction of iron ore agglomerates at high temperatures, the kinetic barrier is mass transfer, or the diffusion of gases. In order to break this barrier, long distance diffusion of gases has to be avoided. The obvious solution to this problem is to bring the reacting particles close together. For a mixture of fine particles of iron ore concentrate and pulverized coal, the distance between reacting particles is of the order of tens of microns, which is smaller than the mean free path of gas at high temperatures. Hence, in this case, the resistance to the reduction reaction due to diffusion is of no significance and the overall reaction rate is then limited by the interfacial chemical reactions which are sensitive to temperature. Therefore, at high temperatures the overall reaction rate of mixtures of fine particles of iron ore and coal is likely to be limited by heat transfer. Furthermore, the enormous interfacial area of such a mixture offers the potential of very high reaction rate.

In order to realise the concepts of LB Furnace, the challenge of facilitating heat transfer from the flame (high oxygen potential) to the reduction sites (low oxygen

potential) without re-oxidation of the sponge iron has to be overcome. With the direct reduction enhanced, close to complete pre-reduction of iron ore before the occurrence of melting can be achieved.

Figure 2.1 is a schematic diagram of the bench-scale LB Furnace. It consists of two major components, one for the production of sponge iron and the other for melting. Sponge iron can be produced and melted in a single reactor.

Mixtures of fine particles of iron ore concentrate and coal, the raw materials for LB Furnace, are mechanically moved with the use of a steel screw feeder through a silicon carbide reaction tube to the combustion chamber where hot gases generated in the reaction tube together with the volatile impurities from coal are burned with air, introduced at ambient temperature, to provide the heat energy required for preheating, carbonization and reduction. The cold end of the reaction tube is sealed off so that all gases exit through the hot end of the tube. This flow of hot reducing gaseous product from the reaction tube to the combustion chamber protects the sponge iron from being re-oxidized by the strongly oxidizing flame a short distance downstream and serves as fuel for combustion. Sponge iron can be produced from raw materials at ambient temperature in a few minutes, which is then dropped from the hot end of the silicon carbide tube into

the melting zone where it is heated by plasma. Flux can be added to the melting chamber directly through the sampling port, or to the coal/ore mixtures.

The LB Furnace has been found, even in bench scale, to be highly energy efficient and it produces liquid metal which makes it easier to integrate with downstream refining processes. Furthermore, it has several significant potential advantages over the Blast Furnace in the area of lower capital and operational costs, environment pollution control due to the elimination of coke manufacturing, and flexibility in terms of production level and nature of products.

### 2.3 Direct reduction and smelting of sulfide concentrates in LB Furnace<sup>(5,6)</sup>

The novel process of ironmaking base on the LB Furnace which is being developed at McMaster University, can be applied, in principle, to the reduction of sulfide concentrates in the non-ferrous metals industry. It consists of the following key steps, of which number (3) is the major concern of this thesis,

- (1) direct reduction of sulfides by coal in the presence of a basic flux (e.g.  $\text{Na}_2\text{CO}_3$ ) to produce metallic solids (e.g. Cu, Fe) and vapours (e.g. Zn, Pb). The vapours are re-oxidized in the flame and collected in dust collecting system,
- (2) separation of slag including  $\text{Na}_2\text{S}$  from the reduced

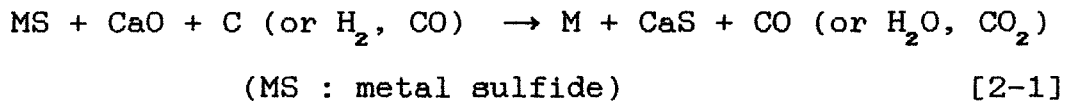
products,

- (3) generation of H<sub>2</sub>S from the resulting slag (Na<sub>2</sub>S),
- (4) conversion of H<sub>2</sub>S to elemental sulfur.

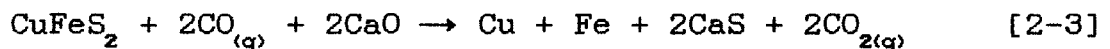
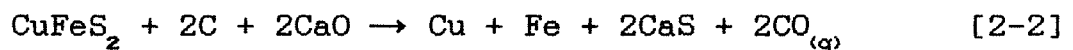
The major potential advantages of this new reduction smelting process over conventional oxidation processes are the positive effect on environmental quality due to the elimination of sulfur dioxide formation and its emission to the atmosphere.

### 2.3.1 Lime enhanced reduction(e.g. CuFeS<sub>2</sub>-C-CaO)

The production of metals by direct reduction of mineral sulfides without the formation of SO<sub>2</sub> has been studied by many authors. The general chemical stoichiometry is as follows :



At sufficiently high temperature, the direct reduction of chalcopyrite (chalcopyrite is used as an example of mineral sulfide throughout the rest of all subsections of 2.3) by coal with lime as flux,[2-2], occurs through the gaseous intermediate CO, [2-3], coupled with "solution loss" reaction, [2-4].



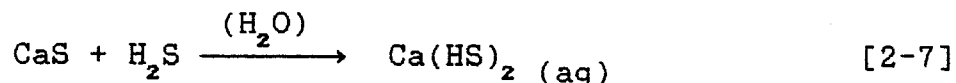
$$K_{2-2} = (P_{\text{CO}})^2 ; \quad K_{2-3} = (P_{\text{CO}_2}/P_{\text{CO}})^2 \quad [2-5,6]$$

Figure 2.2(a) shows the plots of the equilibrium constants  $K_{2-2}$  and  $K_{2-3}$  as a function of temperature, assuming activities of solids concerned being unity. For temperatures that are high enough to be of any practical importance the equilibrium constant  $K_{2-2}$  is of high value, and becomes even more favourable as temperature increases despite the fact that equilibrium of reaction [2-3] shifts to the left with increasing temperature. The direct reduction of chalcopyrite with lime as flux is clearly thermodynamically favourable.

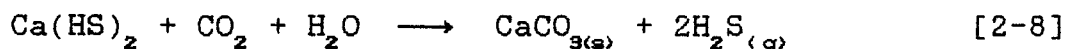
### 2.3.2 Separation of CaS from reduced metals and generation of $H_2S$

Calcium sulfide will be the sulfur containing product if lime is used as flux for the carbothermic reduction of chalcopyrite, reaction [2-2].

An effective way reported in the literature to separate CaS from other solid particles and to generate  $H_2S$  subsequently is to pass a  $H_2S$  containing gas through an aqueous slurry of the CaS mixture. The  $H_2S$  will be consumed by reacting with the CaS to form water soluble  $Ca(HS)_2$  :



Separation from other solid particles can then be accomplished by filtration. Subsequent reaction of the  $Ca(HS)_2$  filtrate with  $CO_2$  gas generates two moles of  $H_2S$  per mole of  $Ca(HS)_2$  :



In the case of direct reduction of chalcopyrite by coal, however, the reduced metal products (copper and iron) are highly susceptible to re-oxidation by hydrogen sulfide to metal sulfides. Therefore, separation of calcium sulfide from other metal products prior to any attempt of generating hydrogen sulfide from calcium sulfide is essential for the recovery of the metal products.

#### 2.3.2.1 Through pyrometallurgical process

In general, separation of reduced metals from other reduction by-products can be done most easily by the formation of liquid slag and metal layers. In this case, however, CaS is stable in the solid state up to very high temperature, at which it decomposes. Hence addition of flux is necessary in order to melt CaS, but unfortunately a CaS rich slag system with low melting point cannot be found in the literature. It appears that a large amount of flux may have to be used. This dilution is undesirable for its negative effect on the kinetics of the conversion of CaS to H<sub>2</sub>S. Besides, the volume of CaS produced is already more than eight times that of copper metal produced. Another large flux addition would mean too large a volume of slag to be practical.

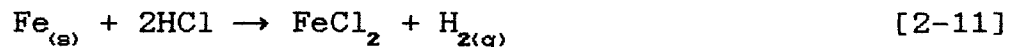
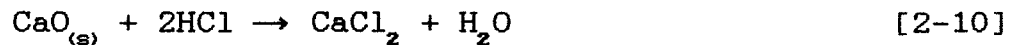
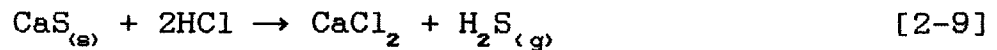
Since pyrometallurgical techniques for the separation of CaS proved unsuccessful, hydrometallurgical alter-

natives are considered.

### 2.3.2.2 Through hydrometallurgical process

The idea of using hydrometallurgical techniques for the separation of CaS is to convert the sulfur of water insoluble CaS into a water soluble form.

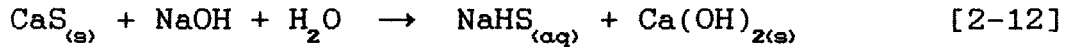
Considering the treatment with acid, HCl solution, the following reactions take place :



Copper is inert to HCl solution and it can easily be separated by filtration from the rest of the reaction products since all chlorides are water soluble. However, the regeneration of HCl by the use of  $\text{CO}_2$ , which is readily available from furnace flue gas, is far from efficient (it has been shown<sup>(6)</sup> by thermodynamic and mass balance calculations that in order to regenerate HCl by  $\text{CO}_2$ , 16 tonnes of aqueous solution has to be recycled for the treatment of 72 grams, i.e. one mole, of CaS solid). Furthermore, the use of acid to separate CaS from other metal products (Cu, Fe) suffers from the serious disadvantage of the generation of  $\text{H}_2\text{S}$  gas, which would re-oxidize copper to copper sulfide (section 2.3.2).

Alternatively, the treatment with base, NaOH solu-

tion, is considered. The reaction

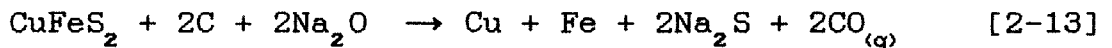


yields sodium hydrosulfide which is water soluble. Hydrogen sulfide would not be generated since an alkaline solution is used; hence no re-oxidation of Cu to CuS. Iron and copper are not reactive with NaOH solution, so the separation of CaS can easily be accomplished by filtration. Reaction [2-12] is thermodynamically feasible, but the kinetics are so sluggish that the use of concentrated NaOH (>2N) is mandatory.

In view of the fact that water insoluble calcium sulfide is eventually converted to water soluble sodium hydrosulfide for filtration separation, the idea of using soda, instead of lime, as flux is investigated. In that case, water soluble Na<sub>2</sub>S will be the sulfur containing product of the carbothermic reduction of sulfide concentrates.

### 2.3.3 Soda enhanced reduction(e.g. CuFeS<sub>2</sub>-C-Na<sub>2</sub>CO<sub>3</sub>)

Equilibrium constant of reaction [2-13], K<sub>2-13</sub>, is very large and increases slowly with temperature.



Unlike CaCO<sub>3</sub>, however, Na<sub>2</sub>CO<sub>3</sub> does not decompose readily to Na<sub>2</sub>O. Hence, the reaction of interest is

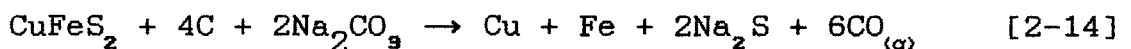
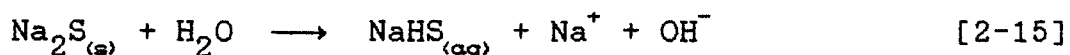


Figure 2.2(b) is a plot of  $K_{2-13}$  and  $K_{2-14}$  as a function of temperature. This shows that  $K_{2-14}$  increases dramatically with temperature, due to the strong entropy effect. At practical reaction temperatures ( $>900^{\circ}\text{C}$ ), reaction [2-14] is thermodynamically favourable. Therefore, soda is the preferred flux over lime for the carbothermic reduction of sulfide concentrates for easier downstream operations.

$\text{Na}_2\text{S}$  can easily be separated from the metal products by simple aqueous leaching.



The resulting basic solution ensures a negligible  $\text{H}_2\text{S}$  equilibrium concentration, so the metal products are free from re-oxidation to metal sulfides.

#### 2.4 Generation of $\text{H}_2\text{S}$ from aqueous $\text{Na}_2\text{S}$ solution

Carbonation process, bubbling with carbon dioxide, is the particularly favourable method for the generation of hydrogen sulfide from aqueous sodium sulfide solution since carbon dioxide is readily available from the LB Furnace flue gas.

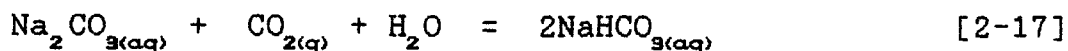
These carbonation processes have been of considerable interest in the past and have been described in the patent literature<sup>(7)</sup>, in particular. However, very few physical-chemical design data is available in the literature particularly in regard to the reaction kinetics,

which is crucial for industrial reactor design. The major objective of this research, therefore, is to study the reaction kinetics of the carbonation reaction of aqueous sodium sulfide solution, in the attempt of generating hydrogen sulfide.

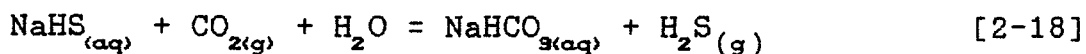
According to D. Freeman and co-workers<sup>(8)</sup>, the principal reaction by which  $H_2S$  can be produced by carbonation of  $Na_2S$  solution is :



where NaHS is the hydrolysis product of dissolution of  $Na_2S$  in water, equation [2-15]. Sodium bicarbonate is regenerated by the carbonation reaction as follows :



Hence, the net reaction of [2-16] and [2-17] is :



The vapour-liquid equilibrium constant,  $K_{2-18}$ , of this  $CO_2$ - $NaHCO_3$ - $Na_2CO_3$ - $Na_2S$ - $H_2O$  system is :

$$K_{2-18} = \frac{a_{NaHCO_3} \cdot P_{H_2S}}{a_{NaHS} \cdot P_{CO_2}} \quad [2-19]$$

$$= \frac{\gamma_{NaHCO_3}}{\gamma_{NaHS}} \cdot K'_{2-18} \quad [2-20]$$

$$\text{where } K'_{2-18} = \frac{[\text{NaHCO}_3] \cdot P_{\text{H}_2\text{S}}}{[\text{NaHS}] \cdot P_{\text{CO}_2}} \quad [2-21]$$

is a convenient description of the carbonation generation of  $\text{H}_2\text{S}$  from aqueous  $\text{Na}_2\text{S}$  solution.

Mai and Babb<sup>(9)</sup> have measured the values of  $K'_{2-18}$  over a temperature range of  $20^\circ\text{C}$  to  $65^\circ\text{C}$ , a pressure range of 1 to 5 atm., and a sodium ion concentration range of 0.10N to 2.0N. They found the effect of pressure on  $K'_{2-18}$  to be negligible, and the effect of temperature and total sodium ion concentration could be expressed as the following correlating equation :

$$K'_{2-18} = (9.746 \times 10^{-4}) C^{0.125} \exp(2275/T) \quad [2-22]$$

where C represents the total sodium ion molar concentration and T the absolute temperature,  $^\circ\text{K}$ .

Figure 2.3 illustrates the dependence of the phase equilibrium constant  $K'_{2-18}$  on temperature and sodium ion concentration. It shows that the effect of total sodium ion concentration is small as compare to that of temperature. Hence, for practical purposes, phase equilibrium constant  $K'_{2-18}$  can be estimated as a temperature dependent constant.

The plot of equilibrium values of  $P_{\text{H}_2\text{S}}/P_{\text{CO}_2}$  verses  $[\text{NaHS}]/[\text{NaHCO}_3]$  is shown in figure 2.4, of which the slopes represent  $K'_{2-18}$  values, for various sodium ion concentrations and temperatures up to  $65^\circ\text{C}$ . Clearly, the equilibrium

partial pressure of  $H_2S$  is promisingly high, and the generation of  $H_2S$  by carbonation of aqueous  $Na_2S$  solution is thermodynamically more favourable at  $25^\circ C$  than at higher temperatures.

## 2.5 Measurement of the extent of $Na_2S$ conversion to $H_2S$

One way to determine the extent of  $Na_2S$  conversion to  $H_2S$  is to measure the amount of  $H_2S$  gas evolved during the course of experiment.

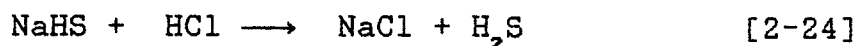
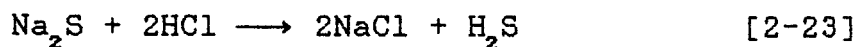
Hydrogen sulfide contaminates mercury (which is a common gas confining media used in many gas analysis apparatus) and is seldom estimated directly by volume in an examination of a gaseous mixture. Instead it is customary to remove  $H_2S$  gas from the gaseous mixture by absorption in aqueous solution before the commencement of analysis. (10)

A common treatment for quantitative analysis of  $H_2S$  gas is to absorb it in a dilute alkaline ammoniacal zinc sulfate solution ( $0.04F ZnSO_4$ ) with the formation of solid zinc sulfide. In general, a large excess of  $ZnSO_4$  is necessary to ensure complete absorption of  $H_2S$ . The absorbed  $H_2S$  is then liberated by acidifying the solution with hydrochloric acid and titrated with potassium iodate using starch as indicator to a permanent blue colour. (11,12)

In the present case of sodium sulfide conversion experiment, however, the exit  $CO_2/H_2S$  gaseous mixture has to pass through well over two litres of dilute ammoniacal

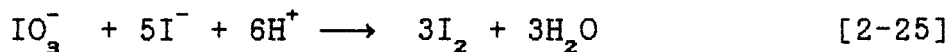
ZnSO<sub>4</sub> solution for complete absorption of H<sub>2</sub>S gas since 150 ml of reaction solution with a 0.43F initial Na<sub>2</sub>S concentration is used. Attempts to increase the concentration of ammoniacal ZnSO<sub>4</sub> solution lead to precipitation of Zn(OH)<sub>2</sub>. Furthermore, the exit gaseous mixture from the reactor contains a large amount of unreacted CO<sub>2</sub> gas, which would quickly lower the pH of the absorbing solution. These considerations make the direct absorption of H<sub>2</sub>S evolved during the course of the present experiments by a basic solution ineffective and impractical. To overcome these difficulties, the residual sulfide concentration of the reacted solution, rather than the amount evolved, is measured in order to determine the extent of conversion.

With the addition of potassium iodide and dilute hydrochloric acid to a sodium sulfide solution, hydrogen sulfide is generated according to the equations<sup>(13)</sup> :

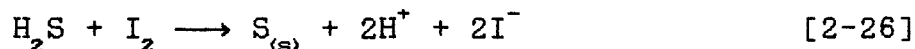


If an appreciable amount of sulfide is present in solution, special precautions (e.g. back titration, use of stoppered titration flask) must be taken to prevent H<sub>2</sub>S loss through volatilization upon addition of acid in the course of volumetric analysis.<sup>(14)</sup> The H<sub>2</sub>S generated has to be titrated at once with potassium iodate to prevent loss. For

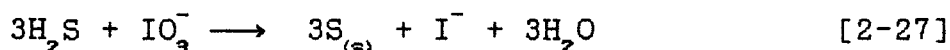
a mixture of potassium iodate and iodide in an acidic media, the position of the equilibrium of equation [2-25] lies by far to the right. (15)



Thus, hydrogen sulfide is oxidized by iodine according to equation [2-26]. (14)



and the overall redox reaction of [2-25] and [2-26] is :

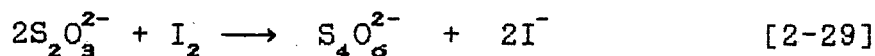


At the titration end-point, the excess iodine reacts with iodide to form the triiodide ion :



which in turn forms a complex with starch that gives the distinctive dark blue colour. (16)

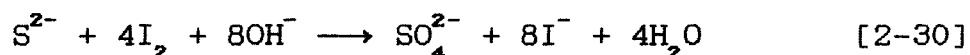
For the practice of back titration to avoid  $\text{H}_2\text{S}$  loss, an excess of potassium iodate is added at the beginning of titration, and the excess iodine generated is later back titrated with sodium thiosulfate according to equation [2-28].



To further prevent the loss of  $\text{H}_2\text{S}$  through volatilization and that of the excess iodine in the case of a back

titration, special stoppered titration flasks have to be used.<sup>(14)</sup>

Kolthoff<sup>(14)</sup> found that, in alkaline solutions, part of the sulfide is oxidized to sulfate in the presence of iodine:



This reaction is appreciable even in a weakly alkaline solution of bicarbonate, and thus can be a major source of error of the volumetric analysis if the solution is not kept acidic during the course of titration. On the other hand, in strongly acidic solutions, iodate will oxidize iodide or iodine to the +1 oxidation state provided some anions such as chloride and bromide are present to stabilize this oxidation state. For instance, in solutions that are greater than 3N in hydrochloric acid, reaction [2-31] proceeds essentially to completion.<sup>(15)</sup>



## 2.6 Chemical kinetics and reaction mechanism<sup>(17,18)</sup>

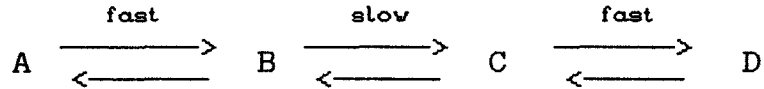
Chemical kinetics is the study of the rates of chemical reactions. The rate of a reaction is expressed as the change in concentration of any reactant or product per unit time. In describing the rate of a reaction, second is the most often used unit of time and molarity is the preferred concentration unit in solution chemistry.

Elementary reactions are reactions that occur in a single stage, with no identifiable intermediates. The rate of an elementary reaction is simply that given by the stoichiometry of the reaction itself. Elementary reactions are generally unimolecular or bimolecular, perhaps occasionally trimolecular.

For an overall chemical reaction, it is not only necessary to know the chemical kinetics, but also the detailed way by which reactants are converted to products. A postulated sequence of elementary reactions which reflects the correct stoichiometry and predicts the correct rate law for the overall reaction is called a reaction mechanism. Thus, the studies of chemical kinetics are closely related to the development of an understanding of reaction mechanisms.

For a sequence of elementary reactions the rate determining step is generally the slow step, as relative to the others in the sequence, of which the reverse reaction is negligible. In other words, the rate of the subsequent rapid reaction which consumes the intermediate is much faster than the backward reaction of the slow rate controlling step. On the other hand, the concentration of any reactive intermediate formed in any rapid step preceding a slow rate determining step can be taken as the equilibrium value. In an open sequence of elementary reactions, the rate of the overall reaction equals to the

rate of the rate determining step. As an example, in the following sequence of elementary reactions converting starting compound "A" to product "D", whereas "B" and "C"



are the reaction intermediates, the conversion reaction from "B" to "C" is the slow step as compared to the other steps. Then the concentration of compound "B" would be in equilibrium with compound A; the reaction converting "C" back to "B" is negligible; and the rate of the overall conversion reaction from "A" to "D" would equal to the rate of the slow rate determining step, namely the reaction converting "B" to "C".

The order of a reaction is the sum of the exponents of concentration factors in an experimental rate law, or reaction order can be used to refer to a particular species.

### 2.7 Gas-liquid reaction

Since the conversion of sodium sulfide to hydrogen sulfide involves the absorption of carbon dioxide into aqueous  $\text{Na}_2\text{S} - \text{NaHCO}_3$  solution, and the desorption of reaction product hydrogen sulfide from the solution to the gas phase, it is therefore necessary to examine the elementary reaction steps of physical and chemical interaction of gas

and liquid.

In general, the phenomenon of mass transfer of any gas-liquid systems with homogeneous reaction in the liquid phase may be broken down into a number of elementary steps, which are summarized as follows<sup>(19)</sup> :

- (a) Diffusion of reactant(s) from the bulk of gas phase to the interface between the two phases.
- (b) Dissolution of gaseous reactant(s) at the interface, at which physical equilibrium may be assumed, i.e. the concentration of dissolved gas at the interface is in equilibrium with the partial pressure of the gas in the gas phase.
- (c) Diffusion of the reactant(s) from the interface towards the bulk of liquid phase.
- (d) Chemical reaction takes place within liquid phase.
- (e) Diffusion of reactant(s) originally present in liquid phase, and of reaction product(s), within liquid phase, due to concentration gradients set up by the chemical reaction.

In the case that involves a production of a volatile reaction product :

- (f) Diffusion of the volatile reaction product from the bulk of liquid phase to the interface.
- (g) Gasification of the volatile reaction product at the interface, at which physical equilibrium may be assumed.

- (h) Diffusion of the volatile reaction product from the interface towards the bulk of gas phase.

### 2.7.1 Physical absorption<sup>(20)</sup>

For the process of physical absorption, by which the gas dissolves in the liquid without chemical reaction with the absorbent, it is found experimentally that the rate of absorption of the gas is given by

$$\bar{R}a = k_L a (A^* - A^0) \quad [2-32]$$

where  $\bar{R}$  is the average rate of absorption of gas per unit area;  $a$  is the interfacial area between the gas and the liquid per unit volume of the system;  $k_L$  is the physical mass transfer coefficient;  $A^*$  is the concentration of dissolved gas which is in equilibrium with the partial pressure of the gas at the interface; and  $A^0$  is the actual concentration of dissolved gas in the bulk of the liquid.

### 2.7.2 The film model

This model was first proposed by Whitman<sup>(21)</sup> in 1923. It suggests a stagnant film of finite thickness  $\delta$  at the surface of the liquid next to the gas, such that there is no convection within the film and dissolved gas gets across it only by diffusion alone. The concentration of the dissolved gas in the film falls from  $A^*$  at the gas liquid interface to  $A^0$  at its inner edge adjacent to the bulk of liquid, of which the composition is kept constant by

agitation, figure 2.5.

For the quasi-steady state diffusion of solute across the film, the compositions of both bulk phases may be considered constant with respect to time, i.e.

$$\frac{\partial A}{\partial t} = 0 . \quad [2-33]$$

In the case of physical absorption without chemical reaction,

$$D_A \frac{\partial^2 A}{\partial x^2} = \frac{\partial A}{\partial t} . \quad [2-34]$$

Hence 
$$D_A \frac{d^2 A}{dx^2} = 0 \quad [2-35]$$

and 
$$D_A \frac{dA}{dx} = \text{constant} , \quad [2-36]$$

where  $A$  and  $D_A$ , respectively, is the concentration and diffusivity of the dissolved gas in liquid phase;  $t$  is the time, and  $x$  is the distance perpendicular to and from the interface towards the liquid bulk. The concentration gradient of  $A$  between  $x = 0$  and  $x = \delta$  is constant, as shown in figure 2.5. Thus,

$$\frac{dA}{dx} = -(A^* - A^0)/\delta \quad [2-37]$$

Since the steady state rate of absorption is

$$\bar{R} = -D_A \left[ \frac{dA}{dx} \right]_{x=0} , \quad [2-38]$$

the film model gives the rate of physical absorption as :

$$\bar{R} = D_A (A^* - A^0)/\delta \quad [2-39]$$

Thus from equation [2-32],

$$k_L = D_A / \delta \quad [2-40]$$

The parameters  $\bar{R}$ ,  $k_L$ ,  $A^*$  and  $A^0$  are as defined previously. The hydrodynamics properties of the system are accounted for by the parameter  $\delta$ , which is affected by liquid turbulence, physical properties of liquid, etc.

Despite the fact that the film model is not very realistic, that a film in agitated system has uniform thickness, it does contain an essential feature of the real system, namely, that the gas must get into the liquid by dissolution and diffusion before it can be transported by convection. Predictions based on the film model are very often remarkably similar, indeed sometimes identical, to those based on more sophisticated models, such as Higbie's model<sup>(22)</sup> and Danckwerts's model<sup>(23)</sup>. In fact it is often preferable to use the film model, in view of its simplicity, rather than the other more sophisticated ones, for the purposes of calculation and prediction.

### 2.7.3 Absorption accompanied by chemical reaction<sup>(24)</sup>

If the dissolved gas reacts with the liquid, or with a substance dissolved in the liquid, the rate of absorption will be determined partly by the hydrodynamic conditions (physical properties of liquid, geometry of absorbing interface, flow rate, etc.) and partly by the physico-chemical properties of the system (solubility of absorbing gas in the absorbent, diffusivity of the gas and

of reactants in liquid, and the kinetics of reactions occurring in the liquid).

The film model (steady state diffusion through a film of uniform thickness  $\delta$ ) with chemical reaction lead to the following equation for chemical absorption :

$$D_A \frac{d^2 A}{dx^2} = r \quad [2-41]$$

where  $r$  is the local rate of reaction that consumes species "A".

Consider the simplest first order irreversible reaction as an example,

$$r = k_1 A , \quad [2-42]$$

where  $k_1$  is the first order reaction rate constant, and  $A$  the local concentration of dissolved gas "A". The film model equation and corresponding boundary conditions are

$$D_A \frac{d^2 A}{dx^2} = k_1 A \quad \left\{ \begin{array}{l} A = A^* \text{ at } x = 0 \\ A = A^0 \text{ at } x = \delta = D_A/k_L \end{array} \right. \quad [2-43]$$

The solution to equation [2-43] is

$$A = \frac{1}{\sinh \sqrt{M}} \left[ A^0 \sinh \left[ x \sqrt{\frac{k_1}{D_A}} \right] + A^* \sinh \left[ \left( \left[ \frac{D_A}{k_L} - x \right] \sqrt{\frac{k_1}{D_A}} \right) \right] \right] \quad [2-44]$$

and

$$\bar{R} = -D_A \left( \frac{dA}{dx} \right)_{x=0} = k_L \left[ A^* - \frac{A^0}{\cosh \sqrt{M}} \right] \frac{\sqrt{M}}{\tanh \sqrt{M}} \quad [2-45]$$

where

$$M = D_A k_1 / k_L^2 \quad [2-46]$$

Typical concentration profile of absorption accompanied by chemical reaction, together with the one of pure physical absorption is shown in figure 2.5.

The absorption rate equations for some higher order irreversible and reversible reactions were reported by Danckwerts. In general, the mathematics is quite involved even for the simple film model, and for some systems there is no analytical solution.

#### 2.7.4 Gas desorption<sup>(25)</sup>

Desorption takes place when the concentration of dissolved gas in the bulk of liquid is greater than that at the surface; hence the partial pressure of gas which would be in equilibrium with the bulk liquid is greater than the partial pressure at the surface.

When the partial pressure in equilibrium with the bulk is much larger than the total pressure at the surface, i.e. a large degree of supersaturation, bubbles will form in the interior of the liquid, and this bubbling will greatly enhance the gas desorption due to increase in surface and liquid turbulence. On the other hand, a small degree of supersaturation does not necessarily imply bubble nucleation because of the increased solubility of small bubbles due to surface tension<sup>(26)</sup>. In other words, although the liquid might be supersaturated relative to the gas phase, it might not be supersaturated relative to small bubbles. Thus, in order for bubbling desorption to take

place, the solution not only has to be supersaturated with dissolved gas, but the supersaturation has to exceed certain degree.

In general, according to Shah et al. (27), supersaturation of a volatile product of a homogeneous liquid phase chemical reaction that enhance the absorption of another gaseous reactant occurs when inequality [2-47] holds

$$D_C H_A / D_A H_C < 1 \quad [2-47]$$

where  $D_A$  and  $H_A$  are, respectively, the diffusivity and Henry's law constant of the absorbing gas, whereas  $D_C$  and  $H_C$  are those of the desorbing volatile product. Satisfaction of equation [2-47] is necessary for, but does not definitely confirm, the occurrence of bubbling desorption. There appears to be no quantitative theory on bubbling desorption.

When the partial pressure in equilibrium with the bulk liquid is less than the total pressure of the gas phase, no bubbling desorption will take place, and the gas will be desorbed by diffusion to the existing surface, a process analogous to gas absorption such that equations derived for absorption may be used for desorption with just minor changes. Equation [2-32] for physical absorption can be used for physical desorption. The difference is only that  $A^\circ$ , the bulk concentration of dissolved gas is greater

than  $A^*$ , the concentration at the interface; thus

$$-\bar{R} = k_L (A^O - A^*) \quad [2-48]$$

where  $-\bar{R}$  is the rate of desorption.

In the case of chemical desorption one is concerned with reactions which produce the dissolved gas rather than destroy it. Unlike chemical absorption, the theory of chemical desorption is much less developed in spite of the fact that in many industrial gas treating plants the absorber is usually coupled with a desorption unit, where the liquid solution is regenerated before being recirculated to the absorber.

Danckwerts reported the general solution for the desorption rate of first order irreversible reactions :

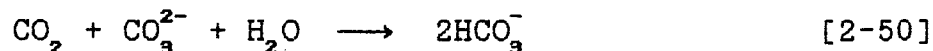
$$-\bar{R} = (A_e - A^*) \sqrt{(D_A k_1 + k_L^2)} \quad [2-49]$$

where  $-\bar{R}$  is the rate of desorption and  $A_e$  is the concentration of the volatile product A, that would be in equilibrium with the liquid of the local composition. The condition for equation [2-49] to be applicable is that the concentration of all reactant species but A is virtually uniform at all points, including the interface; in other words, their concentrations in the liquid film are virtually the same as in the liquid bulk.

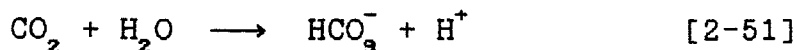
## 2.8 Absorption of carbon dioxide in carbonate-bicarbonate buffer solutions <sup>(28)</sup>

The absorption of carbon dioxide in a carbonate-

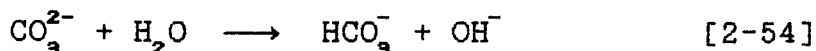
bicarbonate buffer solution is accompanied by the following overall reaction :



Reaction [2-49] is trimolecular, and therefore it is obviously the results of a series of reactions in reality. Carbon dioxide may undergo two sequences of direct reactions in a weakly basic solution that lead to the overall reaction [2-50], namely the reaction with water and with hydroxide ion :



and



### 2.8.1 Reaction between carbon dioxide and water

According to equation [2-51], carbon dioxide reacts with water to form bicarbonate and hydrogen ions. The amount of molecular carbonic acid,  $\text{H}_2\text{CO}_3$ , formed is known to be negligible under all conditions.<sup>(29,30)</sup> The equilibrium constant  $K_{2-51}$ , which is the first acid ionization constant of carbonic acid  $K_{a1}$ , at various temperature and infinite dilution has been reported by Harned and Owen<sup>(31)</sup> and may be summarised by equations [2-55] and [2-56] :

$$K_{2-51} = K_{a1(\text{CO}_2)} = \frac{[\text{HCO}_3^-][\text{H}^+]}{[\text{CO}_2]} \quad [2-55]$$

$$\log K_{a1(\text{CO}_2)} = -3404.7/T + 14.843 - 0.03279T \quad [2-56]$$

where  $K_{a1}$  of carbonic acid is measured in molarity,  $T$  in degrees Kelvin.

The rate of reaction [2-51] is first order with respect to the concentration of carbon dioxide. Values of the forward rate constant  $k_{2-51}$  at various temperature and infinite dilution may be summarised by<sup>(32)</sup> :

$$\log k_{2-51} = 329.850 - 110.541 \log T - 17265.4/T \quad [2-57]$$

where  $T$  is measured in degrees Kelvin. The effect of ionic strength of the solution on  $k_{2-51}$  is negligible<sup>(33)</sup>.

Reaction [2-52] is considered to be instantaneous since it involves only a transfer of proton, and thus it may be assumed that equilibrium is maintained. The equilibrium constant  $K_{2-52}$  is the inverse of the second acid ionization constant  $K_{a2}$  of carbonic acid. The function of  $K_{a2}$  of carbonic acid with temperature as variable at infinite dilution is given by equation [2-60].<sup>(31)</sup>

$$K_{a2(\text{CO}_2)} = \frac{[\text{H}^+][\text{CO}_3^{2-}]}{[\text{HCO}_3^-]} \quad [2-58]$$

$$K_{2-52} = \frac{[\text{HCO}_3^-]}{[\text{H}^+][\text{CO}_3^{2-}]} = 1/K_{a2(\text{CO}_2)} \quad [2-59]$$

$$\log K_{a2}(\text{CO}_2) = -2902.4/T + 6.498 - 0.0238T \quad [2-60]$$

### 2.8.2 Reaction between carbon dioxide and hydroxyl ion

The reaction between carbon dioxide and hydroxide ion, equation [2-53], in the forward direction is first order with respect to the concentration of carbon dioxide and hydroxide ion individually. Hence, the overall kinetics of reaction [2-53] is second order. Values of  $k_{2-53}$  at infinite dilution at various temperature may be summarised by the expression<sup>(32)</sup> :

$$\log k_{2-53} = 13.635 - 2895/T \quad [2-61]$$

It was reported<sup>(32)</sup> that the rate constant  $k_{2-53}$  increases with increasing ionic strength due to sodium chloride ions. Although the effect of ionic strength on  $k_{2-53}$  depends on the kind of ions present, the results for sodium chloride ions can be used to give a rough estimate of  $k_{2-53}$  in a solution of given ionic strength.

Since reaction [2-54] involves only a transfer of proton, it may be considered to be instantaneous, and thus chemical equilibrium may be assumed to prevail at all time.

In a carbonate-bicarbonate buffer solution, the concentration of hydroxide ion depends on the ratio of carbonate to bicarbonate ion concentration according to equation [2-62] :

$$[\text{OH}^-] = K_{2-54} \frac{[\text{CO}_3^{2-}]}{[\text{HCO}_3^-]} = K_{2-54} \beta \quad [2-62]$$

where

$$\beta = \frac{[\text{CO}_3^{2-}]}{[\text{HCO}_3^-]} \quad [2-63]$$

The equilibrium constant  $K_{2-54}$  is actually the ratio of water ionization constant,  $K_w$ , to the second dissociation constant of carbonic acid.

$$K_{2-54} = \frac{K_w}{K_{a2}(\text{CO}_2)} \quad [2-64]$$

where

$$K_w = [\text{H}^+][\text{OH}^-] \quad [2-65]$$

Both equilibrium constants  $K_w$  and  $K_{a2}$  of carbonic acid increase with temperature. Since the effect of temperature on  $K_w$  is stronger than that on  $K_{a2}$  (31,34), the equilibrium constant  $K_{2-54}$  also increases with temperature.

It was noticed that the value of equilibrium constant  $K_{2-54}$  vary markedly with the ionic strength and the species of ion present in the solution<sup>(35)</sup>. In general  $K_{2-54}$  decreases with increasing ionic strength of the solution.

### 2.8.3 Overall absorption rate of carbon dioxide in carbonate-bicarbonate buffer solution

The overall absorption rate of carbon dioxide in

carbonate-bicarbonate solution is clearly the sum of the individual reaction rate of equation [2-51] and [2-53], since both reaction [2-52] and [2-54] are instantaneous. Hence,

$$r_{2-50} = k_{2-51} [\text{CO}_2] + k_{2-53} [\text{OH}^-][\text{CO}_2] \quad [2-66]$$

and from equation [2-62],

$$r_{2-50} = k_{2-51} [\text{CO}_2] + k_{2-53} K_{2-54} \beta [\text{CO}_2] = k_{2-50} [\text{CO}_2] \quad [2-67]$$

where 
$$k_{2-50} = k_{2-51} + k_{2-53} K_{2-54} \beta \quad [2-68]$$

The effect of ionic strength of solution on  $k_{2-51}$  is negligible (section 2.8.1). On the other hand, the product " $k_{2-53} K_{2-54}$ " decreases with ionic strength, but this effect is not significant probably because, with increasing ionic strength,  $k_{2-53}$  increases while  $K_{2-54}$  diminishes (section 2.8.2). Therefore the overall absorption rate constant  $k_{2-50}$  decreases slightly with increasing ionic strength of solution.

All the parameters  $k_{2-51}$ ,  $k_{2-53}$  and  $K_{2-54}$  increase with increasing temperature (section 2.8.2), so that the product " $k_{2-53} K_{2-54}$ " increases rather rapidly. Nijsing and Kramers reported values of " $k_{2-53} K_{2-54}$ " at 20, 25 and 30°C as 0.56, 0.80 and 1.4/sec respectively<sup>(36)</sup>. Therefore, the overall absorption rate constant  $k_{2-50}$  is expected to increase with temperature.

At 25°C and infinite dilution, the value of  $k_{2-51}$

is about 0.026/sec (equation [2-57]). When this value and that of " $k_{2-53}K_{2-54}$ " are inserted into equation [2-68], the overall rate constant of chemical absorption of  $\text{CO}_2$  in carbonate-bicarbonate buffer solutions at  $25^\circ\text{C}$  and infinite dilution is given by :

$$k_{2-50} = 0.026 + 0.80\beta \quad [2-69]$$

Clearly, for any solution that is not almost completely converted to bicarbonate, the reaction of carbon dioxide with water is relatively insignificant as compared to that with hydroxide ion. For instance, at pH 10.0  $\beta$  has a value of 0.46. Thus, the product " $k_{2-53}K_{2-54}\beta$ " equals to 0.37, which is over 14 times greater than  $k_{2-51}$ .

However, it was reported that the reaction between carbon dioxide and water can be catalyzed, and may then become faster than reaction [2-53]. Apart from carbonic anhydrase (an enzyme present in blood) and arsenite<sup>(37)</sup>, the most effective catalysts are the anions of certain weak acids<sup>(38)</sup>. In general, the rate of catalysed reaction is proportional to the concentration of the catalytic species. Therefore, the overall absorption rate of carbon dioxide in solution in the presence of catalyst becomes :

$$\text{Rate} = (k_{2-51} + k_{2-53}[\text{OH}^-] + k_B[\text{B}^-])[\text{CO}_2] \quad [2-70]$$

where  $k_B$  is the catalytic reaction rate constant corresponding to anion  $\text{B}^-$ . Unfortunately, the catalytic rate

constant of hydrosulfide anion does not appear to be in literature.

## 2.9 Solubility of gas in aqueous solution

According to Henry's law, the concentration  $C_A$  of dissolved gas A that is in equilibrium with a partial pressure  $P_A$  of the gas is given by (39):

$$P_A = HC_A \quad [2-71]$$

where H is the Henry's law constant and has dimension l atm/mol. In general the above expression is valid as long as the concentration of dissolved gas is small and the temperature and pressure are far from the critical temperature and pressure of the gas.

If the gas reacts in solution, Henry's law applies to the concentration of unreacted gas, rather than to the total concentration of reacted and unreacted forms of the gas.

In ideal solutions, the Henry's law constant is only temperature dependent and it generally increases with increasing temperature, whereas the solubility of gas decreases.

When considering chemical absorption of gas, it is often necessary to know the solubility of the unreacted gas in solution with which it reacts. In the case of electrolyte solutions, the solubility can be estimated by the empirical method of Van Krevelen and Hoftizer<sup>(40)</sup>,

which relates the solubility in solution to that in pure water at the same temperature by means of the expression :

$$\log(H/H_w) = hI \quad [2-72]$$

where  $H_w$  is the value in pure water;  $h$  is the salting out coefficient and  $I$  is the ionic strength of the solution defined by :

$$I = \frac{1}{2} \sum C_i Z_i^2 \quad [2-73]$$

$C_i$  being the concentration of ions of valency  $Z_i$ .

The value of  $H_w$  of carbon dioxide and hydrogen sulfide at different temperatures are given by V.M.Ramm<sup>(41)</sup> using mole fraction as the concentration unit for the dissolved gas. The corresponding numbers with the more convenient unit of 1 atm/mol are listed in table 2.1.

temperature (°C)	$H_w$ (atm/M)	
	$CO_2$	$H_2S$
20	25.6	8.70
25	29.3	9.81
30	33.4	11.0
35	37.7	12.2
40	41.9	13.4
45	46.2	14.8
50	51.0	15.9
60	61.3	18.5

Table 2.1 Henry's law constant of  $CO_2$  and  $H_2S$  in pure water at various temperatures.

The salting out coefficient  $h$  is the sum of contributions of the gas species  $h_g$  and of the positive and negative ions,  $h_+$  and  $h_-$  respectively, present in solution:

$$h = h_g + h_+ + h_- \quad [2-74]$$

In mixed electrolytes, the value of  $H$ , as suggested by Danckwerts<sup>(42)</sup>, can be estimated by an expression of the form :

$$\log(H/H_w) = h_1 I_1 + h_2 I_2 + \dots \quad [2-75]$$

where  $I_1$  and  $h_1$ , respectively, are the ionic strength and salting out coefficient attributable to species number 1 of the electrolytes.

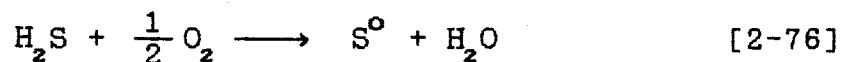
## 2.10 Generation of elemental sulfur from hydrogen sulfide

As mentioned in section 2.3, the final major step of the direct reduction of sulfide concentrates in LB Furnace is the conversion of hydrogen sulfide to elemental sulfur. There are many well established industrial processes for this purpose for the treatment of coke oven gas<sup>(43)</sup>, natural gas and other manufactured gases<sup>(44)</sup>.

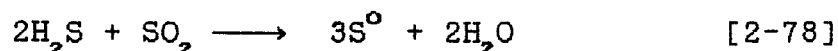
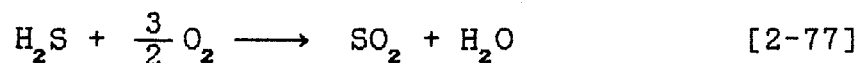
### 2.10.1 Claus process

Probably the most well known and widely used industrial sulfur production process for treating hydrogen sulfide containing gas is the Claus process. It was developed in about 1890 and is applicable for production of sulfur from acid gas streams containing more than about 15 percent H<sub>2</sub>S.

The original Claus process involved the oxidation of hydrogen sulfide with air over a bauxite or iron ore catalyst in a simple reactor with the overall reaction :



The first significant advancement was made in about 1937 by I. R. Farbenindustrie<sup>(45)</sup>. Instead of burning all the H<sub>2</sub>S directly over the catalyst, one-third of the H<sub>2</sub>S was burned to sulfide dioxide in a waste heat boiler. The SO<sub>2</sub> produced was then reacted with the remaining H<sub>2</sub>S over bauxite at 700-750°F.



Actually, the reactions that take place in a Claus reactor are seldom as simple as depicted by equations [2-77,78]. The reactions occurring in the burner and on the catalyst surface are complex and involve many oxygen, sulfur and oxysulfur intermediates. Furthermore, there are several molecular forms of sulfur that can exist, namely  $\text{S}_2$ ,  $\text{S}_6$  and  $\text{S}_8$ . Opekar and Goar<sup>(46)</sup> reported that other molecular sulfur species  $\text{S}_3$ ,  $\text{S}_4$ ,  $\text{S}_5$ , and  $\text{S}_7$  do exist, but their amounts are negligible.

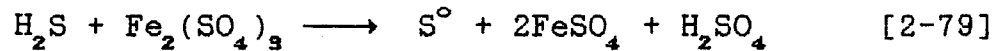
Another development of the Claus process was the high temperature, up to  $1000^\circ\text{C}$ , non-catalytic combustion of  $\text{H}_2\text{S}$  with air to produce elemental sulfur directly. The yield of this non-catalytic generation of sulfur from  $\text{H}_2\text{S}$  can be as high as 90 percent.

#### 2.10.2 Bioreactor-based $\text{H}_2\text{S}$ treatment system

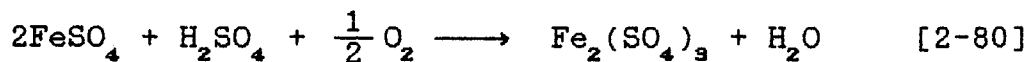
It has been reported that a new bioreactor-based hydrogen sulfide treatment system particularly for  $\text{CO}_2/\text{H}_2\text{S}$  mixtures was recently developed in Japan by Dowa Mining Co., Ltd. and NKK<sup>(6)</sup>. This new process uses bacteria call thiobacillus ferrooxidans (TBFO) to treat  $\text{H}_2\text{S}$  containing gases.

In the absorber of this system, the  $\text{H}_2\text{S}$  of the

incoming raw gas is absorbed and oxidized by a solution of ferric sulfate. Elemental sulfur is produced while ferric sulfate is reduced to ferrous sulfate according to the following equation :



The elemental sulfur produced is separated by dewatering in a sulfur separator, and the ferrous sulfate in the absorbing solution is oxidized back to ferric sulfate by the bacteria, after which the absorbing solution is recirculated to the absorber.



The above absorbent regeneration reaction is extremely slow under normal conditions, but with TBFO the reaction rate can be increased by as much as 500,000 times.

Perhaps the most attractive feature of this new  $\text{H}_2\text{S}$  treatment system is its low operating cost, which is the result of several advantageous aspects of this system. It is operated at ambient temperature and atmospheric pressure which makes energy costs minimal, and the operation and maintenance of the system easier. It does not require any catalysts or special chemicals; only ferric sulfate is used as absorbent. There is no side reactions, therefore no byproducts and no degradation of the absorbing solution. It does not generate any effluent, so there is no need for

waste-water treatment. Furthermore, as the absorbent is acidic, the system has H<sub>2</sub>S selectivity under coexistence of CO<sub>2</sub> in the incoming raw gas.

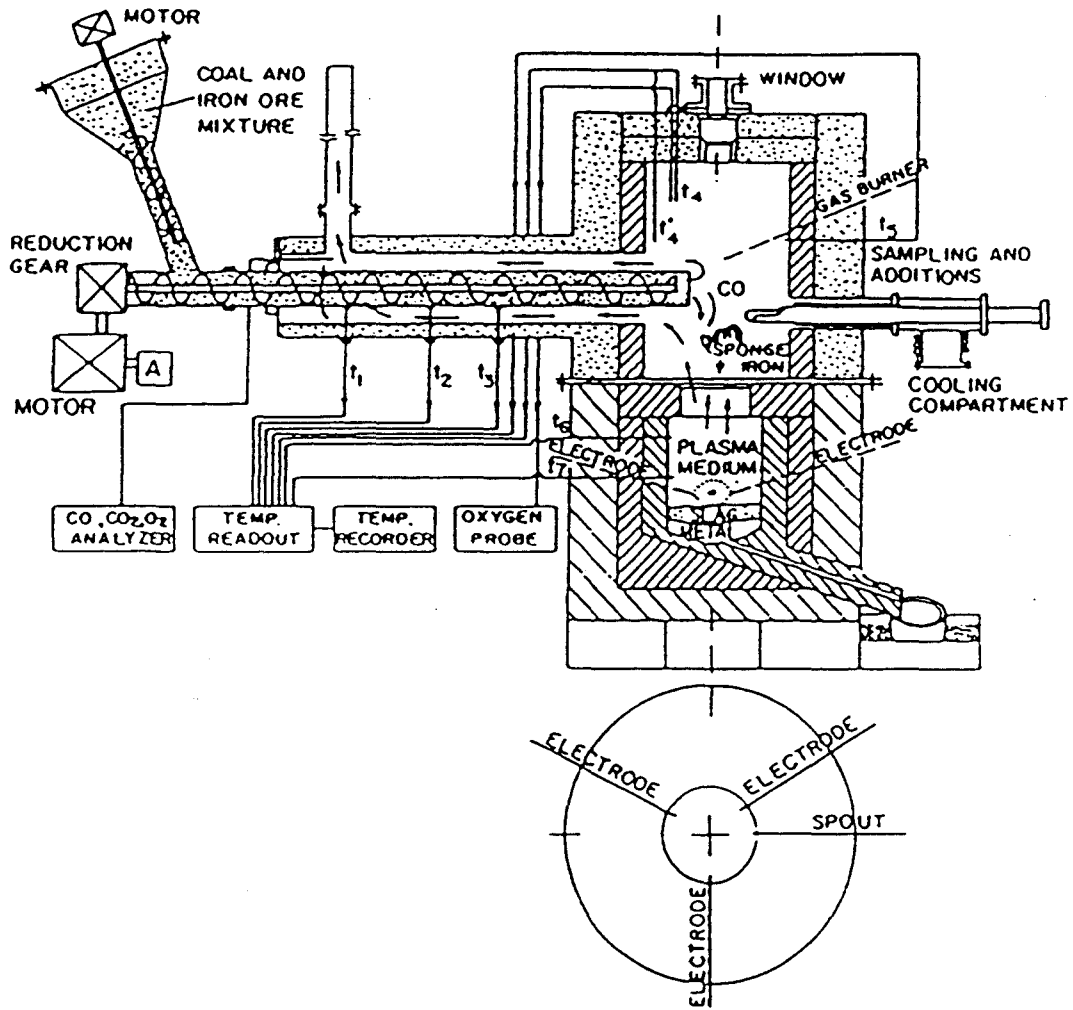


Figure 2.1 Cross section of bench-scale LB Furnace (from ref. 4 )

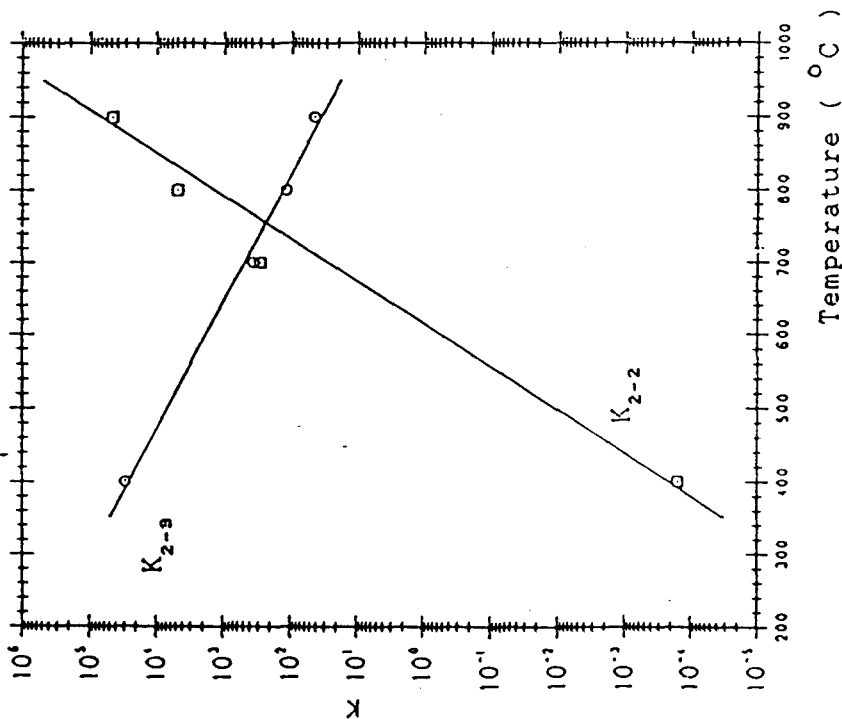


Figure 2.2(a) Lime enhanced carbothermic reduction  
 $\text{CuFeS}_2 + 2\text{C} + 2\text{CaO} \rightarrow \text{Cu} + \text{Fe} + 2\text{CaS} + 2\text{CO}_{(g)}$  (2-2)  
 $\text{CuFeS}_2 + 2\text{CO}_{(g)} + 2\text{CaO} \rightarrow \text{Cu} + \text{Fe} + 2\text{CaS} + 2\text{CO}_{2(g)}$  (2-3)

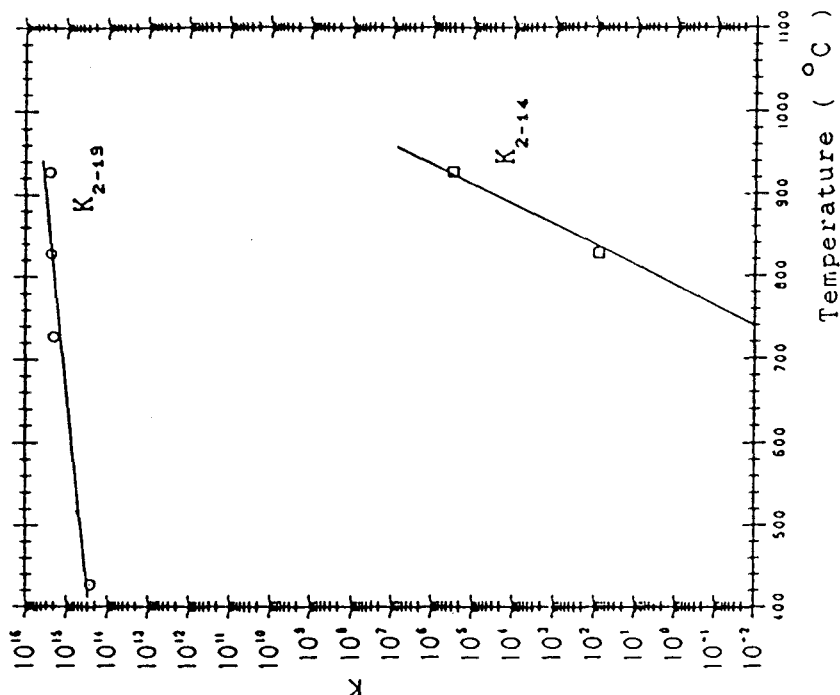


Figure 2.2(b) Soda enhanced carbothermic reduction  
 $\text{CuFeS}_2 + 2\text{C} + 2\text{Na}_2\text{O} \rightarrow \text{Cu} + \text{Fe} + 2\text{Na}_2\text{S} + 2\text{CO}_{(g)}$  (2-13)  
 $\text{CuFeS}_2 + 4\text{C} + 2\text{Na}_2\text{CO}_3 \rightarrow \text{Cu} + \text{Fe} + 2\text{Na}_2\text{S} + 6\text{CO}_{(g)}$  (2-14)

Fig. 2.2(a,b) Equilibrium constant as a function of temperature, for lime or soda enhanced carbothermic reduction of chalcopyrite.

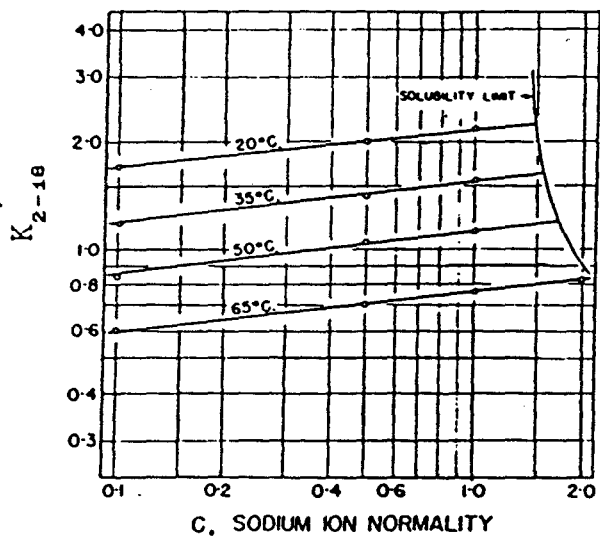


Figure 2.3 Dependence of  $K'_{2-18}$  on total sodium ion concentration.

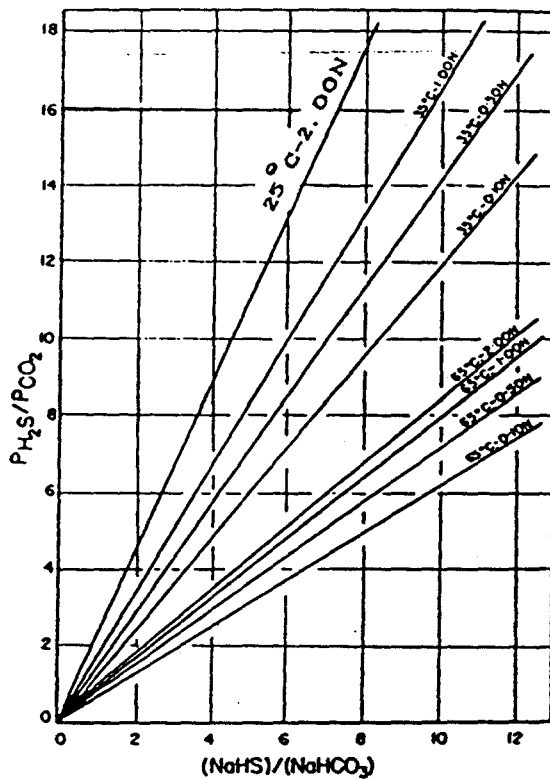
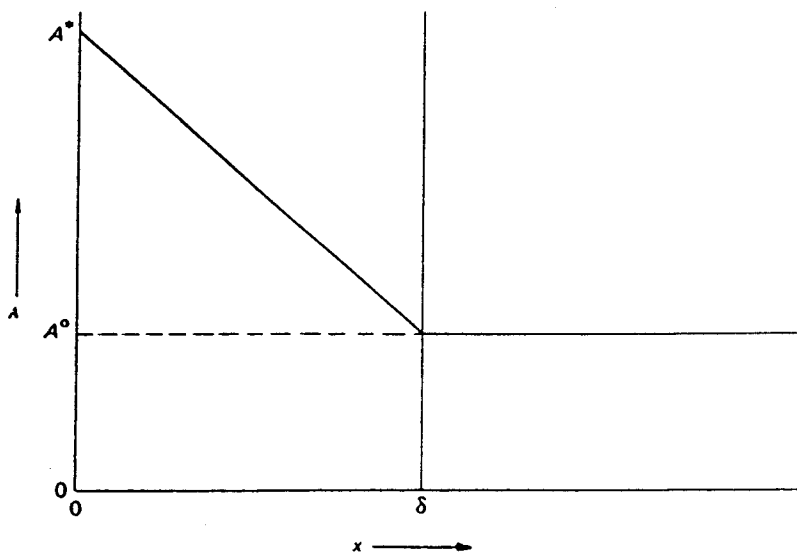
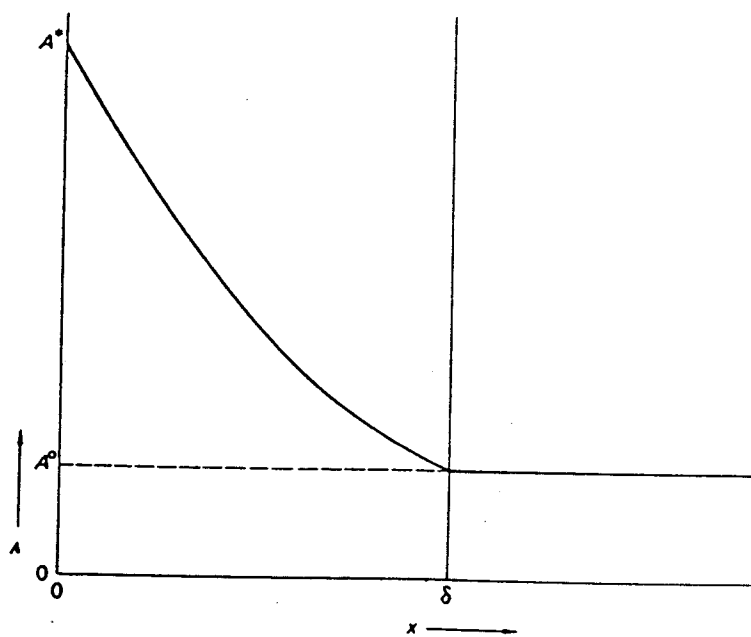


Figure 2.4 Partial pressure ratio of hydrogen sulfide and carbon dioxide over sodium bisulfide-bicarbonate solutions.



(a) Physical absorption



(b) Absorption accompanied by chemical reaction

Figure 2.5 Film model of gas-liquid reaction.

## CHAPTER 3

### EXPERIMENTAL WORK

#### 3.1 Introduction

The desorption of  $H_2S$  from aqueous  $Na_2S$  solution enhanced by  $CO_2$  bubbling was studied with the use of a simple gas washing bottle equipped with fine porosity dispersion cylinder as reactor.

The effects of various physical variables, namely, temperature,  $CO_2$  flow rate,  $CO_2$  partial pressure and sulfide concentration, on  $H_2S$  desorption rate were investigated. Furthermore, the reaction system's interfacial areas at the various pre-determined  $CO_2$  flow rates used in experiments were estimated in order to evaluate the rate constants.

#### 3.2 Experimental design

##### 3.2.1 $Na_2S$ Stock solution

Due to the hygroscopic nature of  $Na_2S$  crystals and the 2% sulphite and sulphate impurities of the BDH reagent grade  $Na_2S$  used, the accurate preparation of  $Na_2S$  solution of a given concentration by accurate weighing of  $Na_2S$  solids followed by dissolution in water is not feasible. Therefore, stock solutions within a close range of the pre-determined concentration (1.3M) were prepared by weighing the approximate amount of  $Na_2S$  solids to dissolve

in distilled water. The exact concentrations were then determined by iodometric titration with excess potassium iodate and back titrated with sodium thiosulphate. Several  $\text{Na}_2\text{S}$  stock solutions were prepared and consumed in the course of this research work. Special attention was paid in trying to get identical concentrations, but due to the fact mentioned above, the concentrations of the  $\text{Na}_2\text{S}$  stock solutions prepared were in the range of 1.22 to 1.33 molar.

### 3.2.2 Physical Variables

Physical variables studied in this research project were (a) temperature, (b)  $\text{CO}_2$  gas flow rate, (c) composition of gas, (d) pressurized system and (e) concentration of reactants.

(a) It is necessary to conduct kinetic study of the  $\text{H}_2\text{S}$  generation process at various temperatures to determine the most desirable temperature for industrial operations. Higher than room temperature operations may be beneficial for the following reasons :

(i) reactions being thermally activated, the kinetics may improve significantly at higher temperature.

(ii) The solubilities of the reactants, both  $\text{Na}_2\text{S}$  and  $\text{NaHCO}_3$ , increase with temperature. This results in more concentrate solution and higher reaction rate, which leads to a smaller reactor with lower capital and operational costs.

(iii) Equilibrium partial pressure of gaseous  $\text{H}_2\text{S}$

over a solution of dissolved  $H_2S$  increases with temperature, i.e. higher temperature enhance  $H_2S$  desorption.

(iv) Since the product out of the LB furnace is hot, the aqueous solution obtained upon dissolution in water is at higher temperature without additional cost.

High reaction temperature, however, has one major draw back, namely, the aqueous  $CO_2$  concentration which would be in equilibrium with the gas phase decreases with increasing temperature. This decrease in  $CO_2$  absorption obviously will lower the driving force of  $H_2S$  generation. Furthermore, it was shown in section 2.4 that higher temperatures are thermodynamically less favourable for the overall reaction.

Accordingly, four temperatures were chosen,  $25^\circ C$ ,  $35^\circ C$ ,  $45^\circ C$  and  $55^\circ C$ , in order to study the effect of temperature on  $H_2S$  generation.

(b) In general, the rate of  $H_2S$  generation increases with  $CO_2$  gas flow rate due to the increase in supply of reactant ( $CO_2$ ), surface area and the turbulence of both gas and liquid phase. It is expected that the effect of increasing  $CO_2$  flow rate on  $H_2S$  generation would be close to linear at the low flow rate region and with diminishing effectiveness as  $CO_2$  flow rate is further increased.

Higher flow rate, however, may leads to a less  $CO_2$

utilization and lower  $H_2S$  concentration in the outlet gas, which may be undesirable for the generation of elemental sulphur since existing technologies for the production of elemental sulphur favour as high a  $H_2S$  content as possible. It is desirable that the  $H_2S$  content of the gaseous mixture be higher than a certain minimum value. Besides, high  $CO_2$  flow rate may cause mechanical difficulty and larger reactor being necessary due to larger gas hold-up volume.

Experiments of five different  $CO_2$  gas flow rates (129, 155, 265, 397 and 495 ml/min) were conducted in order to study the effect of  $CO_2$  flow rate on the kinetics of the  $H_2S$  generation process. High speed movie camera was used to study the bubble size distributions of the various flow rates in order to estimate the interfacial areas.

(c) Since desorption of  $H_2S$  gas from aqueous  $Na_2S$  solution is more favoured by the lowering of pH, which is accomplished by the absorption of  $CO_2$  gas, the kinetics of  $H_2S$  desorption is expected to depend on the  $CO_2$  partial pressure of the inlet gas. Accordingly, four sets of experiments of different  $CO_2$  partial pressures, namely 1 atm, 0.716 atm, 0.417 atm and 0.1213 atm, with  $N_2$  as inert gas to make up to 1 atm total pressure for the systems with lower  $CO_2$  partial pressure, were conducted in order to study the dependence of  $H_2S$  desorption rate on  $CO_2$  partial pressure of inlet gas.

(d) Henry's law, which is usually valid for dilute

system, indicates a linear relationship between concentration of a dissolved gas in solution and the equilibrium gaseous partial pressure. It is important to test the validity of this linear relationship for systems of higher pressure to assess the advantage of using a pressurized reactor. Due to equipment constraint in the laboratory, pressures of only 129 kPa (4 PSIG) and 163 kPa (9 PSIG) were studied.

(e) It is anticipated that the  $H_2S$  generation rate would depend on the concentration of dissolved  $H_2S$ , which is readily in equilibrium with  $HS^-$  ion, in the aqueous  $Na_2S$  solution.

All experiments were isothermal and started off with approximately the same  $Na_2S$  concentrations but terminated after different reaction time. The amount of unreacted sulfide in solution could therefore be directly measured. This gave the concentration of  $Na_2S$  in solution as a function of reaction time, and hence enabled the determination of the dependence of  $H_2S$  desorption rate on sulfide concentration.

### 3.3 Experimental Technique

#### 3.3.1 Description of experimental set up and equipment

A diagram of the experimental set up is shown in figure 3.1 . Coleman instrument grade  $CO_2$  gas, whose mass flow rate was accurately controlled by a Matheson mass flow meter (model 8259,SP-1734), was delivered to the

aqueous  $\text{Na}_2\text{S}-\text{NaHCO}_3$  solution contained in a gas washing bottle used as reactor. The washing bottle was equipped with fritted cylinder of coarse porosity, 40-60 microns, which delivered fine bubbles with diameters less than 1 mm. The dimensions of the reaction bottle are as following : inner diameter 33 mm; dispersion tube outer diameter 8 mm; fritted cylinder 12mm in diameter and 20 mm long; solution mixture depth 16.5 cm without gas bubbling. The reaction bottle was submerged in a water bath whose temperature was controlled to within  $0.5^\circ\text{C}$  by a Brinkmann circulator (model IC-2). The reacted gas after passing through bubblers containing alkaline sodium nitroprusside and/or silver nitrate eventually exited to the fume hood exhaust.

For the iodometric titrations of the reacted solutions, attention was called for and special apparatus was used to minimize the loss of  $\text{I}_2$  and  $\text{H}_2\text{S}$  gas in the course of titration. The burette used, figure 3.2(a), was equipped with an inner  $\text{F} 24$  joint at the tip to match the joint of the titration flask, figure 3.2(b), which had a gum gas expansion bag attached to the side arm to release the pressure of  $\text{H}_2\text{S}$  and  $\text{CO}_2$  gas evolved upon addition of dilute  $\text{HCl}$  acid.

### 3.3.2 Calibration of mass flow meter

The gas mass flow meter and blender used had  $\text{CO}_2$  and  $\text{N}_2$  transducers of a full capacity of, respectively, 2 litres and 3 litres (at standard temperature and pressure)

per minute. The flow setting was a digital display of the percentage of these full capacities, but it was not accurate for flows that were either very large or small with respect to the full capacities. Some of the flow rates used in the experiments were less than 10 % of the full capacities of the transducers, and it was therefore necessary to calibrate the transducers to get the exact flow rates at different percentage settings of our interest.

The exact flow rates were measured under room temperature and atmospheric pressure by using a graduated column with gas introduced at the bottom and soap bubble film formed near the inlet gas opening. By measuring the rising speed of the bubble films the actual flow rates were determined.

To minimize uncertainty, the percentage settings used in the  $H_2S$  conversion experiments were those measured for the preparation of the calibration curves.

### 3.3.3 Experimental procedures

#### 3.3.3.1 Preparation of solutions

(a) Concentrated  $Na_2S$  stock solution was prepared by dissolving about 330 grams of Fisher Scientific reagent grade  $Na_2S \cdot 9H_2O$  crystals in distilled water and made up to one litre. The exact concentration was determined by iodometric titration. Several concentrated  $Na_2S$  stock solutions, ranging from 1.22 to 1.33 molar, were prepared

and consumed in the course of the research.

(b) 0.9 M  $\text{NaHCO}_3$  stock solution was prepared by accurately weighing to the nearest 0.1 mg analytical reagent grade  $\text{NaHCO}_3$  crystals, followed by dissolution in distilled water and quantitatively diluted to one litre.

(c) Potassium iodate is available in a high state of purity and can be used for the direct preparation of standard solutions which are stable indefinitely.

About 6.65 g of Caledon Laboratories Ltd's reagent grade  $\text{KIO}_3$  was weighed accurately to the nearest 0.1 mg and dissolved in about 900 ml of distilled water, which was then transferred quantitatively to a one litre volumetric flask and diluted to the mark to obtain a 0.03 M solution.

(d) On the other hand, thiosulphate solutions are less stable and cannot be used as primary standard. Among the variables affecting the stability of thiosulphate solutions are the presence of microorganisms, concentration and pH value of the solution, and the exposure of the solution to atmospheric oxygen and sunlight. Normality of thiosulphate solutions can decrease by a few percent in a few weeks. The most important single cause of instability is the presence of certain bacteria that metabolize the thiosulphate ion, converting it to sulphate, sulphite and elemental sulphur. Solutions that are sterile are remarkably stable.

Approximately 0.1 N  $\text{Na}_2\text{S}_2\text{O}_3$  solution was prepared

by dissolving 15.81 grams of  $\text{Na}_2\text{S}_2\text{O}_3$  solids in one litre of cool distilled water which was freshly boiled for 10 minutes in a beaker covered with a watch glass. About 0.1 gram of  $\text{Na}_2\text{CO}_3$  was added to the solution which was then transferred to a clean stoppered bottle and stored in the dark.

The exact concentration was later determined by iodometric titration using potassium iodate as primary standard.

(e) Starch solution is the most widely used indicator in iodine titrations which gives an intense blue colour at the presence of a trace of triiodide ion. Aqueous starch suspensions decompose within a few days by bacterial action whose products may consume iodine and interfere with the indicator properties, but the rate of decomposition can be greatly reduced by preparing and storing the indicator in sterile conditions.

A paste of about 2 grams of soluble starch and 10 mg of  $\text{HgI}_2$ , act as preservative, in about 30 ml of water was poured into one litre of boiling distilled water and heated until the solution was clear, which was then transferred to a stoppered bottle for storage when cooled.

About five ml of this starch solution was used for each titration.

### 3.3.3.2 Determination of the concentrations of master and standard solutions

Potassium iodate was used as primary standard, and the kind of burette and titration flask described in 3.3.1 was used for all iodometric titrations in order to minimize the loss of  $\text{H}_2\text{S}$  and  $\text{I}_2$ .

To determine the concentration of standard  $\text{Na}_2\text{S}_2\text{O}_3$ , a buret was cleaned and filled with  $\text{Na}_2\text{S}_2\text{O}_3$  solution. Ten ml aliquot of standard  $\text{KIO}_3$  solution was transferred to a titration flask, and about two grams of iodate-free potassium iodide was added. Ten ml 1.0 N HCl was added and the solution was titrated immediately, to prevent iodine loss, with  $\text{Na}_2\text{S}_2\text{O}_3$  until the colour of the solution became pale yellow. About five ml of starch solution was added and the solution was titrated to the disappearance of the blue colour. Acidity of the solution was checked with pH paper. In the check runs  $\text{Na}_2\text{S}_2\text{O}_3$  was added all at once up to 0.5 ml before end point to minimize  $\text{I}_2$  loss.

To determine the concentration of  $\text{Na}_2\text{S}$  master solution, 2 grams of KI and 5 ml of starch solution was added to 10 ml aliquot of ten-fold diluted  $\text{Na}_2\text{S}$  solution. Ten ml 1.0 N HCl was added and the solution was immediately titrated with  $\text{KIO}_3$  to a deep purple colour to minimize  $\text{H}_2\text{S}$  loss due to the formation and gasification of  $\text{H}_2\text{S}$  upon addition of HCl. Since some  $\text{H}_2\text{S}$  was in the gas phase, the solution was let stand for one minute to ensure complete oxidation. The excess  $\text{KIO}_3$  was then back titrated with  $\text{Na}_2\text{S}_2\text{O}_3$  to colourless and the acidity of solution was

checked. In the check runs,  $\text{KIO}_3$  of just 0.5 ml over the end point was added all at once to minimize the loss of  $\text{H}_2\text{S}$  and  $\text{I}_2$ .

### 3.3.3.3 Conversion of $\text{Na}_2\text{S}$ to $\text{H}_2\text{S}$

For the experiment of converting aqueous  $\text{Na}_2\text{S}$  to  $\text{H}_2\text{S}$  gas with  $\text{CO}_2$  bubbling, the general procedure was as described below.

Fifty ml of  $\text{Na}_2\text{S}$  stock solution was accurately measured and put in the water bath in a stoppered flask for 10 minutes before the start of experiment to let the solution reach experimental temperature. One hundred ml aliquot of  $\text{NaHCO}_3$  stock solution was transferred to the reaction bottle in the water bath and prebubbled for 10 minutes with the pre-determined  $\text{CO}_2$  flow rate in order to flush out all the air and to facilitate the solution to reach the water bath temperature.

At the start of experiment, the  $\text{Na}_2\text{S}$  solution was added to the reaction bottle through the stopcock at the top of the bottle, figure 3.1. Temperature of the water bath was kept constant to within  $0.5^\circ\text{C}$  and the  $\text{CO}_2$  flow rate accurately controlled by a mass flow meter during the course of reaction.

Since the extent of the  $\text{H}_2\text{S}$  generation reaction was determined by measuring the sulfide content difference of the solution before and after reaction, it was necessary to retrieve all the reacted solution and prevent the loss of

$\text{H}_2\text{S}$  through gasification after the pre-determined reaction time when the bubbling of  $\text{CO}_2$  was stopped. Accordingly, at termination time of reaction, the reacted solution was quantitatively and promptly transferred to a beaker and diluted to about 800 ml to minimize further reaction after pH value of the solution was measured by a Fisher Accumet pH meter, model 140. The reaction bottle and dispersion tube was quickly washed many times with distilled water, which was afterwards added to the dilute reacted solution. The solution was then quantitatively transferred to a one litre volumetric flask and made up to the mark with distilled water.

Titration was carried out right away to determine the extent of conversion. About 2 grams of KI was added to a 25 ml aliquot of the diluted reacted solution in a titration flask. Five ml starch solution and 10 ml 1.0 N HCl was added to the solution which was immediately titrated to a colour of purple with  $\text{KIO}_3$  to prevent the loss of  $\text{H}_2\text{S}$  upon addition of HCl. Acidity was checked by pH paper and more 1.0 N HCl solution was added if necessary to ensure the pH value was between 2 and 5. A mixture of  $\text{CO}_2$  and  $\text{H}_2\text{S}$  gas was collected in the gas expansion bag (attached to the side arm of the flask), which was compressed every few seconds for one minute to facilitate the reabsorption and oxidation of the  $\text{H}_2\text{S}$  gas. The excess  $\text{KIO}_3$  was then back titrated with  $\text{Na}_2\text{S}_2\text{O}_3$  to a colourless

end point. Two check runs were conducted and the average value was used to determine the extent of  $\text{Na}_2\text{S}$  conversion.

To prepare for future experiment, the fritted cylinder of the dispersion tube was cleaned with dilute HCl solution after every run to remove the small amount of  $\text{NaHCO}_3$  crystals that formed on the pores in the course of reaction, which would otherwise build up to the extent of completely blocking the gas flow.

It was designed to study one variable at a time, i.e. changing only one variable while keeping the others constant. The extent of conversion at different period of time for four different temperatures,  $25^\circ\text{C}$ ,  $35^\circ\text{C}$ ,  $45^\circ\text{C}$  and  $55^\circ\text{C}$ , with a flow of 129 ml/min pure  $\text{CO}_2$  at atmospheric pressure were measured. Another four higher flow rates, 155, 265, 397 and 495 ml/min of pure  $\text{CO}_2$  at  $35^\circ\text{C}$  and atmospheric pressure were studied.

Three series of lower  $\text{CO}_2$  partial pressure experiments at  $35^\circ\text{C}$ , atmospheric pressure and a flow rate of about 370 ml/min were studied. Nitrogen was used as the inert mixing agent.

For pressurized systems, the experimental set up was the same as before except that the sodium nitroprusside and silver nitrate bottle were replaced by a pressure gauge and a Matheson corrosion resistant low pressure gas regulator (model 3332), figure 3.3, which was closed at the start of experiment in order to build up the pressure and

was not partially opened until the desired pressure was reached. Due to equipment constraint, two higher pressures of only 129 kPa (4 PSIG) and 163 kPa (9 PSIG) were studied. The flow meter setting which corresponded to a flow rate of 397 ml/min at room temperature and atmospheric pressure was used. The actual volumetric flow rates, however, were reduced according to Boyle's law since a mass flow controller was employed. Therefore, the flow rates for the series of 129 and 163 kPa experiments were, respectively, 311 and 246 ml/min. It was noticed that it took the reaction system about 2 minutes to reach 129 kPa, and 4 minutes to 163 kPa.

#### 3.3.3.4 Estimation of interfacial area

Since  $H_2S$  desorption rates measured in the experiments are the products of interfacial areas and a number of other kinetic parameters, it is therefore necessary to estimate the interfacial areas in order to evaluate the rate constants.

##### (i) Bubble size distribution and retention time

With the knowledge of gas flow rate, interfacial area can be determined if average retention time and bubble size distribution are known.

High speed motion picture camera, HYCAM II model 41-0014 which are capable of taking thousands of frames per second, was used to shoot the reaction vessel in hope of estimating bubble size distribution and average retention

time.

The attempt of taking the whole picture of the reaction bottle in order to count the total number of bubbles and trace individual bubble's path in liquid was unsuccessful due to poor resolution of the numerous fine bubbles of the system (majority of the bubbles are less than 1 mm in diameter). Therefore, close up shots of larger magnification at a speed of two hundred frames per second were taken for a small section of the reaction bottle.

The film was analyzed with the use of a high speed movie projector. The speed at which a bubble travels could be determined by measuring the displacement of the bubble for a certain number of frames. Bubble retention time, however, could not be measured with any degree of certainty, since bubbles had sideways and circular motions due to strong turbulence but the pictures of the reaction system only covered a small section of the reaction bottle.

Photographs of the projection image on screen were taken using ordinary camera in order to obtain prints, since prints could not be produced directly from movie films.

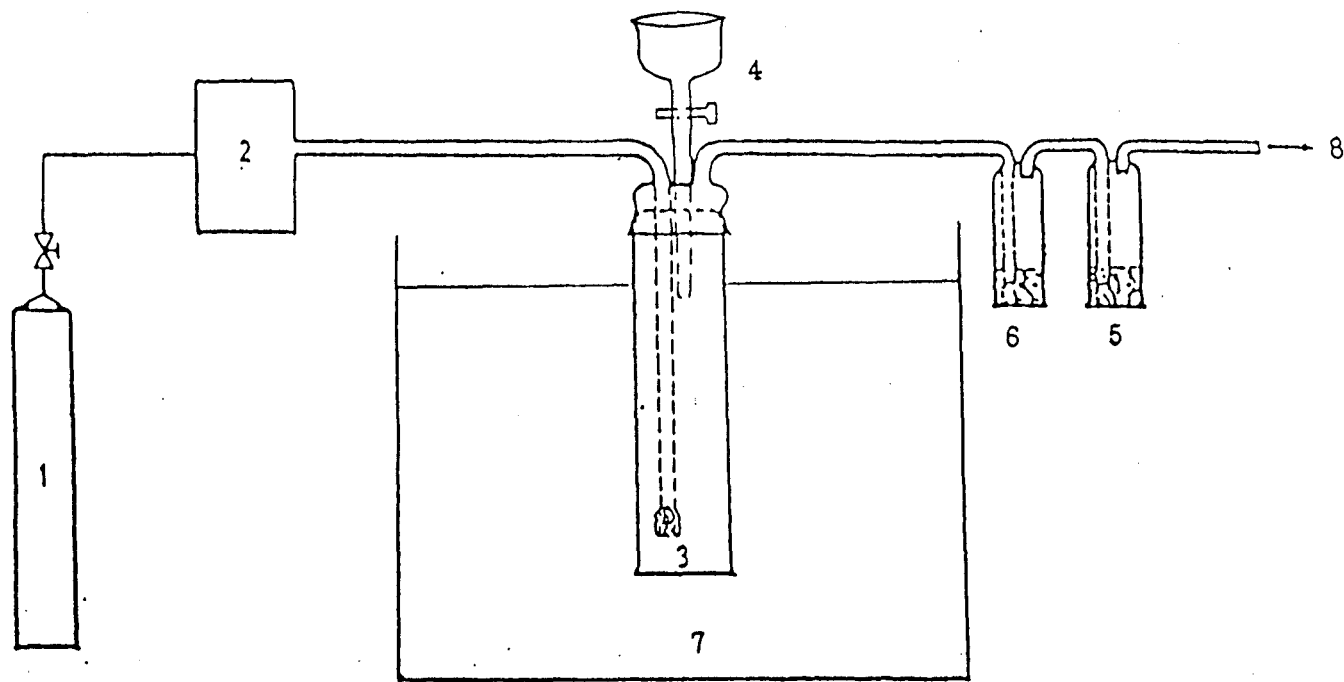
The bubble size distribution of each experimental  $\text{CO}_2$  gas flow rates was estimated by measuring and counting distinguishable in focus bubbles on several corresponding photographs.

(ii) gas hold-up volume

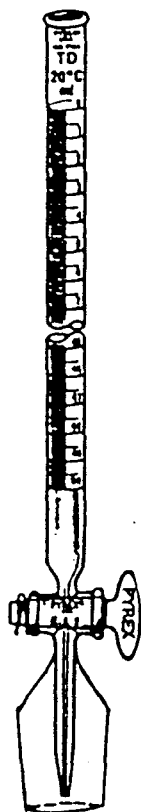
Due to the fact that the retention time of bubbles could not be determined using photographic method, it is therefore necessary to measure gas hold-up volumes in order to evaluate interfacial areas.

Experiments of different flow rates were conducted and the liquid line at different time was marked on the side of the reaction bottle. Water was later added from a burette to the solution, after bubbling was stopped, to bring the liquid line to the marks. The amounts of water added were the estimates of gas hold up volumes, from which, with the knowledge of bubble size distributions, interfacial areas can be evaluated.

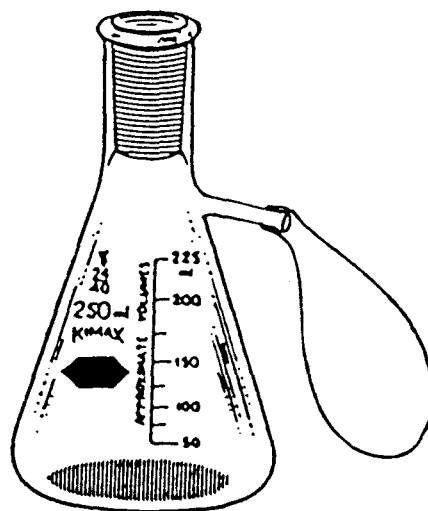
Fig. 3.1 Experimental set-up for  $H_2S$  generation.



- |                          |                                   |
|--------------------------|-----------------------------------|
| 1 - $CO_2$ cylinder      | 5 - Sodium nitroprusside solution |
| 2 - Mass flow controller | 6 - $AgNO_3$ solution             |
| 3 - Reaction bottle      | 7 - Water bath                    |
| 4 - Addition funnel      | 8 - Fumehood exhaust              |



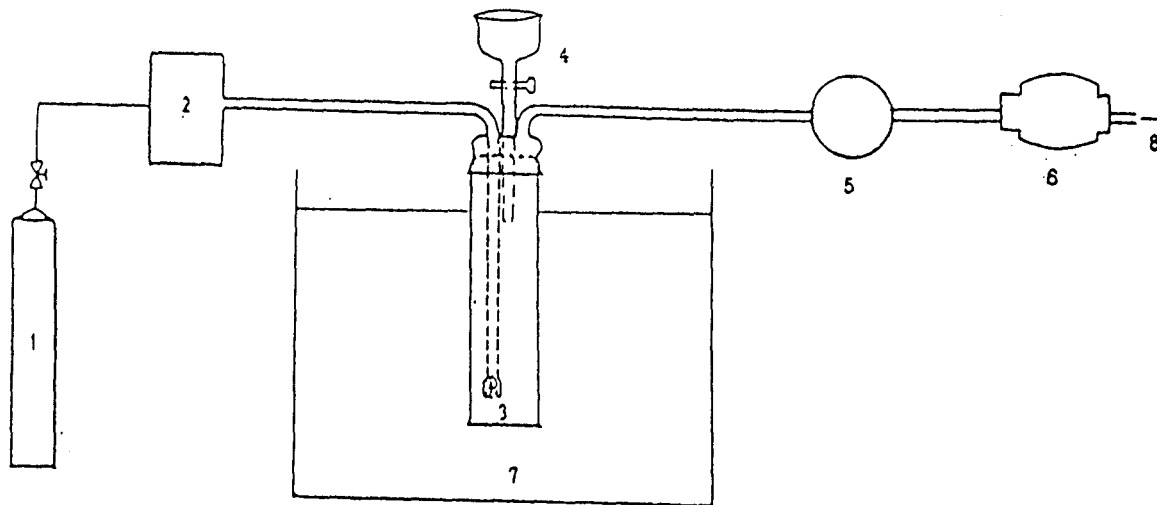
(a)



(b)

Figure 3.2 (a) Titration burette, with inner  $\frac{3}{4}$ " joint at the tip  
(b) Titration flask, with matching joint and gas bag on side arm.

Fig. 3.3 Experimental set-up for pressurised H<sub>2</sub>S generation.



- 1 - CO<sub>2</sub> cylinder
- 2 - Mass flow controller
- 3 - Reaction bottle
- 4 - Addition funnel

- 5 - Pressure gauge
- 6 - Gas regulator
- 7 - Water bath
- 8 - Fumehood exhaust

## CHAPTER 4

### Results

#### 4.1 Summary

The overall rate of conversion of aqueous  $\text{Na}_2\text{S}$  to  $\text{H}_2\text{S}$  by  $\text{CO}_2$  bubbling was found to be strongly dependent on  $\text{CO}_2$  partial pressure and flow rate, but fairly insensitive to reaction temperature. It was also shown that pressurising the reaction system is kinetically advantageous.

The conversion kinetics improve with  $\text{CO}_2$  flow rate and eighty percent conversion can be achieved in less than forty-five minutes even with a rather low flow rate of 155 ml/min at atmospheric pressure.

The bubble size distributions of the five pre-determined flow rates were estimated and interfacial areas determined. The surface areas range from 1.9 to 5.7  $\text{cm}^2/\text{cm}^3$  of solution, from the lowest to highest flow rate. However, deviations in interfacial area among photographs of systems under supposedly the same conditions are in some cases relatively large as compared with that due to variation in  $\text{CO}_2$  flow rates.

#### 4.2 Calibration of mass flow meter

The actual gas flow rate at different mass flow controller settings were determined as described in 3.3.2.

Table 4.1 is a list of the results, which were used to plot the calibration curves in figure 4.1.

To minimize uncertainty, the flow settings used in H<sub>2</sub>S generation experiments were those points measured for the preparation of the calibration curves.

Table 4.2 is a summary of the gas flow volume and composition for the set of various CO<sub>2</sub> partial pressure experiments described in 3.3.3.3.

CO <sub>2</sub> transducer		N <sub>2</sub> transducer	
Flow setting (% of full capacity)	actual flow rate (ml/min)	Flow setting (% of full capacity)	actual flow rate (ml/min)
5.0	45	3.3	105
8.8	129	6.7	218
10.0	155	10.0	326
15.0	265	13.3	433
20.0	397		
25.0	495		

Table 4.1 Actual flow rate of mass flow controller, at room temperature and atmospheric pressure.

(full capacity : CO<sub>2</sub> transducer 2 SLPM  
N<sub>2</sub> transducer 3 SLPM )

CO <sub>2</sub> partial pressure(atm)	CO <sub>2</sub> flow rate (ml/min)	N <sub>2</sub> flow rate (ml/min)	total flow rate(ml/min)
0.121	45	326	371
0.417	155	218	373
0.716	265	105	370
1.000	397	0	397

Table 4.2 Volume and composition of the gas flows of the N<sub>2</sub>-CO<sub>2</sub> mixtures.

### 4.3 Temperature dependence of Na<sub>2</sub>S conversion rate

The residual sulfide concentration after different reaction time of experiments conducted at different reaction temperatures are listed in table 4.3. These values were used to computed the percent conversion of Na<sub>2</sub>S to H<sub>2</sub>S, which are listed in table 4.4 and used to plot the percent conversion verses time curves in figure 4.2.

The effect of temperature on the overall conversion rate of Na<sub>2</sub>S to H<sub>2</sub>S is small, as indicated by figure 4.2.

Time(min)	Temperature			
	25°C	35°C	45°C	55°C
0	0.442	0.442	0.442	0.442
15	0.354	0.361	0.364	0.371
30	0.178	0.195	0.210	0.221
45	0.093	0.115	0.129	0.143
60	0.051	0.061	0.073	0.089
90	0.015	0.020	0.027	0.040
120	0.010	0.011	0.015	0.019
180	0.008	0.008	0.008	0.009

Table 4.3 Residual sulfide concentration (M), as functions of temperature and reaction time. (CO<sub>2</sub> flow rate 129 ml/min; 0.600F [NaHCO<sub>3</sub>]<sub>0</sub>; NaHCO<sub>3</sub> prebubbled for 10 min)

Time(min)	Temperature			
	25°C	35°C	45°C	55°C
15	19.8	18.4	17.7	16.0
30	59.8	55.8	52.4	50.0
45	78.9	74.0	70.8	67.7
60	88.5	86.3	83.5	79.8
90	96.5	95.4	93.9	90.9
120	97.8	97.4	96.7	95.6
180	98.2	98.2	98.1	97.9

Table 4.4 Percent conversion of  $\text{Na}_2\text{S}$  to  $\text{H}_2\text{S}$ , as functions of temperature and reaction time. ( $\text{CO}_2$  flow rate 129 ml/min; 0.600F  $[\text{NaHCO}_3]_0$ ;  $\text{NaHCO}_3$  prebubbled for 10 min)

#### 4.4 The dependence of Na<sub>2</sub>S Conversion on CO<sub>2</sub> flow rate

Table 4.5 is a list of residual sulfide concentrations after different reaction times in experiments with various CO<sub>2</sub> flow rates. The corresponding percent conversions are listed in table 4.6 and are used to plot the curves of percent conversion verses reaction time for different CO<sub>2</sub> flow rates in figure 4.3.

Time(min)	CO <sub>2</sub> flow rate (ml/min)				
	129	155	265	397	495
0	0.442	0.405	0.405	0.418	0.418
5	/	/	/	0.374	0.328
6	/	/	0.388	/	/
10	/	0.388	0.293	0.231	0.178
15	0.361	0.306	0.203	0.134	0.086
30	0.195	0.156	0.065	0.030	0.015
45	0.115	0.074	0.022	0.012	0.006
60	0.061	0.039	0.010	0.006	0.006
90	0.020	0.013	/	/	/

Table 4.5 Residual sulfide concentration (M) after pre-determined reaction time, with various CO<sub>2</sub> flow rates. (At 35°C; 0.600F [NaHCO<sub>3</sub>]<sub>0</sub> ; NaHCO<sub>3</sub> prebubbled for 10 min)

Time(min)	CO <sub>2</sub> flow rate (ml/min)				
	129	155	265	397	495
5	/	/	/	10.6	21.5
6	/	/	4.3	/	/
10	/	4.3	27.7	44.8	57.4
15	18.4	24.4	50.0	67.9	79.4
30	55.8	61.5	83.9	92.9	96.3
45	74.0	81.8	94.5	97.2	98.6
60	86.3	90.3	97.6	98.5	98.6
90	95.4	96.9	/	/	/

Table 4.6 Percent conversion of Na<sub>2</sub>S, in experiments with various flow rates. (At 35°C; 0.600F [NaHCO<sub>3</sub>]<sub>0</sub>; NaHCO<sub>3</sub> prebubbled for 10 min)

Figure 4.3 shows a strong dependence of Na<sub>2</sub>S conversion rate on the inlet CO<sub>2</sub> gas flow rate. Since the gas-liquid interfacial area is proportional, though not linearly as shown later in the chapter, to the gas flow rate, hence figure 4.3 indirectly indicates a strong dependence of reaction rate on interfacial area, which is a common phenomenon of any heterogeneous reactions. The rate controlling step of the overall Na<sub>2</sub>S conversion reaction is therefore likely to be a heterogeneous reaction.

#### 4.5 The dependence of Na<sub>2</sub>S Conversion on partial pressure of CO<sub>2</sub>

The results of the three series of experiments with lower CO<sub>2</sub> partial pressures, together with that of "pure" CO<sub>2</sub> for comparison, are listed in tables 4.7 and 4.8. The numbers in brackets are the pH values of the reaction

Time (min)	CO <sub>2</sub> partial pressure (atm)			
	0.121	0.417	0.716	1.00
0	0.428(/)	0.436(/)	0.436(/)	0.418(/)
5	0.421(10.10)	0.420(9.31)	0.413(8.90)	0.374(/)
10	0.416(9.85)	0.398(8.82)	0.326(8.41)	0.231(8.32)
15	0.412(9.57)	0.339(8.70)	0.234(8.41)	0.134(8.33)
30	0.381(9.22)	0.183(8.63)	0.070(8.43)	0.030(/)
45	0.335(9.13)	0.085(8.63)	0.021(8.43)	0.012(8.30)
60	0.273(9.10)	0.038(8.61)	0.010(8.45)	0.006(/)
90	0.174(9.11)	0.014(8.60)	/	/
120	0.104(9.10)	/	/	/
180	0.037(9.10)	/	/	/

Table 4.7 Residual sulfide concentration (M) and pH value of solution, as functions of inlet gas CO<sub>2</sub> partial pressure and reaction time. (At 35°C; CO<sub>2</sub> flow rate between 370-397ml/min; 0.600F [NaHCO<sub>3</sub>]<sub>0</sub>; NaHCO<sub>3</sub> prebubbled for 10 min)

solutions. The measured pH value of a 0.418F  $\text{Na}_2\text{S}$  ("F" is formality, a concentration unit expressed in number of formal per liter of solvent) and 0.600F  $\text{NaHCO}_3$  solution at time  $t = 0$  (i.e. right after mixing) and  $25^\circ\text{C}$ , and without prebubbling of the  $\text{NaHCO}_3$  solution, is 10.65. The percent conversion curves are plotted in figure 4.4 .

Time(min)	$\text{CO}_2$ partial pressure (atm)			
	0.121	0.417	0.716	1.000
5	1.8	3.7	5.3	10.6
10	2.8	8.7	25.2	44.8
15	3.8	22.3	46.3	67.9
30	11.0	58.0	83.9	92.9
45	21.7	80.6	95.2	97.2
60	36.3	91.2	97.8	98.5
90	59.4	96.8	/	/
120	75.7	/	/	/
180	91.4	/	/	/

Table 4.8 Percent conversion of  $\text{Na}_2\text{S}$  to  $\text{H}_2\text{S}$  after various reaction time, as functions of inlet gas  $\text{CO}_2$  partial pressure. (At  $35^\circ\text{C}$ ;  $\text{CO}_2$  flow rate between 370-397ml/min; 0.600F  $[\text{NaHCO}_3]_0$ ;  $\text{NaHCO}_3$  prebubbled for 10 min)

#### 4.6 Pressurized experiments

The same flow meter setting which corresponded to the CO<sub>2</sub> flow rate of 397 ml/min of the atmospheric system was used in the pressurized experiments. The actual volumetric flow rate, however, was reduced according to Boyle's law since a mass flow controller was employed. Therefore, the flow rates for the two series of 129 kPa (4 PSIG) and 163 kPa (9PSIG) pressurized experiments were 311 and 246 ml/min, respectively.

The results of the pressurized experiments are listed in table 4.9 and 4.10, together with that of the atmospheric system for comparison. The numbers in brackets are pH values. Percent conversion verses time curves are shown in figure 4.5 .

Time (min)	Gaseous pressure		
	atmospheric	4 PSIG	9 PSIG
0	0.418(/)	0.435(/)	0.435(/)
5	0.374(/)	0.373(8.34)	/
10	0.231(8.32)	0.239(8.30)	0.239(8.27)
15	0.134(8.33)	0.148(8.23)	0.153(8.25)
30	0.030(/)	0.030(8.27)	0.031(8.27)
45	0.012(8.30)	0.007(8.25)	0.007(8.27)
60	0.006(/)	0.003(8.25)	0.003(8.27)

Table 4.9 Residual sulfide concentration (M) and pH value of solution, as functions of gaseous pressure and reaction time. (At 35°C; 0.600F [NaHCO<sub>3</sub>]<sub>0</sub>; NaHCO<sub>3</sub> prebubbled for 10 min)

Time (min)	Gaseous pressure		
	atmospheric	4 PSIG	9 PSIG
5	10.6	14.3	/
10	44.8	45.0	45.1
15	67.9	65.9	64.9
30	92.9	93.0	92.8
45	97.2	98.3	98.4
60	98.5	99.3	99.4

Table 4.10 Percent conversion of  $\text{Na}_2\text{S}$  to  $\text{H}_2\text{S}$ , as functions of gaseous pressure and reaction time. (At  $35^\circ\text{C}$ ;  $0.600\text{F}$   $[\text{NaHCO}_3]_0$ ;  $\text{NaHCO}_3$  prebubbled for 10 min)

#### 4.7 Evaluation of interfacial area

The gas hold-up volumes and bubble size distributions for the gas flow rates used in experiments were determined in order to estimate the interfacial areas.

##### 4.7.1 Gas hold-up volume

Table 4.11 is a list of gas hold-up volumes (ml) at various reaction time of experiments with the pre-determined flow rates, whereas table 4.12 shows the corresponding ratios of gas hold-up to total volume (i.e. gas vol. / gas vol. + soln. vol.). Gas hold-up volume is an indication of the gas retention time (the quotient of gas hold-up volume divided by gas flow rate) in solution, which among other things like bubble size distribution affects the total gas-liquid interfacial area.

It was visually observed that there are two distinctive reaction periods as far as bubbling and turbulence are concerned. The first period (extensive CO<sub>2</sub> absorption period) at the beginning of reaction is characterized by the appearance of fewer bubbles and less turbulence, which gradually increases in gas hold-up volume until it fully takes off to the second reaction period (H<sub>2</sub>S generation period) marked by the vast number of bubbles and strong turbulence. The second period has a steady gas hold-up volume at first and shows a small decrease towards the end of reaction. As reflected in tables 4.11 and 4.12, the larger the CO<sub>2</sub> flow rate, the sooner the system converts

from the first period to the second reaction period.

Time (min)	CO <sub>2</sub> flow rate (ml/min)				
	129	155	265	397	495
5	0.60	1.18	4.71	9.28	12.46
10	1.52	2.51	7.84	10.06	12.46
15	3.80	5.34	7.84	10.06	12.46
20	4.49	5.34	7.84	9.47	11.89
30	4.49	4.84	7.33	9.47	11.89
60	4.02	/	/	/	/

Table 4.11 Gas hold-up volume (ml), as functions of CO<sub>2</sub> flow rate and reaction time.

Time (min)	CO <sub>2</sub> flow rate (ml/min)				
	129	155	265	397	495
5	$3.98 \times 10^{-3}$	$7.81 \times 10^{-3}$	$3.04 \times 10^{-2}$	$5.83 \times 10^{-2}$	$7.67 \times 10^{-2}$
10	$1.00 \times 10^{-2}$	$1.65 \times 10^{-2}$	$4.97 \times 10^{-2}$	$6.29 \times 10^{-2}$	$7.67 \times 10^{-2}$
15	$2.47 \times 10^{-2}$	$3.44 \times 10^{-2}$	$4.97 \times 10^{-2}$	$6.29 \times 10^{-2}$	$7.67 \times 10^{-2}$
20	$2.91 \times 10^{-2}$	$3.44 \times 10^{-2}$	$4.97 \times 10^{-2}$	$5.94 \times 10^{-2}$	$7.34 \times 10^{-2}$
30	$2.91 \times 10^{-2}$	$3.13 \times 10^{-2}$	$4.66 \times 10^{-2}$	$5.94 \times 10^{-2}$	$7.34 \times 10^{-2}$
60	$2.61 \times 10^{-2}$	/	/	/	/

Table 4.12 Ratio of gas hold-up to total volume, as functions of CO<sub>2</sub> flow rate and reaction time.

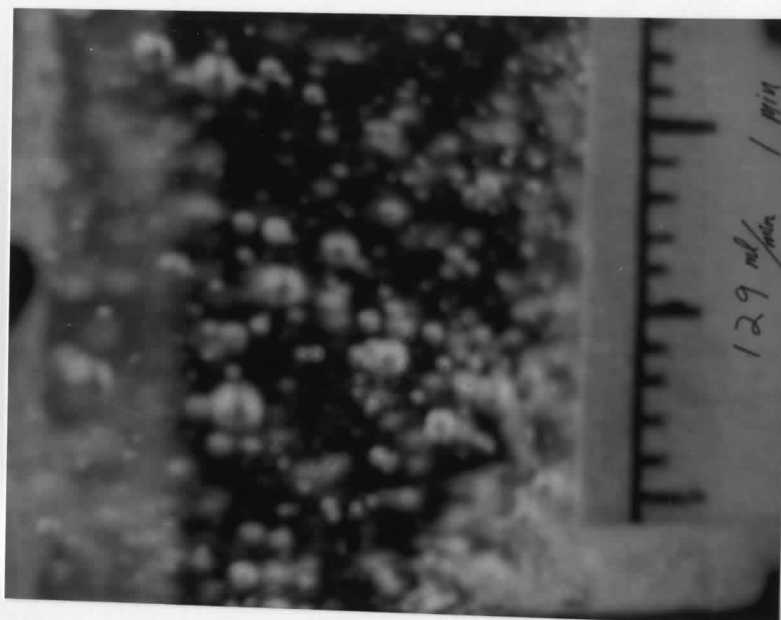
For the experimental procedures employed, as described on page 62, the size of errors associated with the determined values of gas hold-up volume in table 4.11 must be less than 0.20 ml regardless of CO<sub>2</sub> flow rate.

#### 4.7.2 Bubble size distribution and interfacial area

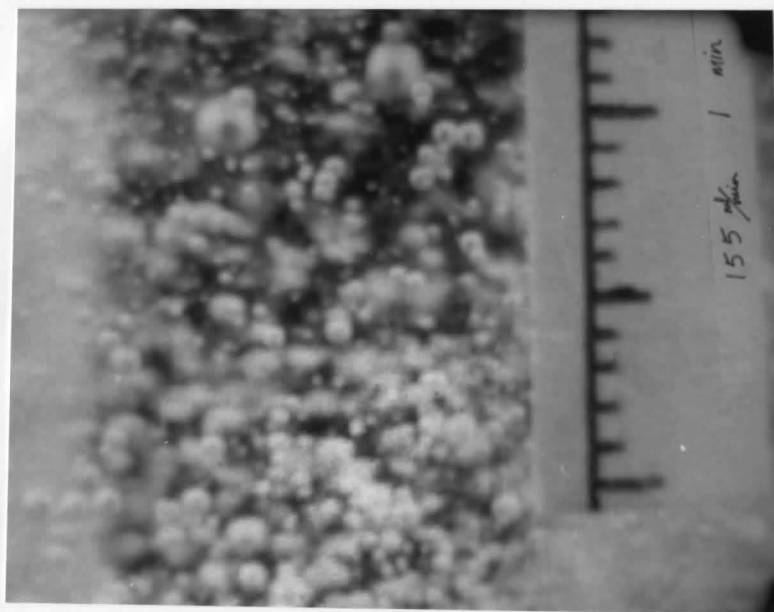
Figure 4.6(a)-(e) are photographs of the two phase system with different flow rates at one minute reaction time (i.e. at first reaction period). The scales on the right hand side of all photographs of bubbles are one centimeter (between the two longest bars, with 10 supposedly equivalent partitions).

Figure 4.7 is the photograph of gas bubbles with  $\text{CO}_2$  flow rate of 155 ml/min at the second reaction period (15 minutes reaction time). This shows a huge amount of indistinguishable bubbles. The appearance of bubbling system at the second reaction period for the other flow rates are similar.

The bubbling of  $\text{CO}_2$  in distilled water is shown in figure 4.8, which shows remarkably larger bubbles than that in reaction solution. The appearance of finer bubbles in reaction solution is because of the lower surface tension of the solution than pure water, due to the disruption of the extensive hydrogen bonding among water molecules upon dissolution of  $\text{Na}_2\text{S}$  and  $\text{NaHCO}_3$  solids.

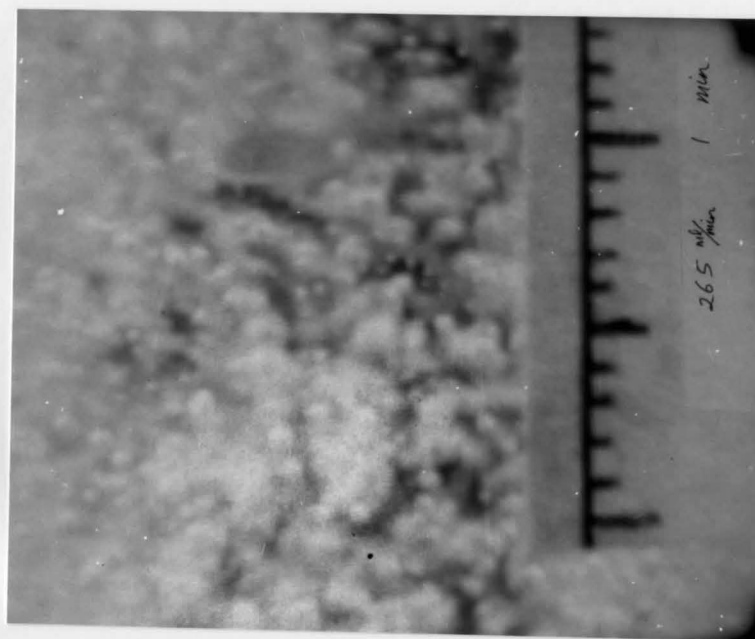


(a)

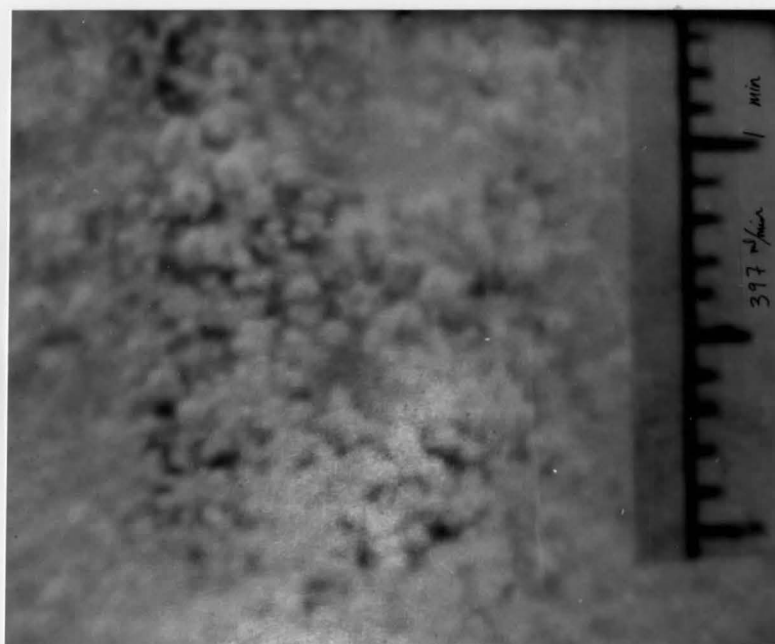


(b)

Fig. 4.6  $\text{CO}_2$  bubbling at 1 min. reaction time  
(a) 129 ml/min , (b) 155 ml/min



(c)



(d)

Fig. 4.6  $\text{CO}_2$  bubbling at 1 min. reaction time  
(c) 265 ml/min , (d) 397 ml/min

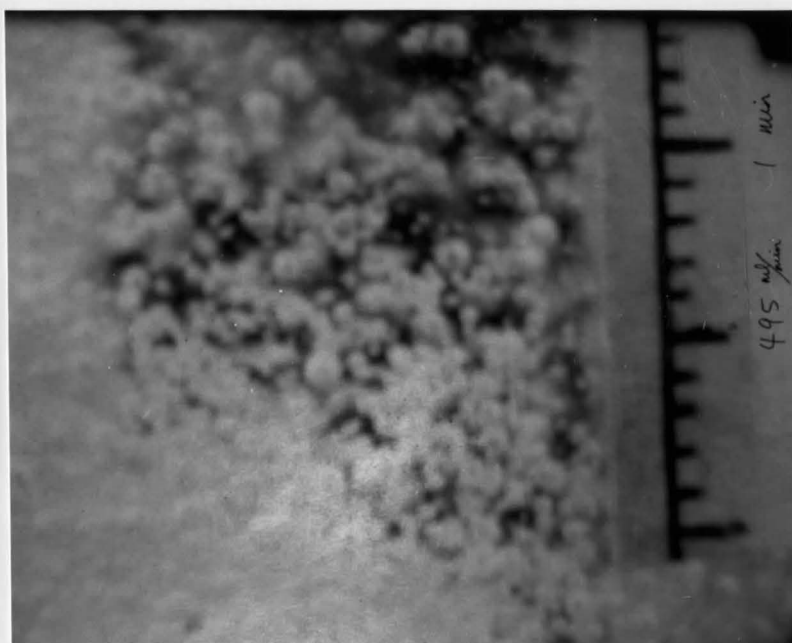


Fig. 4.6 CO<sub>2</sub> bubbling at 1 min. reaction time  
(e) 495 ml/min

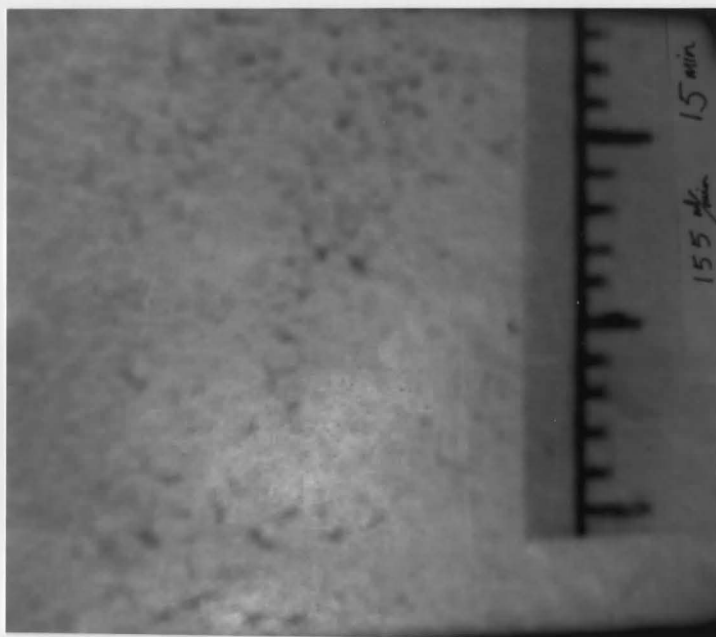


Fig. 4.7  $\text{CO}_2$  bubbling, at a flow rate of 155 ml/min, at the second reaction period (15 min).

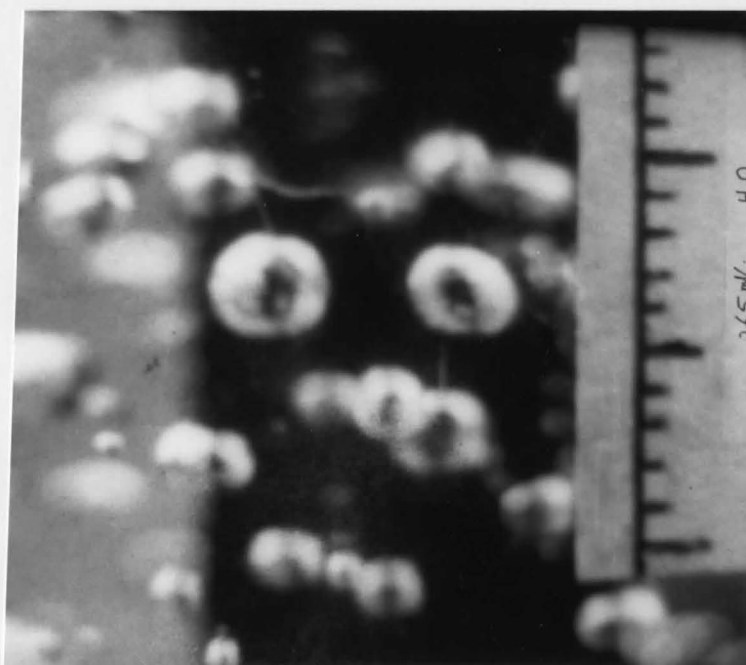


Fig. 4.8  $\text{CO}_2$  bubbling in distilled water, at a flow rate of 265 ml/min.

Bubble size distribution of each pre-determined CO<sub>2</sub> flow rates was estimated by measuring and counting bubbles which are distinguishable and in focus on several corresponding photographs.

Due to the fact that photographs taken in the second reaction period (figure 4.7) are of very poor resolution, those of the first period were used to estimate bubble size distributions and interfacial areas. For the second reaction period it was estimated by assuming that the two reaction periods have similar bubble size distribution which differs only in total number of bubbles.

Table 4.13 lists the bubble size distributions of the five experimental flow rates. Interfacial areas per unit volume of solution were estimated by using the equation as follows,

$$A = \frac{\text{Gas hold up volume}}{\text{Total volume of bubbles measured}} \times \frac{\text{Total surface area of bubbles measured}}{\text{Volume of reaction solution}} \quad [4-1]$$

The steady gas hold up volumes of the second reaction period (table 4.11) were used in the calculations and the volume of reaction solution was 150 ml. Table 4.13 lists the estimated interfacial areas in the system with various CO<sub>2</sub> flow rates.

Number of bubbles with diameter(mm)	CO <sub>2</sub> flow rate (ml/min)				
	129	155	265	397	495
0.3	/	2	3	4	1
0.4	8	12	9	7	4
0.5	4	2	7	7	7
0.6	14	11	14	8	6
0.7	17	7	2	6	10
0.8	12	9	6	10	11
0.9	2	/	6	5	9
1.0	8	4	5	5	2
1.1	2	2	3	3	1
1.2	3	5	2	4	1
1.3	1	/	/	1	1
1.4	3	/	1	/	1
1.6	/	2	/	/	/
Number of bubbles counted	74	56	58	60	54
Total volume of bubbles (cm <sup>3</sup> )	0.023	0.018	0.015	0.017	0.015
Total surface area of bubbles (cm <sup>2</sup> )	1.5	1.1	1.0	1.1	1.0
Gas hold up(cm <sup>3</sup> )	4.49	5.34	7.84	10.06	12.46
Interfacial area (cm <sup>2</sup> /cm <sup>3</sup> of soln)	1.9	2.2	3.6	4.5	5.7

Table 4.13 Summary of bubble size distributions and interfacial areas in the system with various CO<sub>2</sub> flow rates.

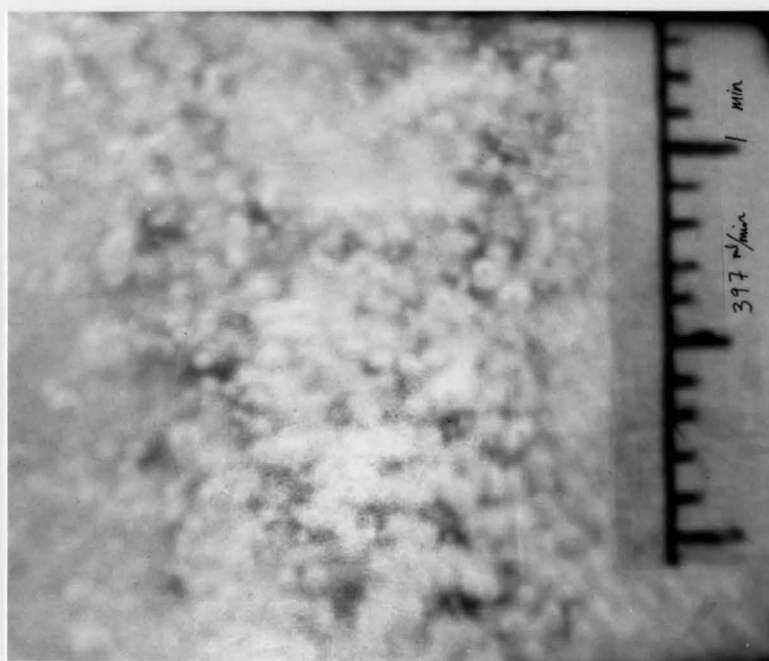
The variations of bubble size distribution and interfacial area among photographs of the systems under supposedly the same conditions are in some cases quite significant. The fluctuation is relatively large in comparison with that due to variation in CO<sub>2</sub> flow rates.

Figure 4.9 (a) and (b) , which are photographs of CO<sub>2</sub> bubbling at a rate of 397 ml/min at one minute reaction time, show the extreme case. It is the pair of photographs that gave the largest deviation in bubble size distribution with the same CO<sub>2</sub> flow rate.

Table 4.14 is a list of bubble size distribution and interfacial area of figure 4.9 (a) and (b). Equation [4-1] was used in the evaluation of interfacial areas. Notice that the upper deviation in interfacial area from the average value  $4.5 \text{ cm}^2/\text{cm}^3$  of soln., (table 4.13) is  $+1.6 \text{ cm}^2/\text{cm}^3$  of soln., (or 36% of average value), and that the lower deviation is  $-0.4 \text{ cm}^2/\text{cm}^3$  of soln., (or 9% of average value). Table 4.14 shows the extents of fluctuation in the system over time and space. It also suggests possible size of error in the determination of interfacial area with limited number of measurements.



(a)



(b)

Fig. 4.9 CO<sub>2</sub> bubbling at a rate of 397 ml/min at one minute reaction time.

Number of bubbles with diameter(mm)	Figure 4.9	
	(a)	(b)
0.3	2	/
0.4	1	4
0.5	/	5
0.6	1	5
0.7	2	2
0.8	3	1
0.9	1	/
1.0	2	1
1.1	1	/
1.2	3	/
Number of bubbles counted	16	18
Total volume of bubbles ( $\text{cm}^3$ )	0.0062	0.0022
Total surface area of bubbles ( $\text{cm}^2$ )	0.38	0.20
Gas hold up ( $\text{cm}^3$ )	10.06	10.06
Interfacial area ( $\text{cm}^2/\text{cm}^3$ of sol.)	4.1	6.1

Table 4.14 Variation in bubble size distribution and interfacial area of figure 4.9 (a & b).

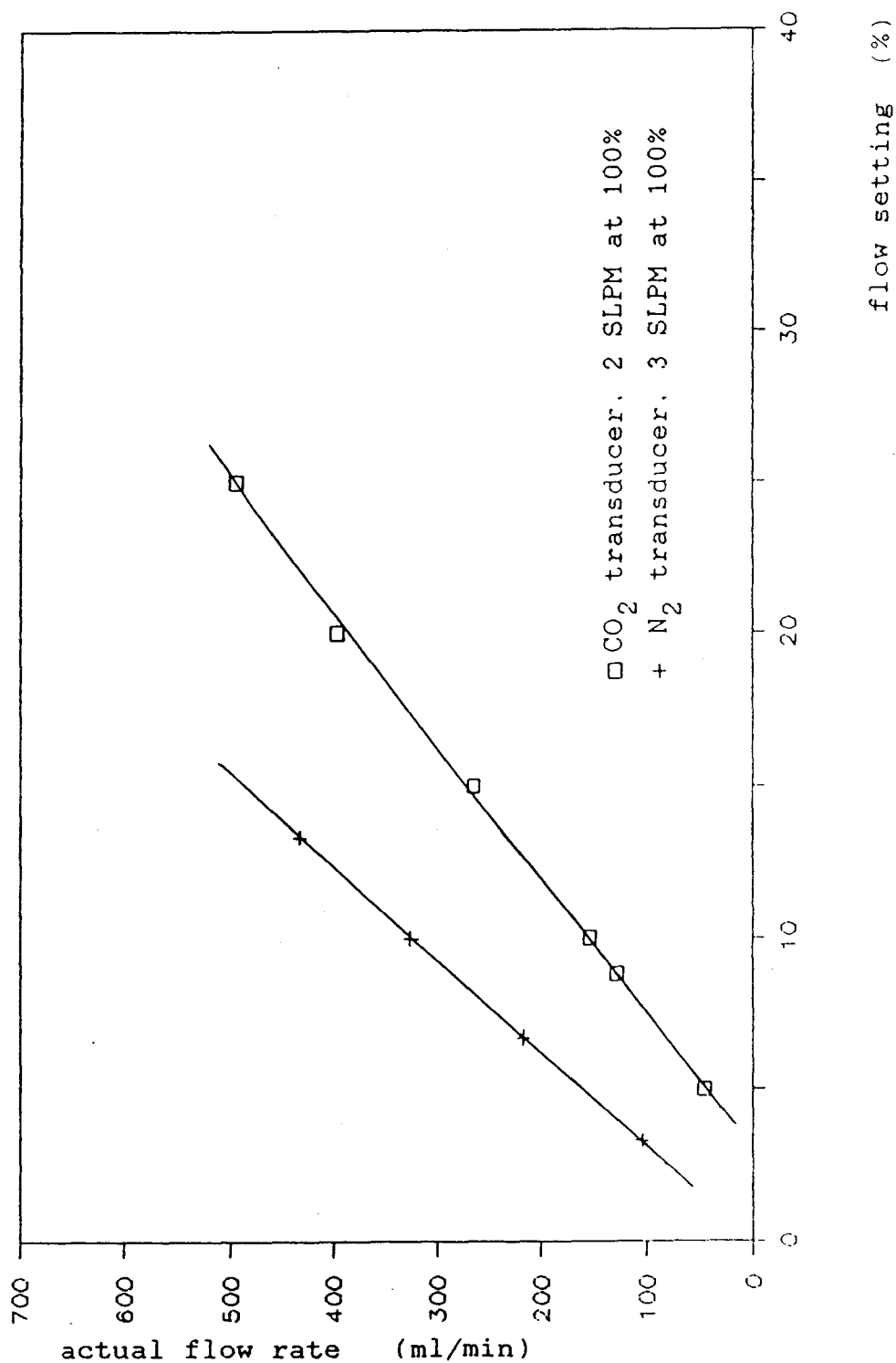


Fig. 4.1 Calibration curve of CO<sub>2</sub> and N<sub>2</sub> transducer of Mathesson mass flow controller.

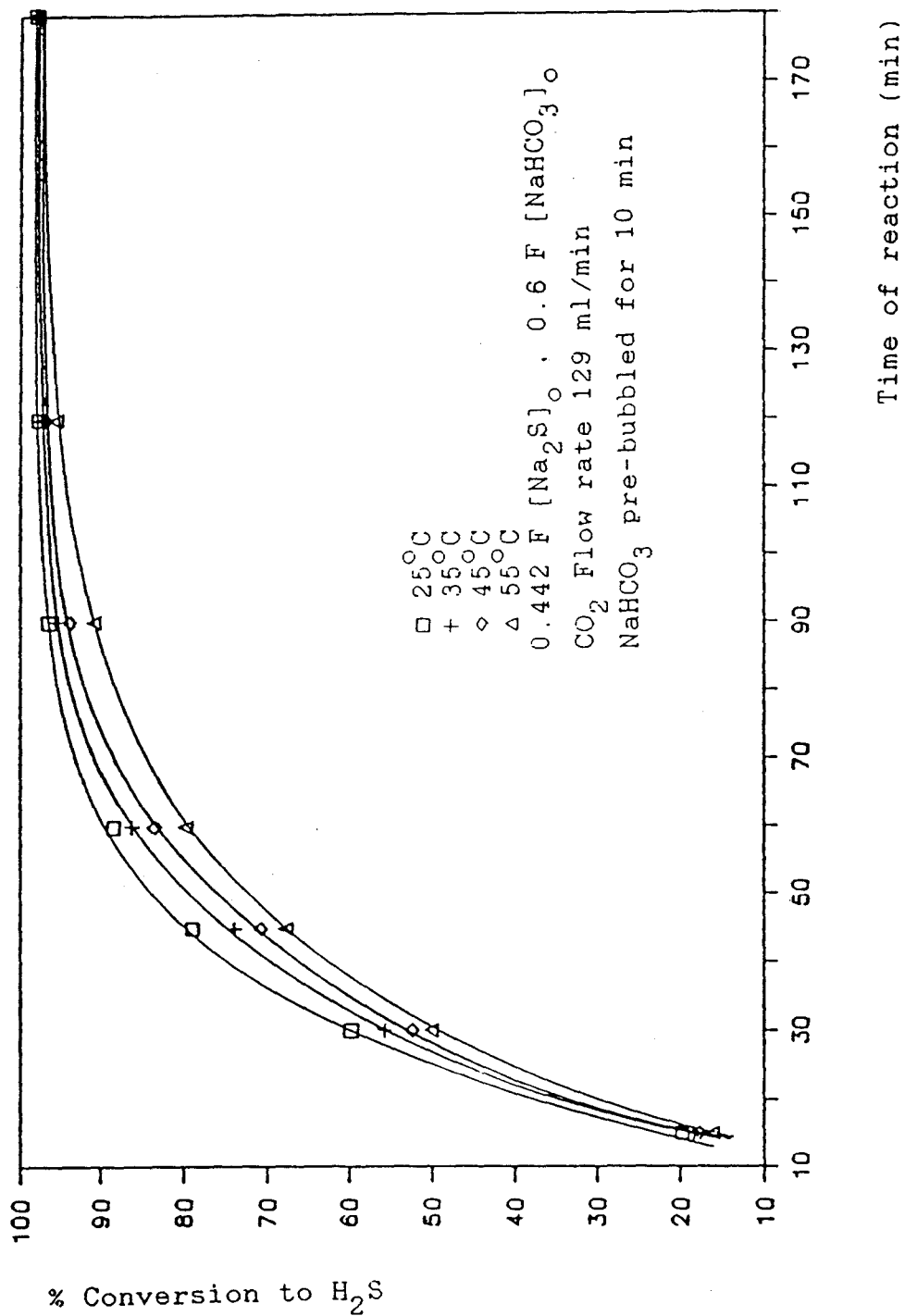


Fig. 4.2 Percent conversion of Na<sub>2</sub>S to H<sub>2</sub>S vs. reaction time at different temperatures.

Fig. 4.3 Percent conversion of  $\text{Na}_2\text{S}$  to  $\text{H}_2\text{S}$  vs. reaction time with different  $\text{CO}_2$  flow rates.

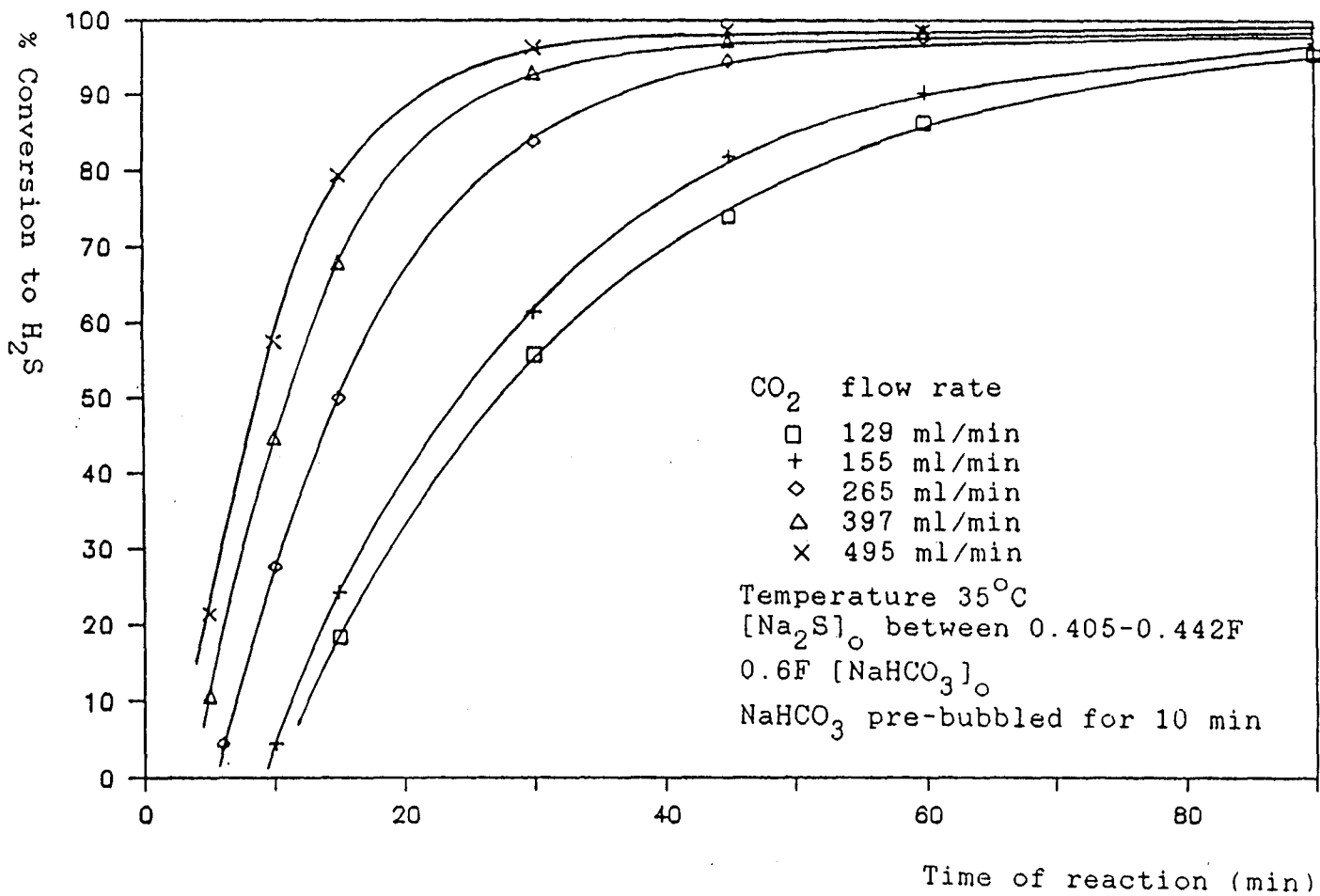


Fig. 4.4 Percent conversion of  $\text{Na}_2\text{S}$  to  $\text{H}_2\text{S}$  vs. reaction time at different  $\text{CO}_2$  partial pressures.

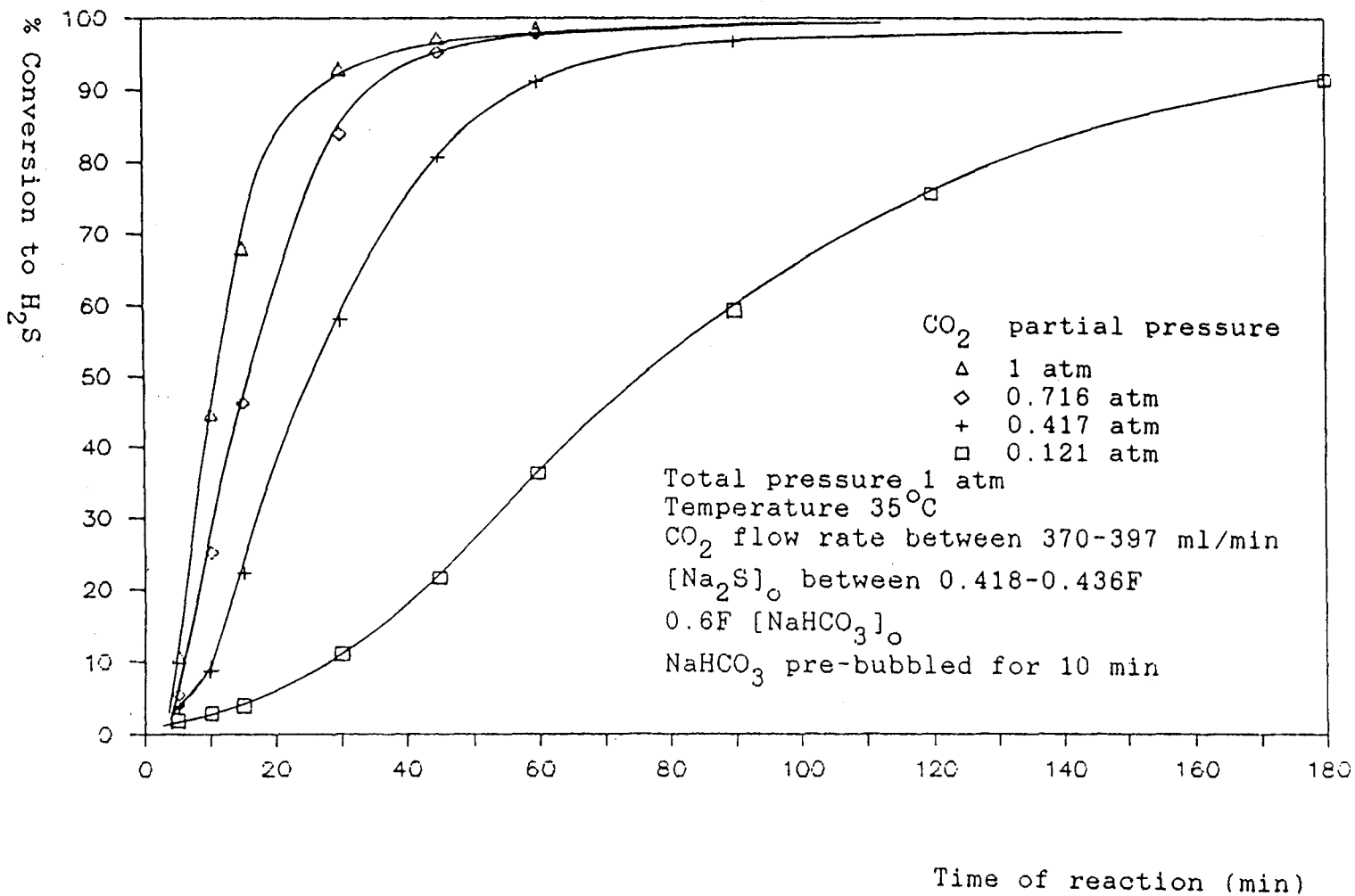
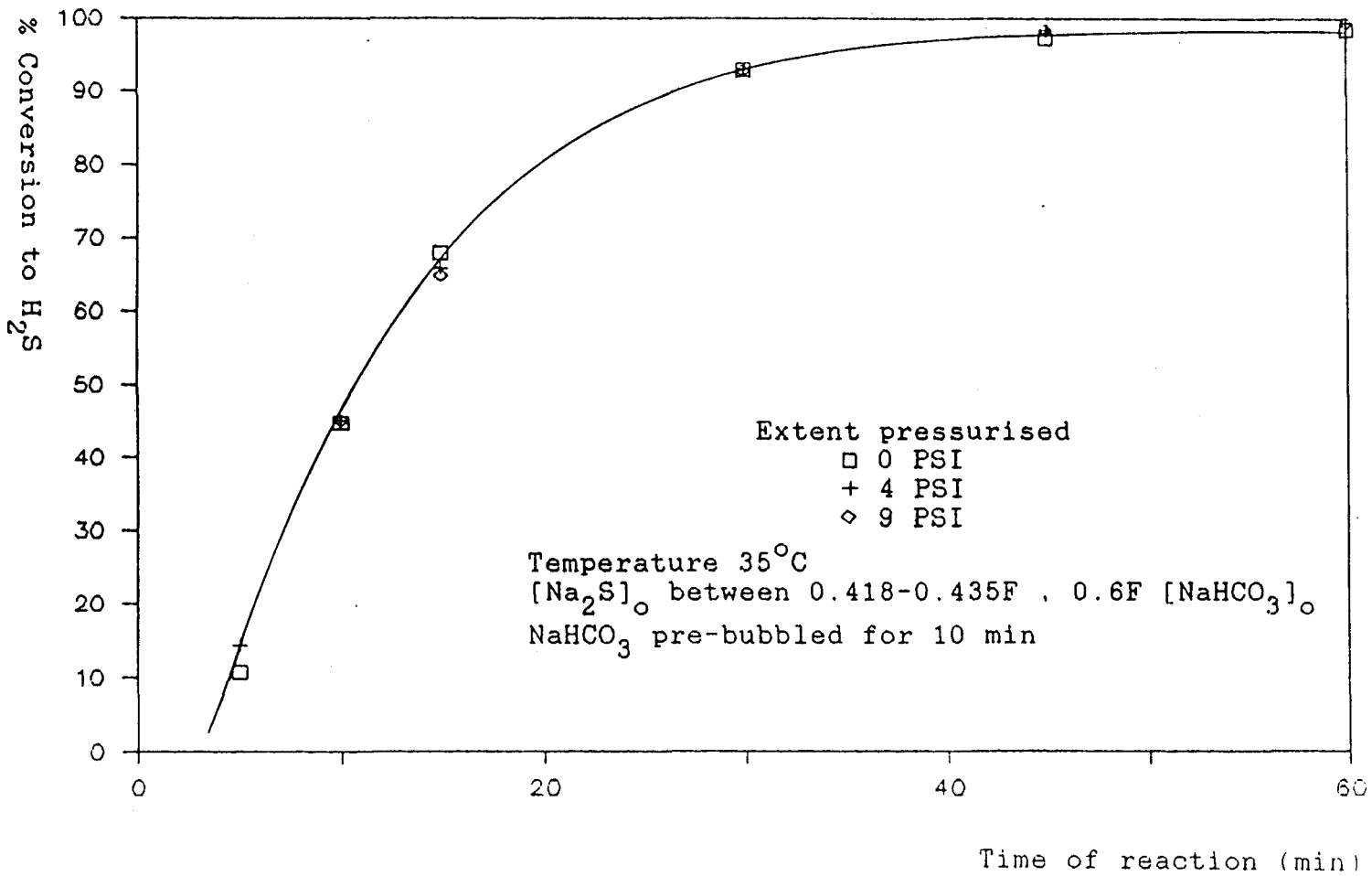


Fig. 4.5 Percent conversion of  $\text{Na}_2\text{S}$  to  $\text{H}_2\text{S}$  vs. reaction time of pressurized systems.



## CHAPTER 5

### Calculations and Discussion

#### 5.1 Ionic composition of NaHCO<sub>3</sub>-Na<sub>2</sub>S solution

In order to study the reaction kinetics of the carbonation conversion of aqueous sodium sulfide to hydrogen sulfide, it is essential to determine the ionic composition ( $[H^+]$ ,  $[CO_3^{2-}]$ ,  $[HS^-]$ ,  $[S^{2-}]$  etc.) of the sodium sulfide-sodium bicarbonate solution before the commencement and during the course of reaction.

##### 5.1.1 At reaction time $t = 0$ , i.e. right before bubbling

Altogether there are seven unknowns, namely  $[HS^-]$ ,  $[S^{2-}]$ ,  $[HCO_3^-]$ ,  $[CO_3^{2-}]$ ,  $[H^+]$ ,  $[OH^-]$  and  $[Na^+]$ ; therefore seven equations are required.

The dissociation constants give three equations :

$$K_{a2}(H_2S) = \frac{[S^{2-}][H^+]}{[HS^-]} \quad [5-1]$$

$$K_{a2}(CO_2) = \frac{[H^+][CO_3^{2-}]}{[HCO_3^-]} \quad [5-2]$$

$$K_w = [H^+][OH^-] \quad [5-3]$$

where  $K_{a2}(H_2S)$  and  $K_{a2}(CO_2)$  are the second acid dissociation constants of hydrosulfuric and carbonic acid, respectively. At 25°C and infinite dilution,  $K_{a2}(H_2S) = 1.2$

$\times 10^{-15}$  and  $K_{a2}(\text{CO}_2) = 4.7 \times 10^{-11}$ (47). In equation [5-3],  $K_w$  is the dissociation constant of water and has a value of  $1.0 \times 10^{-14}$  at  $25^\circ\text{C}$ . All of the three chemical reactions described above are considered to be in equilibrium at all time since they involve only a transfer of proton which is much faster than other chemical and physical processes concerned here.

Another three equations can be written from material balance considerations :

$$[\text{Na}_2\text{S}]_0 = [\text{HS}^-] + [\text{S}^{2-}] \quad [5-4]$$

$$[\text{NaHCO}_3]_0 = [\text{HCO}_3^-] + [\text{CO}_3^{2-}] \quad [5-5]$$

$$[\text{Na}^+] = 2[\text{Na}_2\text{S}]_0 + [\text{NaHCO}_3]_0 \quad [5-6]$$

where  $[\text{Na}_2\text{S}]_0$  and  $[\text{NaHCO}_3]_0$  are, respectively, the initial formal concentrations of  $\text{Na}_2\text{S}$  and  $\text{NaHCO}_3$  of the reaction solution. The above material balance equations are written with the following two assumptions :

- (1) The concentrations of aqueous molecular  $\text{H}_2\text{S}$  and  $\text{CO}_2$  being negligible.
- (2) Complete ionization of aqueous  $\text{Na}_2\text{S}$ .

The first assumption clearly holds since both  $\text{Na}_2\text{S}$  and  $\text{NaHCO}_3$  are alkaline solutions, whereas the second assumption has yet to be justified.

Finally, the requirement of charge balance gives

the seventh equation :

$$[\text{Na}^+] + [\text{H}^+] = 2[\text{S}^{2-}] + 2[\text{CO}_3^{2-}] + [\text{HS}^-] + [\text{HCO}_3^-] + [\text{OH}^-] \quad [5-7]$$

Substitution of equations [5-4,5,6] into [5-7] leads to :

$$[\text{Na}_2\text{S}]_o = [\text{S}^{2-}] + [\text{CO}_3^{2-}] + [\text{OH}^-] - [\text{H}^+] \quad [5-8]$$

Combining equations [5-1] and [5-4] gives :

$$[\text{S}^{2-}] = \frac{[\text{Na}_2\text{S}]_o \cdot K_{a2}(\text{H}_2\text{S})}{K_{a2}(\text{H}_2\text{S}) + [\text{H}^+]} \quad [5-9]$$

Similarly,  $[\text{CO}_3^{2-}]$  can be expressed in terms of the second acid dissociation constant of carbonic acid, the formality of sodium bicarbonate and the  $\text{H}^+$  ion concentration :

$$[\text{CO}_3^{2-}] = \frac{[\text{NaHCO}_3]_o \cdot K_{a2}(\text{H}_2\text{CO}_3)}{K_{a2}(\text{H}_2\text{CO}_3) + [\text{H}^+]} \quad [5-10]$$

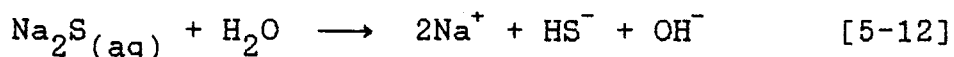
Finally putting equations [5-3,9,10] into [5-8] gives,

$$[\text{Na}_2\text{S}]_o = \frac{[\text{Na}_2\text{S}]_o \cdot K_{a2}(\text{H}_2\text{S})}{K_{a2}(\text{H}_2\text{S}) + [\text{H}^+]} + \frac{[\text{NaHCO}_3]_o \cdot K_{a2}(\text{H}_2\text{CO}_3)}{K_{a2}(\text{H}_2\text{CO}_3) + [\text{H}^+]} + \frac{K_w}{[\text{H}^+]} + [\text{H}^+] \quad [5-11]$$

For a solution of 0.418F  $\text{Na}_2\text{S}$  and 0.600F  $\text{NaHCO}_3$  at  $25^\circ\text{C}$ , the calculated concentration of  $\text{H}^+$  ion using equation [5-11] is  $2.055 \times 10^{-11}\text{M}$ , which corresponds to a pH value of 10.69. The experimentally measured pH value of such a solution is 10.65 (section 4.5), which is in exceptionally good agreement with the calculated value, and thus indirectly justifies the assumption of complete ionization of aqueous  $\text{Na}_2\text{S}$  of the reaction solution. The calculated concentrations of the other ionic species are :  $[\text{HS}^-] = 0.418\text{M}$ ;  $[\text{S}^{2-}] = 2.4 \times 10^{-5}\text{M}$ ;  $[\text{HCO}_3^-] = 0.183\text{M}$ ;  $[\text{CO}_3^{2-}] = 0.417\text{M}$  and  $[\text{Na}^+] = 1.436\text{M}$ . Hence, it is shown that the sulfur of the system initially mainly exists as  $\text{HS}^-$  ion and that the concentration of  $\text{S}^{2-}$  ion is negligible.

The complete ionization of  $\text{Na}_2\text{S}$  in  $\text{Na}_2\text{S}$ - $\text{NaHCO}_3$  solution can also be shown from thermodynamic calculations.

The hydrolysis of sodium sulfide is described by equation [5-12] :



The standard Gibbs free energy of formation,  $\Delta G_f^\circ$ , of  $\text{Na}_2\text{S}_{(\text{aq})}$ ,  $\text{H}_2\text{O}$ ,  $\text{Na}^+$ ,  $\text{HS}^-$  and  $\text{OH}^-$  are, respectively, -104.7, -56.7, -62.6, -6.6 and -37.6 Kcal/mol. (48,49) Thus, the standard Gibbs free energy change of reaction [5-12] is -8 Kcal/mol, which is related to the thermodynamic equilibrium constant according to

$$\Delta G^{\circ} = -RT \ln K \quad [5-13]$$

where R is the gas constant (1.987 cal/mol K), and T is the absolute temperature in degree Kelvin. At 25°C, the thermodynamic equilibrium constant  $K_{5-12}$  equals to  $7.4 \times 10^5$ .

If the activities of the chemical species of reaction [5-12] are approximated by the corresponding molar concentrations, then

$$K_{5-12} = \frac{[\text{Na}^+]^2 [\text{HS}^-] [\text{OH}^-]}{[\text{Na}_2\text{S}]} = \frac{(2x + 0.6)^2 (x) (4.47 \times 10^{-4})}{0.418 - x}$$

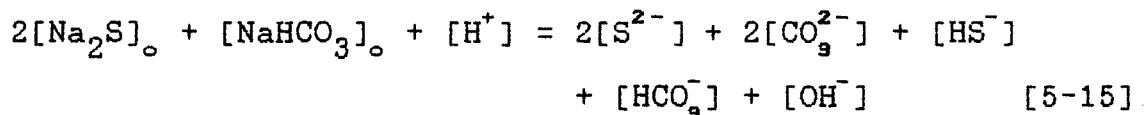
$$= 7.4 \times 10^5 \quad [5-14]$$

where 0.418F is the initial formal concentration of  $\text{Na}_2\text{S}$  and x is the amount of aqueous  $\text{Na}_2\text{S}$  ionized. The experimental pH value is 10.65 which corresponds to a hydroxide ion concentration of  $4.47 \times 10^{-4}\text{M}$ . The solution for x of equation [5-14] is 0.4179M;  $[\text{Na}_2\text{S}]$ ,  $[\text{HS}^-]$  and  $[\text{Na}^+]$  are  $5.2 \times 10^{-10}$ , 0.418 and 1.436M respectively.

Thus it is shown that the equilibrium concentration of aqueous sodium sulfide that remains undissociated in the solution is negligible.

### 5.1.2 During the course of reaction

Since sodium sulfide completely dissociates in the reaction solution, substitution of equation [5-6] to the charge balance equation [5-7] gives :



where  $[\text{Na}_2\text{S}]_0$  and  $[\text{NaHCO}_3]_0$  are the initial formal concentrations of sodium sulfide and sodium bicarbonate respectively.

Combining equations [5-2] and [5-15] gives :

$$[\text{CO}_3^{2-}] = \frac{2[\text{Na}_2\text{S}]_0 + [\text{NaHCO}_3]_0 + [\text{H}^+] - [\text{OH}^-] - [\text{HS}^-] - 2[\text{S}^{2-}]}{2 + ([\text{H}^+]/K_{a2}(\text{CO}_2))} \quad [5-16]$$

The concentration of  $\text{S}^{2-}$  ion is shown to be negligible at reaction time  $t = 0$ , and it remains so during the course of reaction since the pH value of the solution drops as reaction proceeds.

The first acid dissociation constant of  $\text{H}_2\text{S}$  :

$$K_{a1}(\text{H}_2\text{S}) = \frac{[\text{H}^+][\text{HS}^-]}{[\text{H}_2\text{S}]} \quad [5-17]$$

equals  $9.1 \times 10^{-8}$  at  $18^\circ\text{C}$  and infinite dilution.<sup>(48)</sup> The sodium sulfide residual concentration measured at the end of reaction is the total concentration of  $\text{HS}^-$  ion and aqueous  $\text{H}_2\text{S}$ . With the use of equation [5-17], therefore,  $[\text{HS}^-]$  and  $[\text{H}_2\text{S}]$  can be evaluated if the pH of the reaction solution is known. In which case, all the quantities on the right hand side of equation [5-16] are known, so the concentration of  $\text{CO}_3^{2-}$  ion, and hence  $[\text{HCO}_3^-]$ , can be

determined.

The reaction solution pH values of the various  $\text{CO}_2$  partial pressure experiments (0.716, 0.417 and 0.121atm at  $35^\circ\text{C}$ ) were measured and are listed in table 5.1, 5.2 and 5.3. The lowest pH value in the tables is about 8.3, which corresponds to a ratio of  $[\text{HS}^-]$  to  $[\text{H}_2\text{S}]$  of about twenty. In general, the higher pH value of the reaction solution, the higher  $[\text{HS}^-]$  to  $[\text{H}_2\text{S}]$  ratio.

The dissociation constant of water  $K_w$  equals  $2.09 \times 10^{-14}$  at  $35^\circ\text{C}$ .<sup>(48)</sup> The value of  $K_{a2}(\text{CO}_2)$  at  $35^\circ\text{C}$  is determined to be  $5.55 \times 10^{-11}$  using equation [2-59]. The value of  $K_{a1}(\text{H}_2\text{S})$  at  $18^\circ\text{C}$  ( $9.1 \times 10^{-8}$ ) is used as an estimate for that at  $35^\circ\text{C}$ , which does not appear to be in literature.

The concentrations of  $\text{HS}^-$  ion and aqueous  $\text{H}_2\text{S}$  for the various  $\text{CO}_2$  partial pressure experiments are listed in tables 5.1, 5.2 and 5.3, together with that of the other ionic species.

The concentration of sodium ion remains constant through out the course of reaction, and equals to the sum of the initial concentration of sodium bicarbonate and twice of that of sodium sulfide (equation [5-6]).

Time (min)	Sulfide remain(M)	pH	[H <sup>+</sup> ] (x10 <sup>-9</sup> M)	[HS <sup>-</sup> ] (M)
5	0.413	8.90	1.26	0.407
10	0.326	8.41	3.89	0.313
15	0.234	8.41	3.89	0.224
30	0.070	8.43	3.72	0.067
45	0.021	8.43	3.72	0.020
60	0.010	8.45	3.55	0.010

Time (min)	[H <sub>2</sub> S] (M)	[CO <sub>3</sub> <sup>2-</sup> ] (M)	[HCO <sub>3</sub> <sup>-</sup> ] (M)	[CO <sub>2</sub> ] (M)
5	5.64x10 <sup>-3</sup>	0.043	0.978	2.51x10 <sup>-3</sup>
10	1.34x10 <sup>-2</sup>	0.016	1.127	8.95x10 <sup>-3</sup>
15	9.59x10 <sup>-3</sup>	0.017	1.213	9.63x10 <sup>-3</sup>
30	2.75x10 <sup>-3</sup>	0.020	1.364	1.03x10 <sup>-2</sup>
45	8.24x10 <sup>-4</sup>	0.021	1.410	1.07x10 <sup>-2</sup>
60	3.75x10 <sup>-4</sup>	0.022	1.418	1.03x10 <sup>-2</sup>

Table 5.1 Composition of solution, with 0.716 atm partial pressure of CO<sub>2</sub> in the inlet gas. (At 35°C; gas flow rate 370ml/min; NaHCO<sub>3</sub> prebubbled for 10 min; 0.436F [Na<sub>2</sub>S]<sub>0</sub> ; 0.600F [NaHCO<sub>3</sub>]<sub>0</sub>)

Time (min)	Sulfide remain(M)	pH	[H <sup>+</sup> ] (x10 <sup>-9</sup> M)	[HS <sup>-</sup> ] (M)
5	0.420	9.31	0.49	0.418
10	0.398	8.82	1.51	0.391
15	0.339	8.70	2.00	0.332
30	0.183	8.63	2.34	0.178
45	0.085	8.63	2.34	0.083
60	0.038	8.61	2.45	0.037
90	0.014	8.60	2.51	0.014

Time (min)	[H <sub>2</sub> S] (M)	[CO <sub>3</sub> <sup>2-</sup> ] (M)	[HCO <sub>3</sub> <sup>-</sup> ] (M)	[CO <sub>2</sub> ] (M)
5	2.25x10 <sup>-3</sup>	0.097	0.859	8.59x10 <sup>-4</sup>
10	6.51x10 <sup>-3</sup>	0.037	1.007	3.11x10 <sup>-3</sup>
15	7.27x10 <sup>-3</sup>	0.030	1.080	4.40x10 <sup>-3</sup>
30	4.60x10 <sup>-3</sup>	0.029	1.235	5.91x10 <sup>-3</sup>
45	2.13x10 <sup>-3</sup>	0.031	1.326	6.35x10 <sup>-3</sup>
60	9.98x10 <sup>-4</sup>	0.031	1.373	6.88x10 <sup>-3</sup>
90	3.76x10 <sup>-4</sup>	0.031	1.397	7.16x10 <sup>-3</sup>

Table 5.2 Composition of solution, with 0.417 atm partial pressure of CO<sub>2</sub> in the inlet gas. (At 35°C; gas flow rate 373ml/min; NaHCO<sub>3</sub> prebubbled for 10 min; 0.436F [Na<sub>2</sub>S]<sub>0</sub>; 0.600F [NaHCO<sub>3</sub>]<sub>0</sub>)

Time (min)	Sulfide remain(M)	pH	[H <sup>+</sup> ] (x10 <sup>-10</sup> M)	[HS <sup>-</sup> ] (M)
5	0.421	10.10	0.794	0.421
10	0.416	9.85	1.41	0.415
15	0.412	9.57	2.69	0.411
30	0.381	9.22	6.03	0.378
45	0.335	9.13	7.41	0.332
60	0.273	9.10	7.94	0.271
90	0.174	9.11	7.76	0.173
120	0.104	9.10	7.94	0.103
180	0.037	9.10	7.94	0.037

Time (min)	[H <sub>2</sub> S] (M)	[CO <sub>3</sub> <sup>2-</sup> ] (M)	[HCO <sub>3</sub> <sup>-</sup> ] (M)	[CO <sub>2</sub> ] (M)
5	3.67x10 <sup>-4</sup>	0.302	0.432	6.9x10 <sup>-5</sup>
10	6.45x10 <sup>-4</sup>	0.229	0.583	1.67x10 <sup>-4</sup>
15	1.21x10 <sup>-3</sup>	0.153	0.740	4.06x10 <sup>-4</sup>
30	2.51x10 <sup>-3</sup>	0.084	0.910	1.12x10 <sup>-3</sup>
45	2.71x10 <sup>-3</sup>	0.073	0.977	1.48x10 <sup>-3</sup>
60	2.36x10 <sup>-3</sup>	0.073	1.040	1.69x10 <sup>-3</sup>
90	1.47x10 <sup>-3</sup>	0.080	1.123	1.78x10 <sup>-3</sup>
120	9.00x10 <sup>-4</sup>	0.083	1.187	1.92x10 <sup>-3</sup>
180	3.20x10 <sup>-4</sup>	0.087	1.245	2.02x10 <sup>-3</sup>

Table 5.3 Composition of solution, with 0.121 atm partial pressure of CO<sub>2</sub> in the inlet gas. (At 35°C; gas flow rate 371ml/min; NaHCO<sub>3</sub> prebubbled for 10 min; 0.428F [Na<sub>2</sub>S]<sub>o</sub>; 0.600F [NaHCO<sub>3</sub>]<sub>o</sub>)

The  $H^+$  ion concentration of reaction solution increases rapidly at the beginning of reaction, which then gradually levels off to a steady value, as shown in the preceding tables. Therefore, according to equation [5-17], the ratio of aqueous  $H_2S$  concentration to  $HS^-$  ion concentration would increase dramatically at the start of reaction. On the other hand, the total sulfur content of solution decreases due to desorption of  $H_2S$ . Hence, there is a peak in aqueous  $H_2S$  concentration as reaction proceeds. Furthermore, as reflected in tables 5.1-3, the higher  $CO_2$  partial pressure of the inlet gas, the sooner the peak in  $H_2S$  concentration occurs, because of higher acidity of inlet gas with higher  $CO_2$  partial pressure. In the contrary, a minimum in carbonate ion concentration appears in the course of reaction. This is due to rapid lowering in the ratio of  $[CO_3^{2-}]$  to  $[HCO_3^-]$  at the beginning of reaction (equation [5-2]), and the increase in total  $CO_2$  content of solution (i.e.  $[CO_3^{2-}] + [HCO_3^-] + [CO_2]_{aq}$ ) resulting from  $CO_2$  absorption.

## 5.2 Exit gas composition

The carbonation conversion of aqueous sodium sulfide to hydrogen sulfide is a system of simultaneous absorption of carbon dioxide and desorption of hydrogen sulfide.

With the knowledge of the reaction solution's

composition at various reaction time, as listed in tables 5.1-3, the amount of carbon dioxide absorbed and hydrogen sulfide desorbed over the time intervals can be evaluated. Therefore, knowing the composition and flow rate of the incoming gas, the average outgoing gas composition over the time periods can in turn be determined. This value can be used to compare with the vapour-liquid equilibrium constant  $K_{2-18}'$  of the  $\text{CO}_2\text{-NaHCO}_3\text{-Na}_2\text{CO}_3\text{-Na}_2\text{S-H}_2\text{O}$  system (chapter 2.4) to measure the efficiency and the feasibility of further significant improvement in yield of the present contacting pattern.

#### 5.2.1 H<sub>2</sub>S desorbed

The amount of H<sub>2</sub>S desorbed from the reaction solution over a period of time is simply the difference in residual sulfide concentration of the solution between the beginning and the end of the time interval.

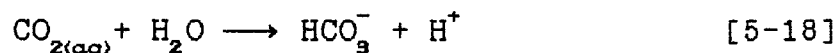
For instance, the number of mole of H<sub>2</sub>S desorbed in the 6-10 minute interval of table 5.2 is  $(0.420\text{M} - 0.398\text{M}) \times 150\text{ml} = 3.3 \times 10^{-3}$  mole, where 150ml is the volume of the reaction solution. The amounts of H<sub>2</sub>S desorbed over the time intervals of the partial pressure experiments (corresponding to the data in tables 5.1-3) are listed in tables 5.4-6.

#### 5.2.2 CO<sub>2</sub> absorbed

The amount (no. of mole) of CO<sub>2</sub> absorbed by the reaction solution over a period of time is the difference

in the total amount of carbonate, bicarbonate and aqueous carbon dioxide of the solution (the amount of  $\text{H}_2\text{CO}_3$  is negligible, section 2.8.1) between the end and the beginning of the time interval.

The concentrations of carbonate and bicarbonate have been determined in section 5.1.2. On the other hand, it is necessary to assume equilibrium of equation [5-18] of the reaction solution,



in order to estimate the concentration of  $\text{CO}_{2(\text{aq})}$ . The error introduced in so doing should not be significant since the concentration of aqueous  $\text{CO}_2$  is by far lower than that of bicarbonate ion as shown in tables 5.1-3. Besides, shortly after the commencement of reaction the pH value of the reaction solution drops to a steady value, which suggests a steady aqueous  $\text{CO}_2$  concentration. Hence, there would be no contribution to the absorption of  $\text{CO}_2$  gas from the variation of aqueous  $\text{CO}_2$  concentration shortly after the start of reaction.

From equation [5-18], the equilibrium concentration of  $\text{CO}_{2(\text{aq})} = [\text{HCO}_3^-] \times [\text{H}^+] / K_{5-18}$ . The value of  $K_{5-18}$  at  $35^\circ\text{C}$  and infinite dilution is  $4.90 \times 10^{-7}$  (equation [2-56], section 2.8.1) The equilibrium aqueous  $\text{CO}_2$  concentrations of the solutions of the  $\text{CO}_2$  partial pressure experiments are listed in tables 5.1-3. The amounts of  $\text{CO}_2$  absorbed

over the corresponding time intervals are listed in tables 5.4-6.

The calculation of the amount of  $H_2S$  desorbed from and  $CO_2$  absorbed by the reaction solution confirms the results of the gas hold up experiments (section 4.7.1, table 4.11). As shown in tables 5.4 and 5.5, the amount of  $CO_2$  absorbed is more than that of  $H_2S$  desorbed at the early stage of reaction, e.g. 6-10 minute intervals. Since the experimental pressure and temperature are constants, the flow volume decreases as the inlet  $CO_2$  gas bubbles through the solution and renders a smaller gas hold up and turbulence. On the other hand, at the later stage of reaction the amount of  $CO_2$  absorbed approximately equals to that of  $H_2S$  desorbed, so there is no significant change in the volume of gas flow, which results in larger gas hold up volume and stronger turbulence.

A criteria for the occurrence of bubbling desorption of a volatile product in a liquid phase reaction which facilitates the absorption of another gaseous reactant is the supersaturation of the reaction solution. Supersaturation occurs when the total partial pressure of reactant and product which would be in equilibrium with the bulk liquid is greater than the total pressure at the surface, at which case equation [2-47] holds.

$$D_{CA} / D_{AC} < 1 \quad [2-47]$$

As discussed in section 2.7.4, satisfaction of equation [2-47] is necessary for, but does not definitely confirm the occurrence of bubbling desorption. The diffusivity of  $\text{CO}_2$  ( $D_A$ ) and  $\text{H}_2\text{S}$  ( $D_C$ ) in water at  $16^\circ\text{C}$  are  $1.6 \times 10^{-5}$  and  $1.7 \times 10^{-5} \text{ cm}^2/\text{sec}$ , respectively.<sup>(50)</sup> The Henry's law constant of  $\text{CO}_2$  ( $H_A$ ) and  $\text{H}_2\text{S}$  ( $H_C$ ) in water at  $25^\circ\text{C}$  are respectively 29.4 and 9.8 atm/M.<sup>(41)</sup> These values are used as estimates in the calculations of the present  $\text{Na}_2\text{S}-\text{NaHCO}_3$  system. The product " $D_C H_A$ " is more than three times greater than " $D_A H_C$ ", so the inequality [2-47] is not justified. Thus, theoretical calculations using the physical data for water system show that the reaction solution is not supersaturated and bubbling desorption would not take place.

### 5.2.3 Outgoing gas $P_{\text{H}_2\text{S}}$ to $P_{\text{CO}_2}$ ratio

The amount of  $\text{CO}_2$  in the outgoing gas is simply the amount supplied in the inlet gas less that absorbed by the reaction solution, and the partial pressure ratio of  $\text{H}_2\text{S}$  to  $\text{CO}_2$  of the outgoing gas is the same as the molar ratio.

For the series of 0.716 atm  $\text{CO}_2$  partial pressure experiments (265ml/min  $\text{CO}_2$ , 105ml/min  $\text{N}_2$ ), the amount of  $\text{CO}_2$  supplied is 265 ml/min, or 11.06 mol/min since one mole of gas has a volume of 24.1 litre at room temperature  $20^\circ\text{C}$ . Therefore, there is a total of  $5.53 \times 10^{-2}$  mole of  $\text{CO}_2$  supplied to the reaction solution over a five minutes

period. Using the 6-10 minute interval (table 5.4) as an example, the total amount of  $\text{CO}_2$  in the outgoing gas over this period is  $3.61 \times 10^{-2}$  mole (i.e.  $5.53 \times 10^{-2} - 1.92 \times 10^{-2}$ ). Hence, the mean outgoing gas partial pressure ratio of  $\text{H}_2\text{S}$  to  $\text{CO}_2$  of this interval is 0.362 (i.e.  $1.30 \times 10^{-2} / 3.61 \times 10^{-2}$ ). The outgoing gas  $P_{\text{H}_2\text{S}}$  to  $P_{\text{CO}_2}$  ratios of the other time intervals and  $\text{CO}_2$  partial pressure experiments are listed in tables 5.4-6.

Time interval (min)	$\text{H}_2\text{S}$ desorbed (mole)	$\text{CO}_2$ absorbed (mole)	Mean outgoing gas $P_{\text{H}_2\text{S}}$ to $P_{\text{CO}_2}$ ratio
6 - 10	$1.30 \times 10^{-2}$	$1.92 \times 10^{-2}$	0.362
11 - 15	$1.38 \times 10^{-2}$	$1.32 \times 10^{-2}$	0.327
16 - 30	$2.46 \times 10^{-2}$	$2.32 \times 10^{-2}$	0.242
31 - 45	$7.4 \times 10^{-3}$	$7.0 \times 10^{-3}$	0.050
46 - 60	$1.7 \times 10^{-3}$	$1.4 \times 10^{-3}$	0.011

Table 5.4 Average  $P_{\text{H}_2\text{S}}$  to  $P_{\text{CO}_2}$  ratio of outgoing gas, of the 0.716 atm  $\text{CO}_2$  partial pressure experiments. (corresponds to the data in table 5.1)

Time interval (min)	H <sub>2</sub> S desorbed (mole)	CO <sub>2</sub> absorbed (mole)	Mean outgoing gas P <sub>H<sub>2</sub>S</sub> to P <sub>CO<sub>2</sub></sub> ratio
6 - 10	3.3x10 <sup>-3</sup>	1.34x10 <sup>-2</sup>	0.175
11 - 15	8.8x10 <sup>-3</sup>	1.02x10 <sup>-2</sup>	0.402
16 - 30	2.34x10 <sup>-2</sup>	2.33x10 <sup>-2</sup>	0.319
31 - 45	1.47x10 <sup>-2</sup>	1.41x10 <sup>-2</sup>	0.178
46 - 60	7.1x10 <sup>-3</sup>	7.0x10 <sup>-3</sup>	0.079
60 - 90	3.6x10 <sup>-3</sup>	3.6x10 <sup>-3</sup>	0.019

Table 5.5 Average P<sub>H<sub>2</sub>S</sub> to P<sub>CO<sub>2</sub></sub> ratio of outgoing gas, of the 0.416 atm CO<sub>2</sub> partial pressure experiments. (corresponds to the data in table 5.2)

Time interval (min)	H <sub>2</sub> S desorbed (mole)	CO <sub>2</sub> absorbed (mole)	Mean outgoing gas P <sub>H<sub>2</sub>S</sub> to P <sub>CO<sub>2</sub></sub> ratio
6 - 10	7.5x10 <sup>-3</sup>	1.17x10 <sup>-2</sup>	-0.315
11 - 15	6.0x10 <sup>-3</sup>	1.22x10 <sup>-2</sup>	-0.212
16 - 30	4.7x10 <sup>-3</sup>	1.53x10 <sup>-2</sup>	0.364
31 - 45	6.9x10 <sup>-3</sup>	8.6x10 <sup>-3</sup>	0.354
46 - 60	9.3x10 <sup>-3</sup>	9.4x10 <sup>-3</sup>	0.497
61 - 90	1.49x10 <sup>-2</sup>	1.36x10 <sup>-2</sup>	0.349
91 - 120	1.05x10 <sup>-2</sup>	1.00x10 <sup>-2</sup>	0.228
121 - 180	1.01x10 <sup>-2</sup>	9.4x10 <sup>-3</sup>	0.215

Table 5.6 Average P<sub>H<sub>2</sub>S</sub> to P<sub>CO<sub>2</sub></sub> ratio of outgoing gas, of the 0.121 atm CO<sub>2</sub> partial pressure experiments. (corresponds to the data in table 5.3)

It is desirable to have as high a  $H_2S$  content in the exit gas as possible for the downstream production of elemental sulfur. As shown in tables 5.4-6, a high  $P_{H_2S}$  to  $P_{CO_2}$  ratio of about 0.4 can be attained. This corresponds to a 28%  $H_2S$  content in the exit gas for an incoming gas flow of pure  $CO_2$ . It has to be point out that the ratios of tables 5.4-6 are mean values over a certain period of time. The instantaneous ratio at a particular time within an interval can be much higher than the mean value of the interval. Furthermore, the flow rate of these experiments is 370 ml/min, which is fairly high for the size of the reaction vessel used (chapter 3.3.1). A lower gas flow rate would lead to better  $CO_2$  utilization and higher exit gas  $H_2S/CO_2$  ratio; hence an even higher  $H_2S$  content in the exit gas.

With the use of equations [2-21] and [2-22], or figure 2.4, it can be shown that the outgoing gas partial pressure ratios of  $H_2S$  to  $CO_2$  of tables 5.4 and 5.5 are generally above 60% of the corresponding equilibrium values. By equation [2-22], the value of  $K_{2-18}'$  at  $35^\circ C$  and a total sodium ion concentration of 1.47M (i.e. 0.436F  $Na_2S$  + 0.600F  $NaHCO_3$ ) is about 1.65. Using 6-10 minute interval of table 5.1 as an example, the mean  $[HS^-]/[HCO_3^-]$  is about 0.347 (i.e. average of 0.407/0.978 and 0.313/1.127, concentration values from table 5.1). Hence, by equation [2-21], the equilibrium  $P_{H_2S}$  to  $P_{CO_2}$  ratio is about 0.57

(i.e.  $1.65 \times 0.347$ ). The experimental value of  $P_{\text{H}_2\text{S}}/P_{\text{CO}_2}$  is 0.362 (table 5.4), which is 63% of the equilibrium value. For the second time interval of table 5.4, 11-15 minute, the experimental  $P_{\text{H}_2\text{S}}/P_{\text{CO}_2}$  value (0.327) is about 86% of the corresponding equilibrium value (0.38). Thus, it shows that the present contacting pattern is highly effective, and any major improvement in yield without significant sacrifice in reaction kinetics is unlikely.

The total amount of  $\text{CO}_2$  supplied in five minutes by the gas flow of 0.121 atm  $\text{CO}_2$  partial pressure (326ml/min  $\text{N}_2$ , 45ml/min  $\text{CO}_2$ ) is  $9.4 \times 10^{-3}$  mole. However, the calculated amount of  $\text{CO}_2$  absorbed for the first two intervals of table 5.6 are larger than the amount supplied, which render the obviously incorrect negative  $P_{\text{H}_2\text{S}}/P_{\text{CO}_2}$  values of the first two intervals of table 5.6. The previously measured  $\text{CO}_2$  flow rate was first suspected to be at fault, so the flow rate was re-measured by the method of a moving film along a graduated column as described in section 3.3.2. However, the  $\text{CO}_2$  flow rate was found to be the same as previously measured, i.e. 45ml/min.

A closer examination of table 5.3 suggests that the first few pH values of the reaction solution might probably be the sources of error. As shown in table 5.3, the pH value decreases from 10.10 at  $t = 5$  minute to 9.85 at  $t = 10$  minute, a drop of 0.25 pH unit. In the subsequent five minutes interval, the pH value drops a further 0.28 unit

(pH = 9.57 at t = 15 minute), which is an even bigger decrease than that in the preceding five minutes interval. This indicates an experimental error since the pH value of the reaction solution is expected to decrease rapidly at the beginning of reaction and taper off to a steady value afterwards, as depicted by the data in tables 5.1 and 5.2.

If the pH value at time t = 15 minute of table 5.3 were 9.67, (instead of the measured value 9.57, i.e. a difference of 0.1, while keeping all of the other values the same so as to see the effect of a small error in pH value on the overall results) the total amount of CO<sub>2</sub> absorbed in the 10-15 minute interval and the mean  $P_{H_2S}/P_{CO_2}$  value would have been  $8.2 \times 10^{-3}$  mole (which is now less than the total amount of CO<sub>2</sub> supplied) and 0.536, respectively. Hence, it shows that errors in pH value measurements are likely to be the cause of the poor results of the early part of the 0.121 atm CO<sub>2</sub> partial pressure reaction.

Other possible sources of error are the values of equilibrium constants used in the calculations. Equilibrium constants  $K_{a2}(CO_2)$  and  $K_w$  at 35°C are used, whereas the value of  $K_{a1}(H_2S)$  at 18°C is used as an estimate for 35°C, which does not appear to be in literature.

It is previously mentioned in section 2.8.2 that  $K_{2-54}$ , which equals to  $K_w/K_{a2}(CO_2)$ , decreases with increasing ionic strength. The dissociation constant of

water  $K_w$  is expected to be relatively independent of ionic strength since it is the solvent and is abundant. Hence,  $K_{a2}(\text{CO}_2)$  increases with ionic strength, and, by equation [5-2], so does the ratio of carbonate to bicarbonate ions for a constant  $\text{H}^+$  ion concentration. Due to charge balance constraint, i.e. equation [5-15], an increase in carbonate ion would lead to a decrease in bicarbonate ion by twice the amount. Therefore, while keeping all other parameters unchanged ( $\text{H}^+$ , etc), an increase in ionic strength would decrease the total amount of  $\text{HCO}_3^-$  and  $\text{CO}_3^{2-}$  of the solution, and hence decrease the amount of  $\text{CO}_2$  absorbed. Since the value of  $K_{a2}(\text{CO}_2)$  for infinite dilution is used, the calculated amount of  $\text{CO}_2$  absorbed is likely to be an over estimate which, in extreme cases, could lead to calculated amount of  $\text{CO}_2$  absorbed being greater than that supplied.

On the other hand, the uncertainty due to the effect of ionic strength on  $K_{a2}(\text{H}_2\text{S})$  would be insignificant since the concentration of  $\text{S}^{2-}$  ion is negligible anyway (section 5.1.2).

### 5.3 Reaction kinetics of carbonation conversion of aqueous sodium sulfide to hydrogen sulfide

Figure 5.1 shows the plots of  $\ln(C/[\text{Na}_2\text{S}]_0)$  against reaction time, where C is the total sulfide concentration, for the four reaction temperatures studied. It indicates a common reaction pattern exhibited by all four of the plots, i.e. the carbonation conversion of  $\text{Na}_2\text{S}$  to  $\text{H}_2\text{S}$  starts off

with a slow reaction period, which is followed by a fast conversion period indicated by the linear regions of the plots, and finally tapers off to a slow finishing period.

Figures 5.2, 5.3 and 5.4 are, respectively, the similar plots for the CO<sub>2</sub> flow rate, CO<sub>2</sub> partial pressure and pressurized experiments. All the plots of these figures show the same reaction pattern perceptible in figure 5.1.

This reaction pattern is in fact in good agreement with other experimental observations and measurements. For instance, it can be shown by comparing table 4.11 with figure 5.2 (both of which are results of the CO<sub>2</sub> flow rate experiments) that the small gas hold up period at the beginning of reaction coincides with the initial slow reaction period, while the subsequent large gas hold up stage matches with the fast conversion period (the linear regions of the plots of figure 5.2). On the other hand, the initial slow reaction period of the plots of figure 5.3 matches well in time with the stage of rapid increase in solution's acidity at the beginning of reaction as shown in tables 5.1-3 (both figure 5.3 and tables 5.1-3 are results of the CO<sub>2</sub> partial pressure experiments), whereas the fast conversion period coincides with the stage of steady pH value. These comparisons of experimental results suggest that the reaction kinetics, gas hold up volume and acidity of reaction solution are highly correlated.

At the commencement of reaction the Na<sub>2</sub>S-NaHCO<sub>3</sub>

solution is basic, with a pH value of about 10.6 (sections 5.1.1 and 4.5). Upon bubbling with carbon dioxide, large amount of  $\text{CO}_2$  is absorbed in the solution with little  $\text{H}_2\text{S}$  desorption. Consequently, the gas volume in solution decreases (i.e. a smaller gas hold up volume) as  $\text{CO}_2$  bubbles through the solution, of which the acidity increases rapidly. As the solution's acidity rises, the rate of  $\text{CO}_2$  absorption gradually slows down because of the decrease in driving force (equations [2-62] and [2-69]), whereas the desorption rate of  $\text{H}_2\text{S}$  increases since aqueous  $\text{H}_2\text{S}$  concentration increases with the acidity of solution (equation [5-17]). This leads to a larger gas hold up volume. Eventually a steady pH value is reached and the amount of  $\text{CO}_2$  absorbed is roughly equal to that of  $\text{H}_2\text{S}$  desorbed.

The linear regions of the plots of  $\ln(C/[\text{Na}_2\text{S}]_0)$  vs reaction time suggest that the rate of  $\text{H}_2\text{S}$  generation is first order with respect to residual sulfide concentration, but since the majority of residual sulfide exists as  $\text{HS}^-$  ion (over 95%, tables 5.1-3), it may be assumed that the rate is first order with respect to  $\text{HS}^-$  ion. The slopes of these linear regions of figures 5.1-4 are listed in tables 5.7-10 respectively. On the other hand, since the driving force for the  $\text{H}_2\text{S}$  generation is the absorption of  $\text{CO}_2$ , it is expected that the rate of reaction is somehow dependent on the gas phase  $\text{CO}_2$  partial pressure. Therefore, the

differential rate equation may be written as follows

$$-\frac{dc}{dt} = akc(P_{\text{CO}_2})^n \quad [5-19]$$

where  $a$  and  $k$  are the gas-liquid interfacial area and overall  $\text{H}_2\text{S}$  generation rate constant respectively;  $c$  is the total sulfide concentration and  $n$  is the reaction order with respect to the gas phase  $\text{CO}_2$  partial pressure. The integrated form of equation [5-19] is

$$\left[ \frac{1}{P_{\text{CO}_2}} \right]^n \ln \left[ \frac{C}{[\text{Na}_2\text{S}]_0} \right] = -akt \quad [5-20]$$

Thus, in the case which  $n$  equals to the actual reaction order with respect to gas phase  $\text{CO}_2$  partial pressure, plots of  $[\ln(C/[\text{Na}_2\text{S}]_0)]/(P_{\text{CO}_2})^n$  verses reaction time for the results of the four different  $\text{CO}_2$  partial pressure experiments would yield linear regions of identical slopes. Figures 5.3, 5.5 and 5.6 show the plots for  $n$  equals to zero, one and two, respectively, for the results of the four different  $\text{CO}_2$  partial pressure experiments. Reaction order with respect to a particular species is unlikely to be higher than two.

Comparison among figures 5.3, 5.5 and 5.6 shows that the carbonation conversion of  $\text{Na}_2\text{S}$  to  $\text{H}_2\text{S}$  is likely to be first order with respect to gas phase  $\text{CO}_2$  partial pressure. As shown in figure 5.5, the deviation in slope of the linear regions of the three higher  $\text{CO}_2$  partial pressure

experiments is small, whereas the slope of the lowest  $\text{CO}_2$  partial pressure is somewhat steeper. The slopes of these plots are listed in table 5.11. The discrepancy in slope is probably due to the fact that the values of  $\text{CO}_2$  partial pressure of the inlet gas flows are used in the calculations because there is no information on the variation of gas phase  $\text{CO}_2$  partial pressure with position of the reaction column. Gas phase  $\text{CO}_2$  partial pressure is expected to decrease due to the absorption of  $\text{CO}_2$  by reaction solution as gas bubbles rise through the solution column.

Since the carbonation conversion of aqueous  $\text{Na}_2\text{S}$  to  $\text{H}_2\text{S}$  is first order with respect to both sulfide concentration and gas phase  $\text{CO}_2$  partial pressure, the integrated rate equation [5-20] becomes

$$\ln\left(\frac{C}{[\text{Na}_2\text{S}]_0}\right) = -akP_{\text{CO}_2} t \quad [5-21]$$

Thus, the slope of a plot  $\ln(C/[\text{Na}_2\text{S}]_0)$  verses reaction time equals to the product " $-akP_{\text{CO}_2}$ "; hence rate constant  $k$  can be determined from the measured slopes. The interfacial areas of the various predetermined gas flow rates are listed in table 4.13. For the case of the pressurized experiments, the interfacial areas are estimated by the use of figure 5.7, which shows the plot of interfacial area against gas flow rate. The calculated rate

constant values are tabulated in the same tables next to the slope values.

Temperature (°C)	Slope (sec <sup>-1</sup> )	Rate Constant k (cm sec <sup>-1</sup> atm <sup>-1</sup> )
25	-0.0431	0.022
35	-0.0391	0.020
45	-0.0354	0.018
55	-0.0315	0.016

Table 5.7 Slopes of the linear regions of the plots of figure 5.1, together with the calculated rate constants.

CO <sub>2</sub> flow rate (ml/min)	Slope (sec <sup>-1</sup> )	Rate Constant k (cm sec <sup>-1</sup> atm <sup>-1</sup> )
129	-0.0391	0.020
155	-0.0463	0.021
265	-0.0740	0.021
397	-0.101	0.023
495	-0.124	0.022

Table 5.8 Slopes of the linear regions of the plots of figure 5.2, together with the calculated rate constants.

CO <sub>2</sub> partial pressure (atm)	Slope (sec <sup>-1</sup> )	Rate Constant k (cm sec <sup>-1</sup> atm <sup>-1</sup> )
1.00	-0.101	0.023
0.716	-0.0790	0.025
0.417	-0.0489	0.026
0.121	-0.0156	0.029

Table 5.9 Slopes of the linear regions of the plots of figure 5.3, together with the calculated rate constants.

Gaseous Pressure	Slope (sec <sup>-1</sup> )	Rate Constant k (cm sec <sup>-1</sup> atm <sup>-1</sup> )
atmospheric	-0.101	0.022
4 PSIG	-0.101	0.021
9 PSIG	-0.102	0.021

Table 5.10 Slopes of the linear regions of the plots of figure 5.4, together with the calculated rate constants.

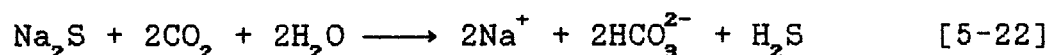
CO <sub>2</sub> partial pressure (atm)	Slope (sec <sup>-1</sup> atm <sup>-1</sup> )	Rate Constant k (cm sec <sup>-1</sup> atm <sup>-1</sup> )
1.00	-0.101	0.023
0.716	-0.110	0.025
0.417	-0.117	0.026
0.121	-0.129	0.029

Table 5.11 Slopes of the linear regions of the plots of figure 5.5, together with the calculated rate constants.

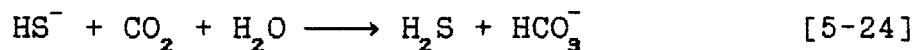
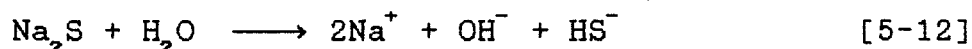
#### 5.4 Reaction mechanisms and rate determining step of the carbonation conversion of aqueous sodium sulfide to hydrogen sulfide

##### 5.4.1 Reaction mechanisms

The overall aqueous reaction of the carbonation conversion of  $\text{Na}_2\text{S}$  to  $\text{H}_2\text{S}$



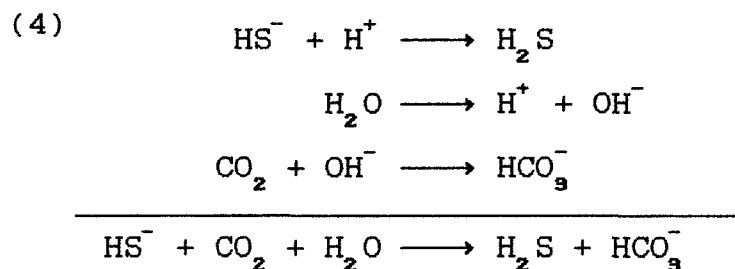
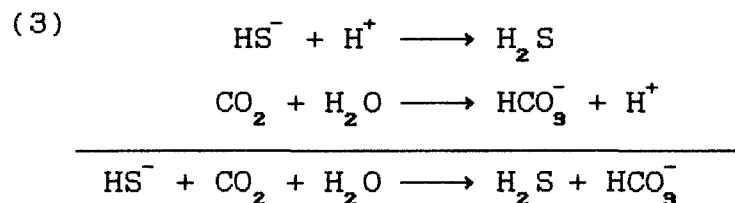
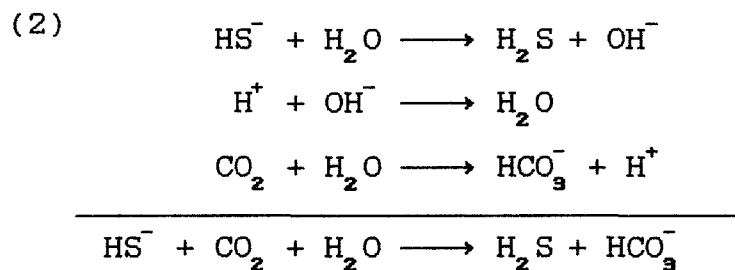
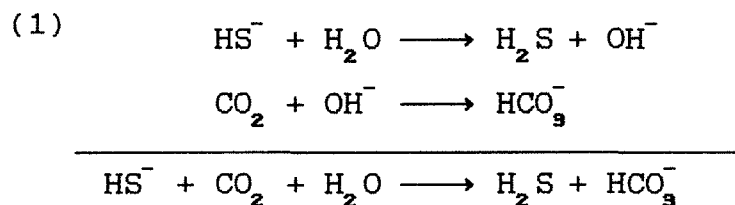
is made up of a number of reactions that may be broken down as follows :

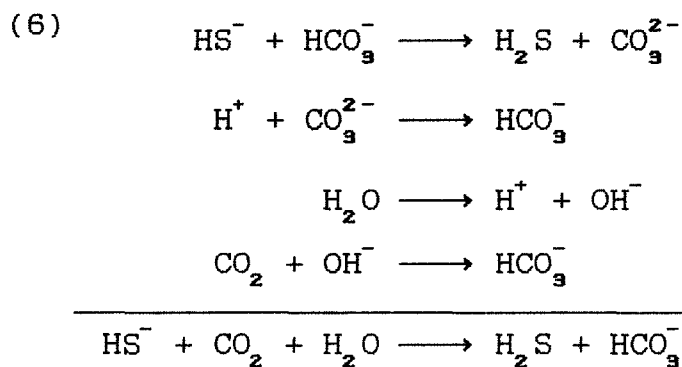
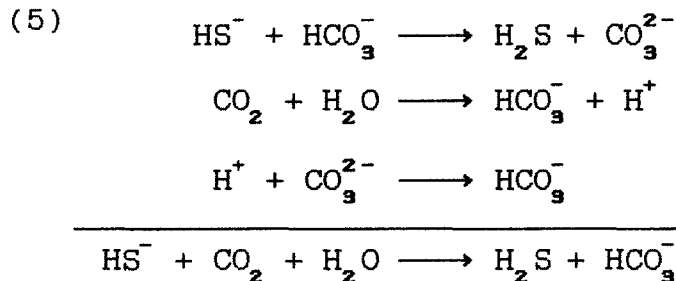


Equation [5-12] is the hydrolysis of sodium sulfide which is shown in section 5.1.1 to go essentially to completion in the present case of  $\text{Na}_2\text{S}$ - $\text{NaHCO}_3$  system. Equation [5-23] is believed to be the major reaction which takes place at the first reaction period of the carbonation reaction that rapidly increases the solution's acidity. On the other hand, the subsequent fast conversion period is dominated by the  $\text{H}_2\text{S}$  generation reaction, equation [5-24], which is of the greatest interest in the study of reaction kinetics, section 5.3.

Equation [5-24] is still a trimolecular reaction,

and it is likely to be made up in reality by a sequence of reactions. The most probable reaction sequences that result in the overall equation [5-24] are described below :

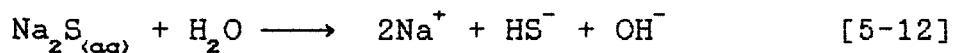




Reaction sequences (5) and (6) are unlikely to be of any importance since they both involve a reaction between two similarly charged ionic species, namely  $\text{HS}^-$  and  $\text{HCO}_3^-$  ions. On the contrary, sequences (1) and (2) are most likely to represent the actual reactions, because here  $\text{HS}^-$  ion reacts with water molecule which is the medium and is abundant, to give aqueous  $\text{H}_2\text{S}$  molecule.

Therefore, the mechanism of carbonation conversion of aqueous  $\text{Na}_2\text{S}$  to gaseous  $\text{H}_2\text{S}$  may then be summarized as follows :

(A) Ionization of sodium sulfide to  $\text{HS}^-$  ion in liquid phase :

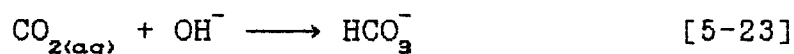
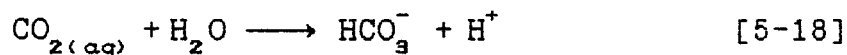


(B) Absorption of carbon dioxide :

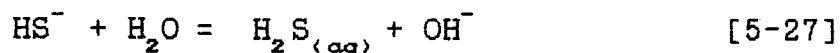
- (1) Diffusion of  $\text{CO}_2$  from the bulk of gas phase to the gas-liquid interface.
- (2) Dissolution of  $\text{CO}_2$  at the interface at which physical equilibrium may be assumed.



- (3) Diffusion of dissolved  $\text{CO}_2$  from the interface towards the bulk of liquid.
- (4) Chemical reaction within liquid phase which leads to an increase in acidity of reaction solution.



(C) Generation of aqueous hydrogen sulfide :



(D) Desorption of hydrogen sulfide :

- (1) Diffusion of  $\text{H}_2\text{S}$  from bulk of liquid towards gas-liquid interface due to the concentration gradient

set up by the chemical reaction.

(2) Gasification of  $H_2S$  at the interface.



(3) Diffusion of gaseous  $H_2S$  from the interface towards the bulk of gas.

#### 5.4.2 Rate determining step

The ionization of aqueous sodium sulfide to  $HS^-$  ion in the present  $Na_2S-NaHCO_3$  system is a homogeneous reaction which goes to completion at the initial state of the conversion reaction as discussed previously in section 5.1.1. Thus, the supply of reactant  $HS^-$  ion is not rate limiting and hence equation [5-12] may not be the rate determining step of the overall  $Na_2S$  conversion reaction.

The homogeneous liquid phase  $H_2S$  generation reactions [5-26] and [5-27] may be considered to be instantaneous and in equilibrium at all time since only a transfer of proton is involved, which is fast in comparison to other reactions considered here. Thus, the generation of aqueous  $H_2S$  is not the rate limiting step either.

The other possible rate controlling steps left are the absorption of  $CO_2$  and desorption of  $H_2S$ , which are both heterogeneous reactions. This is in accordance with the results of the gas flow rate experiments which suggest that the rate determining step is likely to be heterogeneous reaction (section 4.4). If the aqueous concentration of

either  $\text{CO}_2$  or  $\text{H}_2\text{S}$  is in equilibrium with its partial pressure in the gas phase, then the heterogeneous reaction involving the other gas would be the rate limiting step. Therefore, solubility of gas in the present  $\text{Na}_2\text{S-NaHCO}_3$  system is needed in order to determine if equilibrium of the gas is established between the gas and liquid phase.

As discussed in section 2.7, the solubility of a gas in an electrolyte solution may be estimated by equation [2-72].

$$\log(H/H_w) = hI \quad [2-72]$$

where  $H$  is the Henry's law constant of the gas in the electrolyte solution;  $H_w$  is that in pure water;  $h = h_g + h_+$  +  $h_-$  is the salting out coefficient, and  $I$  is the ionic strength of the solution. Furthermore, in the case of mixed electrolytes, Danckwerts<sup>(42)</sup> suggested that the value of  $H$  may be given by equation [2-75].

$$\log(H/H_w) = h_1 I_1 + h_2 I_2 + \dots \quad [2-75]$$

The major ionic species of the present  $\text{Na}_2\text{S-NaHCO}_3$  system are  $\text{HS}^-$ ,  $\text{HCO}_3^-$ ,  $\text{CO}_3^{2-}$  and  $\text{Na}^+$  ions (section 5.1), so the solution may be treated as mixed electrolytes of  $\text{NaHS}$ ,  $\text{NaHCO}_3$  and  $\text{Na}_2\text{CO}_3$ . As reaction proceeds, the ionic composition of the reaction solution changes, and so does the solubility of  $\text{CO}_2$  in the solution. However emphasis is put on the second fast conversion period, which is of the

greatest interest in the study of the reaction kinetics.

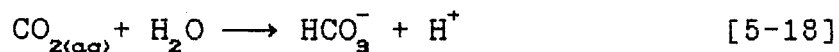
Using the ionic composition at time  $t = 15$  min of table 5.1 as an example, the concentrations of  $\text{HS}^-$ ,  $\text{HCO}_3^-$  and  $\text{CO}_3^{2-}$  are, respectively, 0.224, 1.213 and 0.017M, whereas that of  $\text{Na}^+$  ion remains unchanged during the course of reaction at 1.472M. It is assumed that the salting out coefficients  $h_g$ ,  $h_+$  and  $h_-$  are not temperature sensitive<sup>(51)</sup>, and the values<sup>(51)</sup> at 25°C are used. Thus, the value of the product "hI" of NaHS =  $(-0.2277 - 0.0183 + 0.3718)[1/2(0.224 + 0.224)] = 0.028$ . Similarly, the products of "hI" of  $\text{NaHCO}_3$  and  $\text{Na}_2\text{CO}_3$  are 0.2214 and  $6.6 \times 10^{-3}$  respectively. From table 2.1,  $H_w$  equals to 37.7 atm/M at 35°C. Therefore, by equation [2-72], the calculated estimate of the Henry's law constant of  $\text{CO}_2$  for the reaction solution at 35°C is 68.0 atm/M. Similar calculations are performed for the compositions at other reaction time of the second fast conversion period (10-45 min, figure 5.3), of which the results are listed in table 5.12. It shows that variation in Henry's law constant of  $\text{CO}_2$  is small as reaction proceeds.

Take reaction time  $t = 30$  min of the 0.716 atm  $\text{CO}_2$  partial pressure experiment as an example, the aqueous  $\text{CO}_2$  concentration that would be in equilibrium with the gas phase is  $1.03 \times 10^{-2}$  M ( $0.716 \text{ atm} / 69.4 \text{ atm M}^{-1}$ ). The concentrations of  $\text{H}^+$  and  $\text{HCO}_3^-$  ions are  $3.72 \times 10^{-9}$  M and

Reaction time(min)	"hI"			log(H/H <sub>w</sub> )	H (atm/M)
	NaHS	NaHCO <sub>3</sub>	Na <sub>2</sub> CO <sub>3</sub>		
10	0.039	0.206	0.0062	0.251	67.3
15	0.028	0.221	0.0066	0.256	68.0
30	0.0084	0.249	0.0078	0.265	69.4
45	0.0025	0.257	0.0082	0.268	69.9

Table 5.12 Solubility of CO<sub>2</sub> in reaction solution at various reaction time of the 0.716 atm CO<sub>2</sub> partial pressure experiments.

1.364M respectively (table 5.1). By equation [2-56], the equilibrium constant  $K_{5-18}$  at 35°C is  $4.9 \times 10^{-7} M$ .



Thus, the aqueous CO<sub>2</sub> concentration that would be in equilibrium with the H<sup>+</sup> and HCO<sub>3</sub><sup>-</sup> concentrations is  $1.04 \times 10^{-2} M$  ( $3.72 \times 10^{-9} M \times 1.364 M / 4.9 \times 10^{-7} M$ ), which is practically the same concentration that would be in equilibrium with the CO<sub>2</sub> partial pressure of the gas phase. Hence, it is shown that the gas phase CO<sub>2</sub> partial pressure is in equilibrium with the liquid phase CO<sub>2</sub>, H<sup>+</sup> and HCO<sub>3</sub><sup>-</sup> concentrations.

Similar calculations for the other CO<sub>2</sub> partial pressure experiments show consistent results. For instance,

at time  $t = 30$  min. of the  $0.417$  atm  $\text{CO}_2$  partial pressure reaction, the Henry's law constant  $H$  of  $\text{CO}_2$  equals to  $68.5$  atm  $\text{M}^{-1}$  ( $\log H/H_v = 0.259$ ; concentration data from table 5.2). Thus, an aqueous  $\text{CO}_2$  concentration of  $6.09 \times 10^{-3} \text{M}$  would be in equilibrium with the gas phase  $\text{CO}_2$  partial pressure. On the other hand, equilibrium considerations of reaction [5-28] indicate that an aqueous  $\text{CO}_2$  concentration of  $5.90 \times 10^{-3} \text{M}$  would be in equilibrium with the liquid phase  $\text{H}^+$  and  $\text{HCO}_3^-$  ion concentrations. Similarly, at time  $t = 90$  min. of the  $0.121$  atm  $\text{CO}_2$  partial pressure reaction,  $H = 68.3$  atm  $\text{M}^{-1}$  ( $\log H/H_v = 0.258$ ; concentration data from table 5.3). Thus, an aqueous  $\text{CO}_2$  concentration of  $1.77 \times 10^{-3} \text{M}$  would be in equilibrium with the gas phase  $\text{CO}_2$  partial pressure. Equilibrium considerations of reaction [5-28] indicate that an aqueous  $\text{CO}_2$  concentration of  $1.78 \times 10^{-3} \text{M}$  would be in equilibrium with the liquid phase  $\text{H}^+$  and  $\text{HCO}_3^-$  ion concentrations.

Therefore, it is shown that the absorption of  $\text{CO}_2$  gas is a relatively fast reaction, and that the desorption of  $\text{H}_2\text{S}$  gas must be the rate limiting step.

### 5.5 Pressurized reaction system

At first glance figure 4.5 might suggest that the two pressurized systems (4 PSIG and 9 PSIG) have little difference in overall conversion rate of  $\text{Na}_2\text{S}$  as compare to that of the atmospheric system. However, the pressurized systems' volumetric flow rate were reduced according to

Boyle's law, as discussed in section 4.6, and that section 4.4 shows the strong dependence of conversion rate on inlet  $\text{CO}_2$  gas volumetric flow rate. Hence, figure 4.5 actually indirectly suggests the advantage of using a pressurized reactor to increase the reaction rate per unit area of gas-liquid interface.

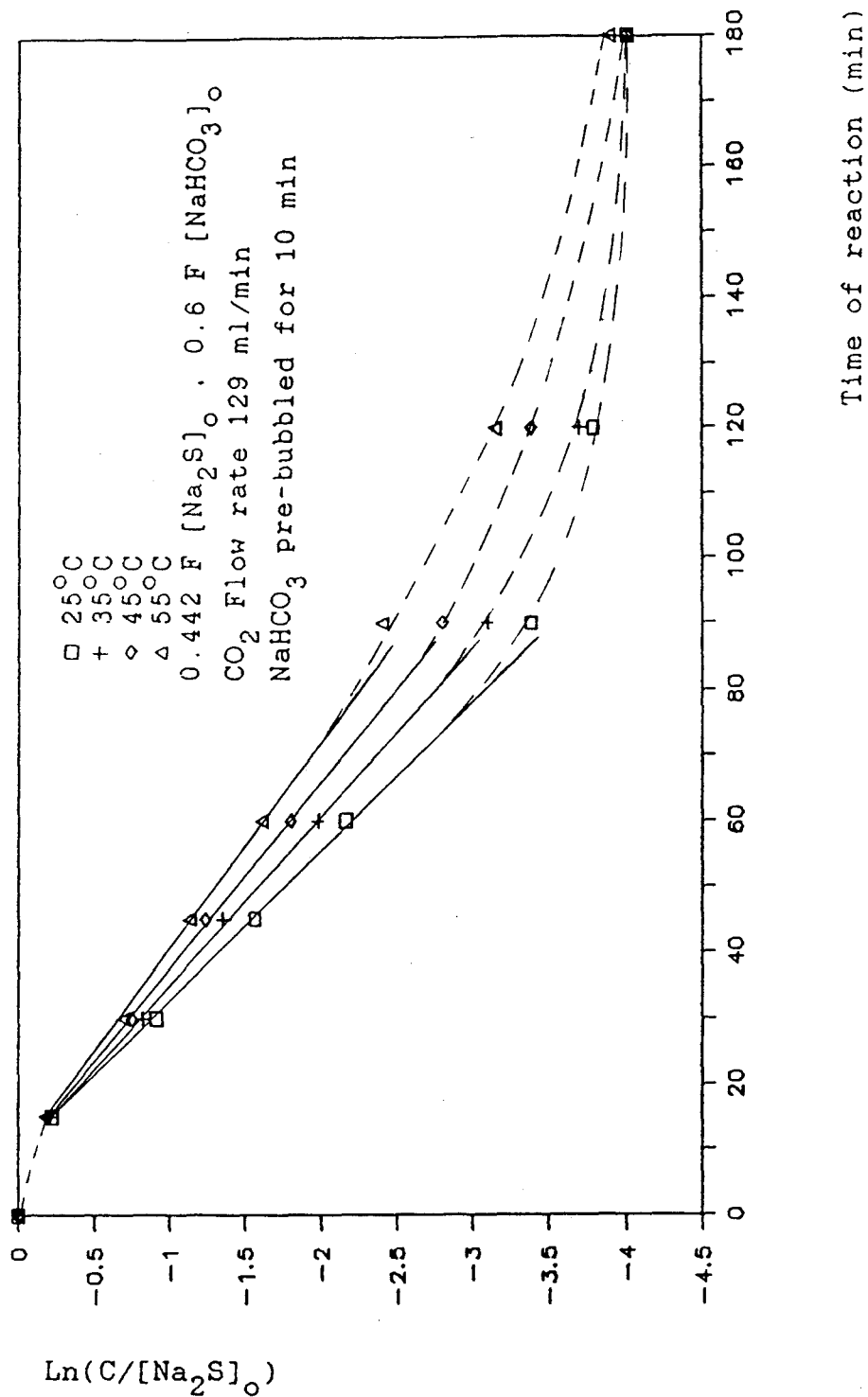


Figure 5.1 Ln(C/[Na<sub>2</sub>S]<sub>0</sub>) versus reaction time at different temperatures.

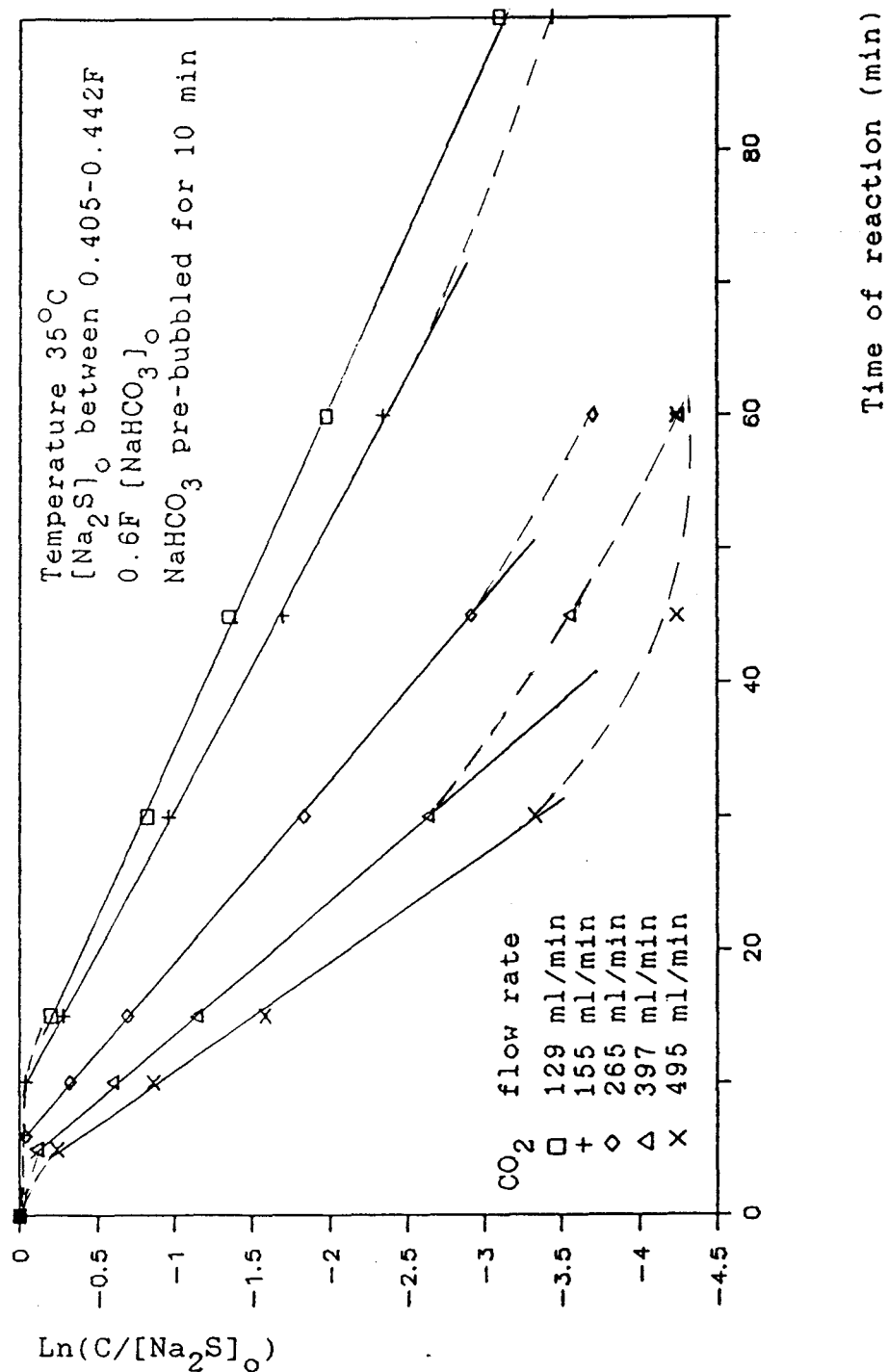
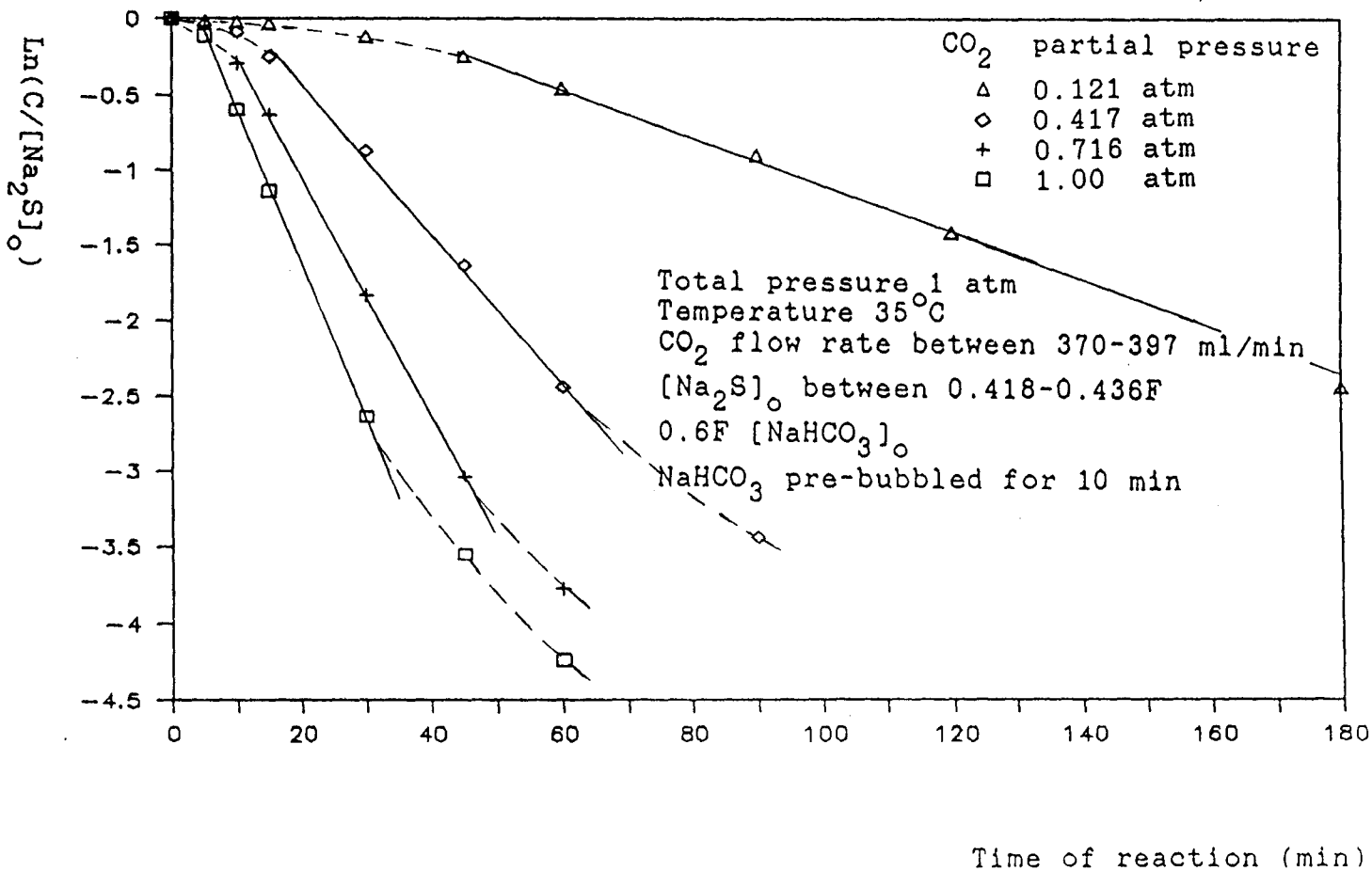


Figure 5.2  $\text{Ln}(C/[\text{Na}_2\text{S}]_0)$  versus reaction time with different  $\text{CO}_2$  flow rates.

Figure 5.3  $\ln(C/[Na_2S]_0)$  versus reaction time at different  $CO_2$  partial pressures.



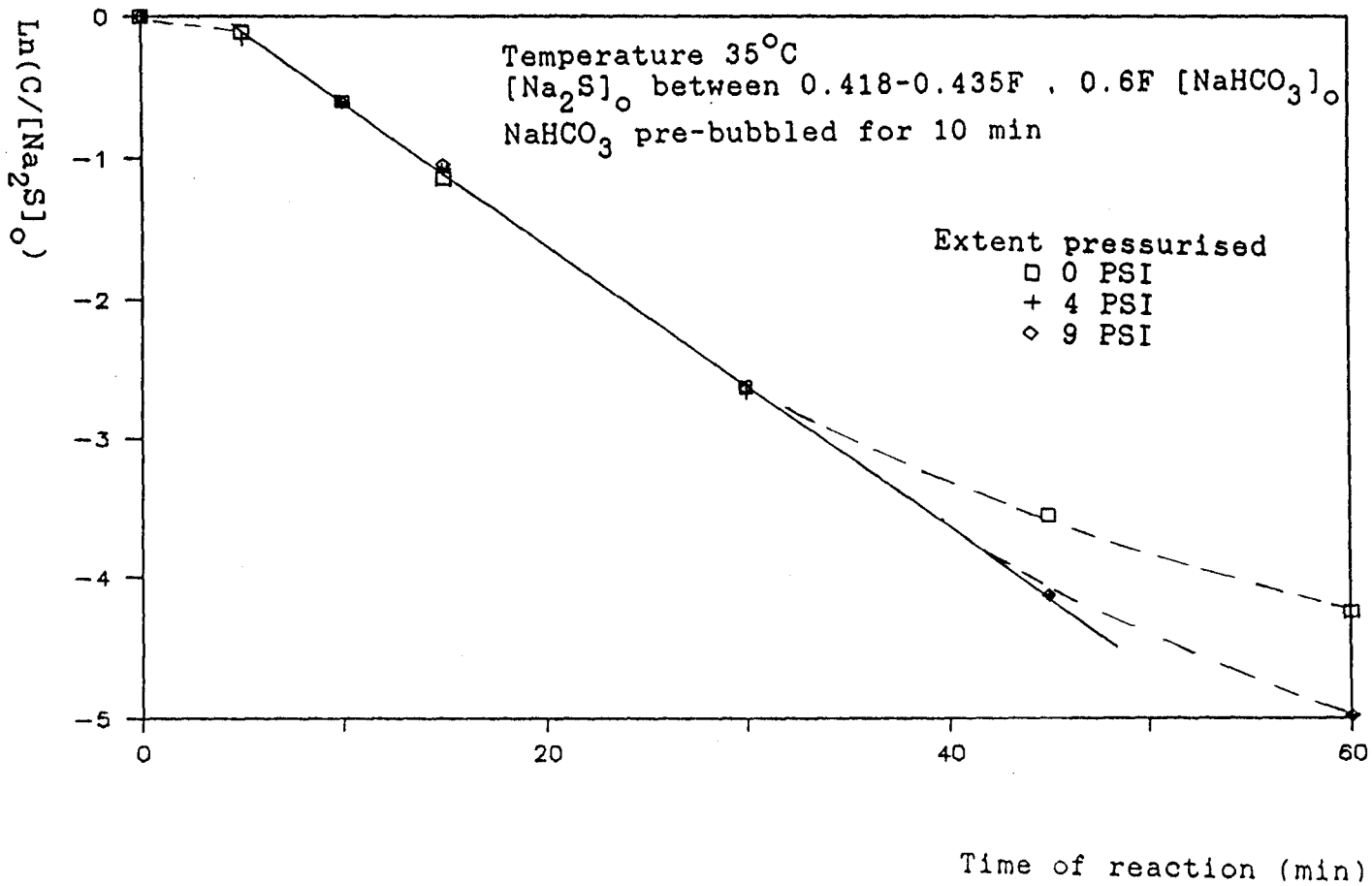


Figure 5.4  $\ln(C/[\text{Na}_2\text{S}]_0)$  verses reaction time of pressurized systems.

Figure 5.5  $[\ln(C/[Na_2S]_o)]/P_{CO_2}$  verses reaction time at different  $CO_2$  partial pressures.

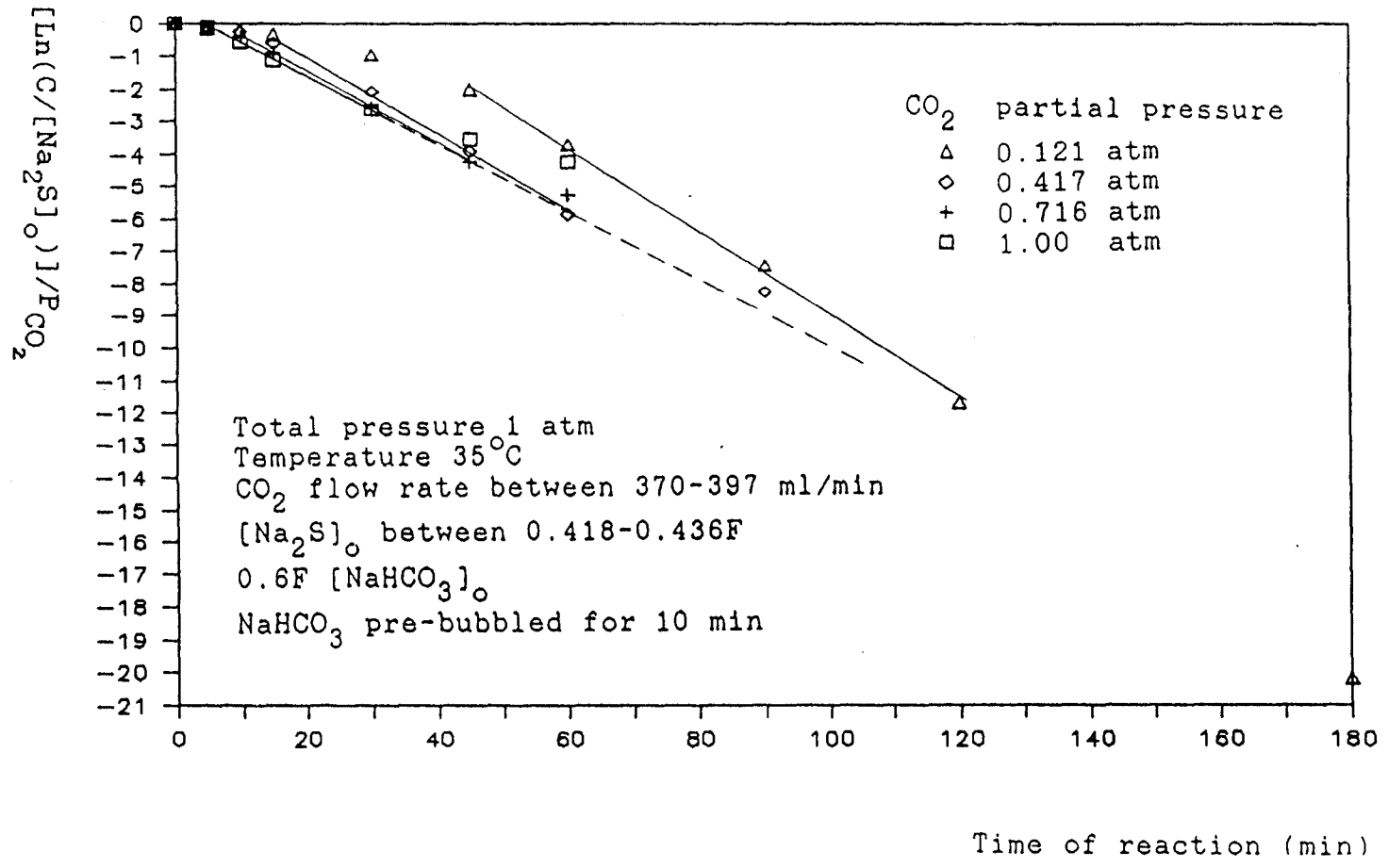
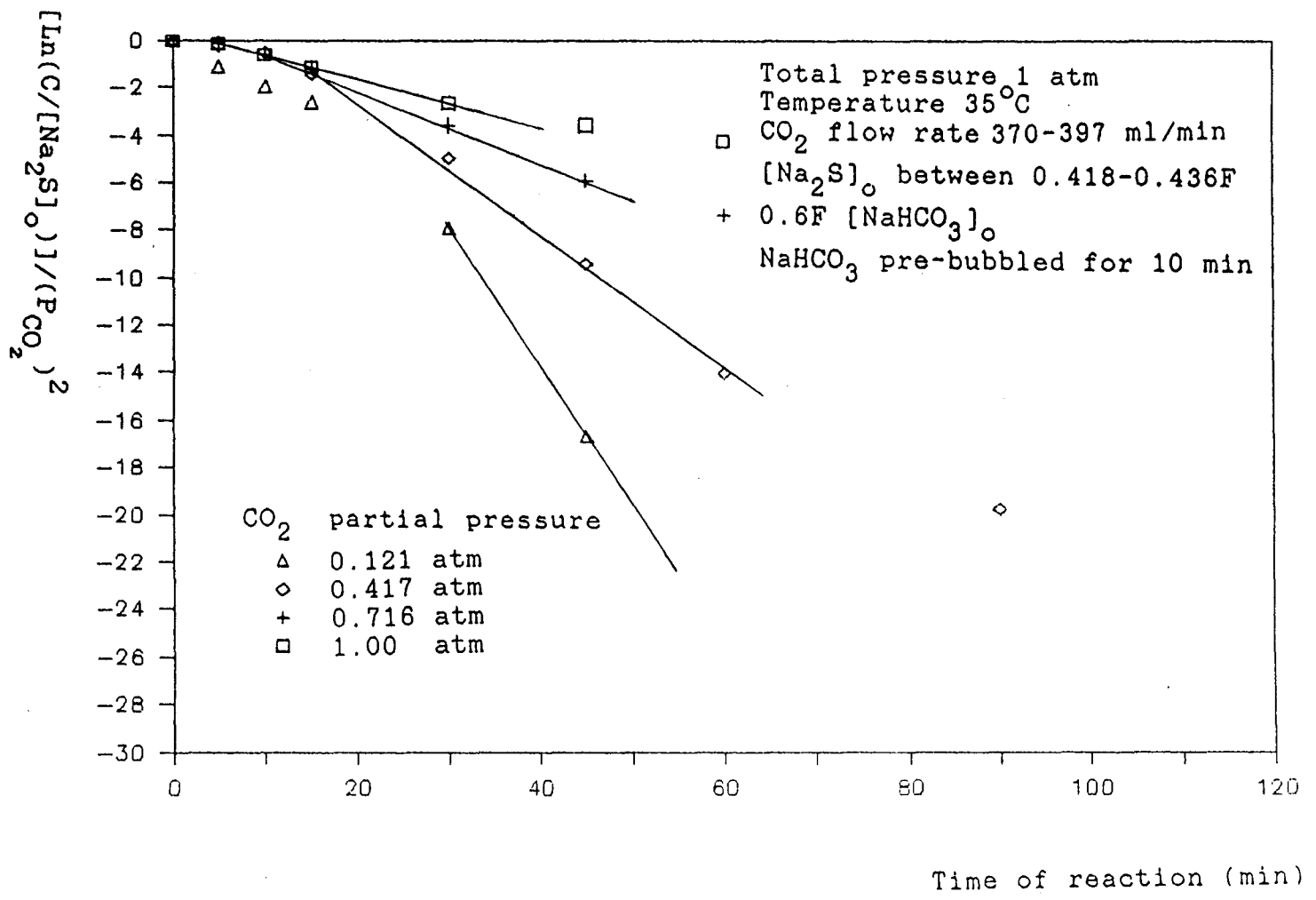


Figure 5.6  $[\ln(C/[Na_2S]_0)]/(P_{CO_2})^2$  verses reaction time at different  $CO_2$  partial pressures.



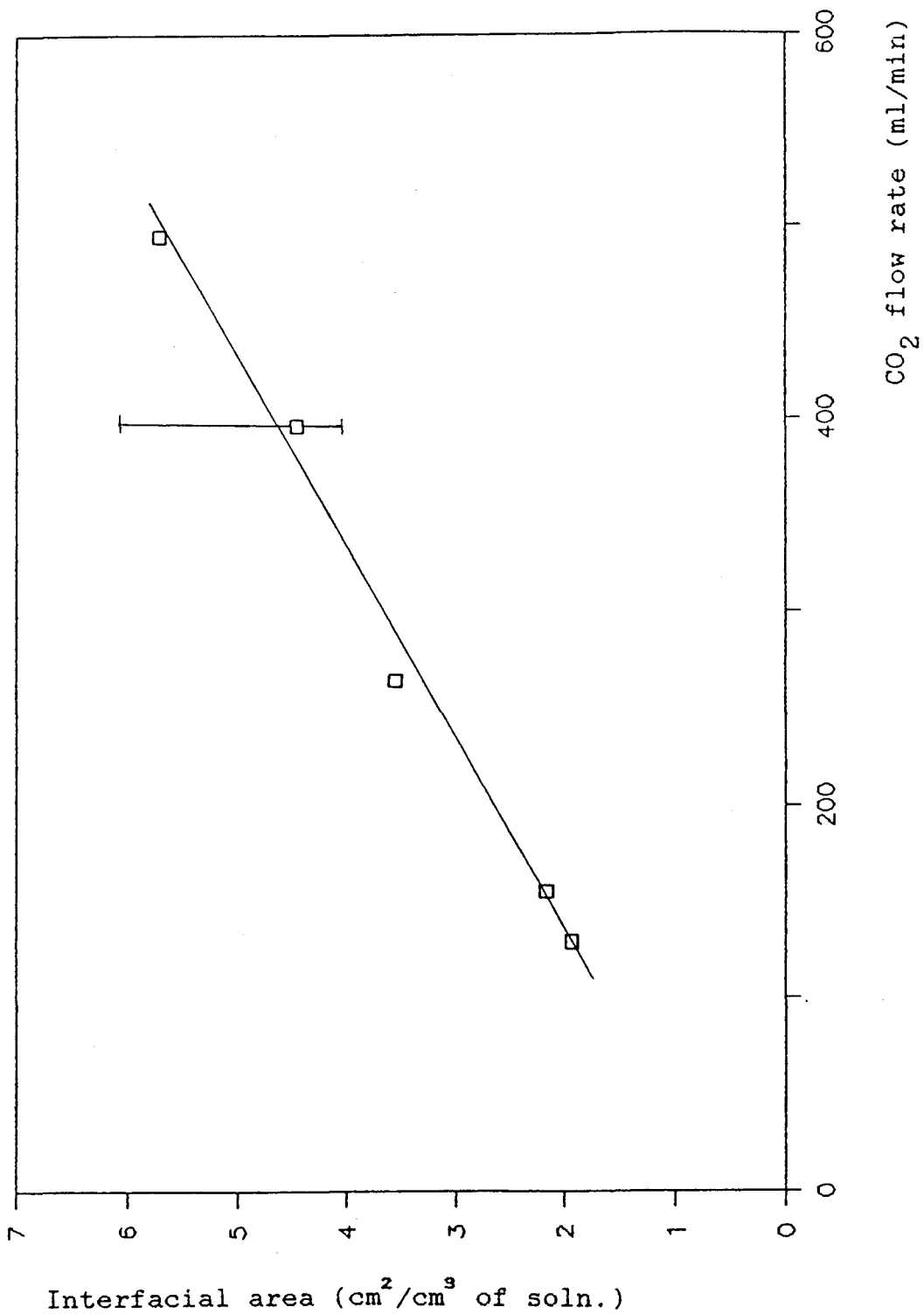


Figure 5.7 Gas-liquid interfacial area verses gas flow rate.

## CHAPTER 6

### Conclusions

Carbonation conversion of aqueous sodium sulfide to gaseous hydrogen sulfide is shown to be feasible. Eighty percent conversion can be achieved in 45 minutes under atmospheric pressure, at 35°C and with a CO<sub>2</sub> flow rate of 155 ml/min into a reactor containing 150 ml of reaction solution. Exit gas composition of up to thirty percent H<sub>2</sub>S can be attained. The main conclusions of this work are listed as follows :

- (1) Dependence of Na<sub>2</sub>S conversion rate on temperature is relatively small as compared to that of CO<sub>2</sub> flow rate and partial pressure.
- (2) The carbonation conversion of Na<sub>2</sub>S shows three distinguishable reaction periods. In the first period the acidity of reaction solution increases rapidly but with little Na<sub>2</sub>S conversion. On the contrary, the second reaction period is marked by fast Na<sub>2</sub>S conversion but with little change in the pH value of reaction solution. As Na<sub>2</sub>S depletes, to over 90% completion, the fast conversion period tapers off to the final slow reaction period.
- (3) The carbonation conversion of Na<sub>2</sub>S is first order with respect to HS<sup>-</sup> ion and P<sub>CO<sub>2</sub></sub>.
- (4) The rate determining step of the carbonation conversion

of aqueous  $\text{Na}_2\text{S}$  to gaseous  $\text{H}_2\text{S}$  is the desorption of  $\text{H}_2\text{S}$  gas.

- (5) The use of a pressurized reaction system is kinetically advantageous.

### Reference

- (1) Rosenqvist, terkel. Principles of Extractive Metallurgy. McGraw-Hill Book Company, 1983, 215-225.
- (2) Henold, K.L., and Walmsley, F.. Chemical Principles, Properties, and Reactions. Addison-Wesley Publishing Company, 1984, 610-611.
- (3) Lu W-K, Bryk, C., and Gou, H.Y.. "The LB Furnace For Smelting Reduction Of Iron Ores", Process Technology Proceedings, Washington, Vol.6 (1986), 1065-1075.
- (4) Lu W-K, and Gou, H.Y.. "The Development Of a Smelting Reduction Process", Proceedings Of Shengyang International Symposium On Smelting Reduction, China, 1986, 485-497.
- (5) Lu W-K. "Investigations Into The Feasibility Of Direct Reduction And Smelting Of Sulfide Ores In a LB Furnace". A submission to Department of Supply And Services, and Department of Energy, Mines and Resources, Canada, from Department of Materials Science and Engineering, McMaster University, Ontario, Canada. April, 1986.
- (6) Lu W-K. Final report of an "Investigation Into The Development Of a Process To Produce Elemental Sulfur From The Direct Smelting Of a Sulfide Concentrate" submitted to Canmet, EMR, Ottawa, Canada, by the Department of Materials Science and Engineering, McMaster University, Ontario, Canada. July, 1988.
- (7) Miller, Ralph. "Recovery Of Concentrated H<sub>2</sub>S From SO<sub>2</sub> Contained In Flue Gas". United States Patent, patent number 4,588,567. May 13, 1986.

- (8) Freeman, D.N., Ciriacks, J.A., and Wehn, W.E..  
"Efficient Recovery Of Chemicals For High-Yield Sulphite-Anthraquinone Pulping". International Sulphite Conference, 1986, Quebec, Canada.
- (9) Mai, K.L., and Babb, A.L.. "Vapor-Liquid Equilibria By Radioactive Tracer Techniques". Industrial And Engineering Chemistry, Vol.47, No.9 (1955), 1749-1756.
- (10) McCulloch, A.. "Gas Analysis", H.F. & G.Witherby, LTD. London, 1938, 28.
- (11) Karchmer, J.H.. "The Analytical Chemistry Of Sulfur And Its Compounds", Wiley-Interscience, 1970. Part 1, 106-107.
- (12) McCulloch, A.. "Gas Analysis", H.F. & G.Witherby, LTD. London, 1938, 109-110.
- (13) Furman, N.H.. "Standard Methods Of Chemical Analysis" D. Van Nostrand Company, Inc., Princeton, New Jersey, 1962. Vol.1, 1028.
- (14) Kolthoff, I.M., and Belcher, R.. "Volumetric Analysis" Interscience Publishers, Inc., New York, 1957. Vol.3, 291-292.
- (15) Skoog, D.A., and West, D.M.. "Fundamentals Of Analytical Chemistry". Holt, Rinehart and Winston, 1976. 353-354.
- (16) Skoog, D.A., and West, D.M.. "Fundamentals Of Analytical Chemistry". Holt, Rinehart and Winston, 1976. 329.
- (17) Espenson, J.H., "Chemical Kinetics and Reaction Mechanisms", McGraw-Hill Book Company, 1981.
- (18) Wilkinson, F., "Chemical Kinetics and Reaction Mechanisms", Van Nostrand Reinhold Company, 1980.
- (19) Astarita, Giovanni. "Mass Transfer With Chemical

- Reaction". Elsevier Publishing Company, 1967, 1.
- (20) Danckwerts, P.V.. "Gas-Liquid Reactions", McGraw Hill Book Company, 1970, 97-98.
- (21) Whitman, W.G.. "The Two-Film Theory Of Gas Absorption" Chemical And Metallurgical Engineering, Vol.29 (1923), 146-148.
- (22) Higbie, R., "The Rate Of Absorption Of a Pure Gas Into a Still Liquid During Short Periods Of Exposure", Transactions of American Institute of Chemical Engineers, Vol.35 (1935), 365-389.
- (23) Danckwerts, P.V., "Significance of Liquid-Film Coefficients in Gas Absorption", Ind. Engng. Chem. Ind. Edn., Vol.43 (1951), 1460.
- (24) Danckwerts, P.V.. "Gas-Liquid Reactions", McGraw Hill Book Company, 1970, 103-111.
- (25) Danckwerts, P.V.. "Gas-Liquid Reactions", McGraw Hill Book Company, 1970, 264-267.
- (26) Brian, P.L.T., Vivian, J.E., and Matiatos, D.C., "A Criteria For Supersaturation In Simultaneous Gas Absorption and Desorption", Chemical Engineering Science, Vol.22 (1967), 7-10.
- (27) Shah, Y.H., Juvekar, Y.A., and Sharma, M.M., "Criteria For Supersaturation During Simultaneous Absorption-Desorption", Chemical Engineering Science, Vol.31 (1976), 671-680.
- (28) Astarita, Giovanni. "Mass Transfer With Chemical Reaction". Elsevier Publishing Company, 1967, 131-133.
- (29) Berg, D., and Patterson, A., "The High Field Conductance Of Aqueous Solution Of CO<sub>2</sub> At 25°C. The True Ionization Constant Of Carbonic Acid", Journal of American Chemical Society, Vol.75 (1953), 5197.
- (30) Patterson, A., and Ettinger, R., "NMR Studies Of The

- CO<sub>2</sub>-Water Equilibrium", Zettschrift Fur Elektrochemie Vol.64 (1960), 98-110.
- (31) Harned, H.S., and Owen, B.B., "The Physical Chemistry Of Electrolyte Solutions", Reinhold Publishing Corp., New York, 1958.
- (32) Pinsent, B.R.W., Pearson, L., and Roughton, F.J.W., "The Kinetics Of Combination Of CO<sub>2</sub> and OH<sup>-</sup>", Transaction of the Faraday Society, Vol.52 (1956) 1512-1520.
- (33) Roughton, F.J.W., and Booth, V.H., "Catalytic Effect Of Buffers On The Reactions: CO<sub>2</sub> + H<sub>2</sub>O → H<sub>2</sub>CO<sub>3</sub> ", Biochemical Journal, Vol.32 (1938), 2049-2069.
- (34) Henold, K.L., and Walmsley, F.. Chemical Principles, Properties, and Reactions. Addison-Wesley Publishing Company, 1984, 431.
- (35) Näsänen, R., "The Second Dissociation Constant Of Carbonic Acid In Sodium Chloride and Potassium Chloride Solutions", Acta Chim. Fenn., Vol.B19 (1946), 90.
- (36) Nijsing, R.A.T.O., and Kramers, H., 1st Europ. Symp. Chem. React. Eng., Amsterdam, 1957.
- (37) Riesenfeld, F.C., and Blohm, C.L., "Acid Gas Removal Processes Compared", Hydrocarbon Processing and Petroleum Refiner, Vol.41 (1962), No.4, 123-127.
- (38) Sharma, M.M., and Danckwerts, P.V., "Catalysis By Brönsted Bases Of The Reaction Between CO<sub>2</sub> And Water", Transactions Of The Faraday Society, Vol.59 (1963), 386-395.
- (39) Gianetto, A., and Silveston, P.L., "Multiphase Chemical Reactors", Hemisphere Publishing Corporation, 1986, 81-83.
- (40) Van Krevelen, D.W., and Hoftijzer, P.J., Chimie et

Industrie, Numero Speciale du XXIe Congres International de Chimie Industrielle, Bruxelles, 1948, 168.

- (41) Ramm, V.M., "Absorption Of Gases", Israel Program For Scientific Translation Press, Jerusalem, 1968, 18-21.
- (42) Danckwerts, P.V., "Gas-Liquid Reactions", McGraw Hill Book Company, 1970, 18-20.
- (43) Lu W-K., "Treatment Of Coke Oven Gas", McMaster University Press, McMaster Symposium, 1977.
- (44) Maddox, R.N., "Gas And Liquid Sweetening", Campbell Petroleum Series, 1974.
- (45) Gamson, B.W., and Elkins, R.H., "Sulfur From Hydrogen Sulfide", Chemical Engineering Progress, Vol.49 (April 1953), 203-215.
- (46) Opekar, P.C., and Goar, B.G., Proceedings of 45th Annual Meeting Of NGPA.
- (47) Meites, L., "Handbook Of Analytical Chemistry", McGraw-Hill Book Company, Inc., 1963, 1-21.
- (48) Weast, R.C., and Lide, O.R., "CRC Handbook Of Chemistry And Physics", CRC Press, Inc. 1989.
- (49) Barner, H.E., and Scheuerman, R.V., "Handbook Of Thermodynamical Data For Compounds And Aqueous Species", Wiley-Interscience Publication, 1978.
- (50) Akgerman, A., and Gainer, J.L., "Diffusion Of Gases In Liquids", Ind. Eng. Chem. Fundam., Vol.11, No.3, 1972, 373-379.
- (51) Gianetto, A., and Silveston, P.L., "Multiphase Chemical Reactors", Hemisphere Publishing Corporation, 1986, 90.